INVESTIGATION OF THE
ATMOSPHERIC OZONE FORMATION POTENTIAL
OF PARA TOLUENE ISOCYANATE AND
METHYLENE DIPHENYLENE DIISOCYANATE

Final Report to the
Chemical Manufacturers Association
Diisocyanates Panel

by

William P. L. Carter, Dongmin Luo, and Irina L. Malkina

March 8, 1999

College of Engineering
Center for Environmental Research and Technology
University of California
Riverside, California 92521

ABSTRACT

Environmental chamber experiments and computer model calculations were conducted to assess the atmospheric ozone formation potentials of para toluene isocyanate (PTI), which is an analogue for methylene diphenylene diisocyanate (MDI), a compound of commercial importance which might be emitted into the atmosphere. MDI could not be studied directly because of its low vapor pressure, but PTI is considered to be a good analogue to MDI because of structural similarities. The experiments consisted of determining the effects of adding PTI on ozone formation, NO oxidation, and integrated OH radical levels in three different simulated photochemical smog systems in ~5000-liter, blacklight-irradiated Teflon environmental chambers. The rate constant for the reaction of PTI with hydroxyl radicals, its major expected atmospheric fate, was measured, and found to be essentially the same as that for toluene. PTI was found to have very small effects on ozone formation and OH radical levels under higher NO_x conditions, but was found to cause reduced ozone yields and OH radical levels in lower NO_x experiments. Although the mechanism for PTI's atmospheric reactions is unknown, the results of the experiments could be fit by simple parameterized models assuming significant formation of a cresol-like product, approximately 10% radical inhibition, some NO to NO_2 conversion, and some formation of a photoreactive product which is represented in the model by methyl glyoxyl.

The parameterized model which best fit the PTI chamber data and the PTI OH radical rate constant were used to estimate a mechanism to predict the atmospheric impact of MDI, which is essentially a dimer of PTI. It is concluded that MDI will probably have negative impacts on ozone formation under atmospheric conditions where NO_x limited or most favorable for ozone formation, which was the case in most of the scenarios used in this study to represent ozone exceedence episodes in various areas of the United States. However, MDI was calculated to have positive impacts and form comparable or more ozone than ethane under higher NO_x, MIR conditions where ozone is sensitive to VOC emissions. Therefore, MDI is expected to be a less general ozone inhibitor than TDI, which based on a previous study is expected to be an ozone inhibitor under all conditions.

ACKNOWLEDGEMENTS

TABLE OF CONTENTS

LIST OF TABLES

LIST OF FIGURES

INTRODUCTION

Ozone in photochemical smog is formed from the gas-phase reactions of volatile organic compounds (VOCs) and oxides of nitrogen (NO_x) in sunlight. Although Los Angeles has one of the worst ozone problems in the United States, other areas of the country also have episodes where ozone exceeds the federal air quality standard. Ozone control strategies in the past have focused primarily on VOC controls, though the importance of NO_x control has become recognized in recent years. VOC and NO_x controls have differing effects on ozone formation. NO_x is required for ozone formation, and if the levels of NO_x are low compared to the levels of reactive VOCs, then changing VOC emissions will have relatively little effect on ozone. Since NO_x is removed from the atmosphere more rapidly than VOCs, ozone in areas far downwind from the primary sources tend to be more NO_x limited, and thus less responsive to VOC controls. VOC controls tend to reduce the rate that O_3 is formed when NO_x is present, so VOC controls are the most beneficial in reducing O_3 in the urban source areas, where NO_x is relatively plentiful, and where O_3 yields are determined primarily by how rapidly it is being formed. Because of this, any comprehensive ozone control strategy should involve reduction of emissions of both NO_x and VOCs.

Many different types of VOCs are emitted into the atmosphere, each reacting at different rates and having different mechanisms for their reactions. Because of this, they can differ significantly in their effects on ozone formation, or their "reactivities". Some compounds, such as CFCs, do not react in the lower atmosphere at all, and thus make no contribution to ground-level ozone formation. Others, such as methane, react and contribute to ozone formation, but react so slowly that their practical effect on ozone formation in urban atmospheres is negligible. Still others, such as volatile silicone compounds (Carter et al, 1992) react in such a way that they inhibit ozone formation in the atmosphere. Obviously, it does not make sense to regulate such compounds as ozone precursors. In recognition of this, the EPA has exempted certain compounds from such regulations on the basis of having "negligible" effects on ozone formation. Although the EPA has no formal policy on what constitutes "negligible" reactivity, in practice it has used the ozone formation potential of ethane as the standard in this regard. This is because ethane is the most reactive of the compounds that the EPA has exempted to date. Therefore, the ozone formation potential of a compound relative to ethane is of particular interest when assessing whether it might be a likely candidate for exemption from regulation as an ozone precursor.

Toluene diisocyanate (TDI) and methylene diphenylene diisocyanate (MDI) are used in a number of manufacturing processes, and the appropriateness of regulating them as an ozone precursors is of interest to their users and suppliers. We had previously studied the atmospheric ozone impacts of TDI and found it to be an ozone inhibitor under all atmospheric conditions which were considered (Carter et

al, 1997a). This suggests that other aromatic isocyanates, such as MDI, might be ozone inhibitors as well. However, the atmospheric reactions of MDI have not been studied, and its structure, having a single isocyanate group on each aromatic ring rather than two like TDI, could result in its having different reactivity characteristics. Therefore, additional data were needed to evaluate whether MDI may also be an ozone inhibitor in the atmosphere.

MDI is calculated to have a vapor pressure of approximately 17 ppb at 300°K (80°F). Although emissions of a compound with such a low vapor pressure would be slow, significant emissions might occur if the compound is exposed to the atmosphere for a sufficient amount of time, or if the process where the compound is used involves high temperature. However, this vapor pressure is too low for it to be practical to directly study MDI's ozone impacts using currently available experimental methods. Therefore, it is necessary to use a more indirect method to obtain information concerning the likely effects of MDI on ozone formation in the atmosphere.

MDI consists of two isolated aromatic rings joined by a methylene group, each with a single isocyanate group in a *para* position relative to the methylene. Because aromatic hydrocarbons react in the atmosphere primarily by addition of OH radicals to the aromatic ring (e.g., see Atkinson, 1990, and references therein), it is reasonable to expect that this is the primary reaction mode for aromatic isocyanates as well. TDI has been found to have a slightly higher rate constant for reaction with OH radicals than does toluene (Becker et al, 1988), which is consistent with the assumption that most of the reaction is at the aromatic ring[1]. This suggests that a good analogue for MDI would be two para toluene isocyanate (PTI) molecules, each of which, like MDI, has an aromatic ring with an isocyanate group *para* to an alkyl group. Therefore, the mechanism for the reaction following OH radical addition to the aromatic ring should be similar in both cases. For this reason, if PTI can be shown to have the same type of ozone inhibiting characteristics as does TDI, it is reasonable to conclude that MDI will similarly be an ozone inhibitor. In any case, ozone reactivity data obtained for PTI can provide a significantly improved basis for estimating likely atmospheric ozone impacts for MDI, and significantly reduce the uncertainty range.

To obtain data needed to determine the ozone impact of PTI and thus improve our estimates for MDI, the Diisocyanate Panel of the Chemical Manufacturers Association contracted the College of Engineering Center for Environmental Research and Technology (CE-CERT) to carry out the

---

[1] The alternative mode of reaction is abstraction from a side group, which would be methyl groups in the case of toluene and TDI. This mode of reaction occurs somewhat less than 10% of the time in the case of toluene (Atkinson, 1990, and references therein.) Since this reaction is not expected to be strongly affected by substituents on the aromatic ring, it is reasonable to expect this to have a similar rate for TDI. Therefore, if this were the only mode of reaction of OH with TDI, the total rate constant would be estimated to be ~10 times lower than the total OH rate constant for toluene, which is not the case.

2

environmental chamber experiments to measure the ozone impacts of PTI various simulated atmospheric conditions, to develop and evaluate models for its effects on ozone and other observations which are consistent with these data, and then to use these models to derive an atmospheric reactivity model for MDI which can be used to estimate its likely ozone impacts under a variety of atmospheric conditions. The results of this study are documented in this report.

METHODS

Environmental Chamber Experiments

      Overall Experimental Approach

Most of the environmental chamber experiments for this program consisted of measurements of "incremental reactivities" of PTI under various conditions. These involve two types of irradiations of model photochemical smog mixtures. The first is a "base case" experiment where a mixture of reactive organic gases (ROGs) representing those present in polluted atmospheres (the "base ROG surrogate") is irradiated in the presence of oxides of nitrogen (NO_x) in air. The second is the "test" experiment which consists of repeating the base case irradiation except that the VOC whose reactivity is being assessed is added. The differences between the results of these experiments provide a measure of the atmospheric impact of the test compound, and the difference relative to the amount added is a measure of its reactivity. These data can then be used to test the ability of various chemical mechanisms or models for PTI's atmospheric reactions to predict the reactivities of similar compounds, such as MDI, under various conditions in the atmosphere.

To provide data to test predictions of reactivities of PTI under varying atmospheric conditions, three types of incremental reactivity experiments were carried out:

1. Mini-Surrogate Experiments. The base case for this type of experiment employed a simplified ROG surrogate and relatively high NO_x levels and low ROG/NO_x ratios. Low ROG/NO_x ratios represent "maximum incremental reactivity" (MIR) conditions (Carter, 1994a), which are most sensitive to VOC effects. Low ROG/NO_x experiments are useful because they provide a sensitive test for the model, and also because it is most important that the model correctly predict a VOC's reactivity under conditions where the atmosphere is most sensitive to the VOCs. The ROG mini-surrogate mixture employed consisted of ethene, n-hexane, and m-xylene. This same surrogate was employed in our previous studies (Carter et al, 1993a,b; 1995a,b.), and was found to provide a more sensitive test of aspects of the mechanism concerning radical initiation and termination effects than the more complex surrogates which more closely represent atmospheric conditions (Carter et al, 1995b). This high sensitivity to these important mechanistic effects makes the mini-surrogate experiments highly useful for mechanism evaluation.

2. Full Surrogate Experiments. The base case for this type of experiment employed a more complex ROG surrogate under somewhat higher, though still relatively low, ROG/NO_x conditions. While less sensitive to radical initiation and termination effects in the mechanisms of the VOCs studied, they provide a means to test other aspects of the mechanisms, such as numbers of NO to NO_2 conversions, etc.

4

Furthermore, experiments with a more representative ROG surrogate are needed to evaluate the mechanism under conditions that more closely resembling the atmosphere. The ROG surrogate employed was the same as the 8-component "lumped molecule" surrogate as employed in previous studies (e.g., Carter et al. 1995b), and consists of n-butane, n-octane, ethene, propene, trans-2-butene, toluene, m-xylene, and formaldehyde. Calculations have indicated that use of this 8-component mixture will give essentially the same results in incremental reactivity experiments as actual ambient mixtures (Carter et al. 1995b).

    3. <u>Full Surrogate, low NO_x Experiments</u>. The base case for this type of experiment employed the same 8-component lumped molecule surrogate as used in the full surrogate experiments described above, except that lower NO_x levels (higher ROG/NO_x ratios) were employed to represent NO_x-limited conditions. Such experiments are necessary to assess the ability of the model to properly simulate reactivities under conditions where NO_x is low. The initial ROG and NO_x reactant concentrations were comparable to those employed in our previous studies (Carter et al. 1995b).

    An appropriate set of control and characterization experiments necessary for assuring data quality and characterizing the conditions of the runs for mechanism evaluation were also carried out. These are discussed where relevant in the Modeling Methods or Results sections.

Environmental Chamber

    The environmental chamber system employed in this study was the CE-CERT "Dividable Teflon Chamber" (DTC) with a blacklight light source. This consists of two ~5000-liter 2-mil heat-sealed FEP Teflon reaction bags located adjacent to each other and fitted inside an 8' x 8' x 8' framework, and which uses two diametrically opposed banks of 32 Sylvania 40-W BL black lights as the light source. The lighting system in the DTC was found to provide so much intensity that only half the lights were used for irradiation. The air conditioner for the chamber room was turned on before and during the experiments. Four air blowers which are located in the bottom of the chamber were used to help cool the chamber as well as mix the contents of the chamber. The CE-CERT DTC is very similar to the SAPRC DTC which is described in detail elsewhere (Carter et al, 1995b,c).

    The DTC is designed to allow simultaneous irradiations of experiments with and without added test reactants under the same reaction conditions. Since the chamber is actually two adjacent FEP Teflon reaction bags, two mixtures can be simultaneously irradiated using the same light source and with the same temperature control system. These two reaction bags are referred to as the two "sides" of the chamber (Side A and Side B) in the subsequent discussion. The sides are interconnected with two ports, each with a box fan, which rapidly exchange their contents to assure that base case reactants have equal concentrations in both sides. In addition, a fan is located in each of the reaction bags to rapidly mix the reactants within each chamber. The ports connecting the two reactors can then be closed to allow separate injections on each side, and separate monitoring of each side.

Experimental Procedures

The reaction bags were flushed with dry air produced by an AADCO air purification system for 14 hours (6 PM - 8 AM) on the nights before experiments. The continuous monitors were connected prior to reactant injection and the data system began logging data from the continuous monitoring systems. The reactants were injected as described below (see also Carter et al, 1993a,, 1995c). The common reactants were injected in both sides simultaneously using a three-way (one inlet and two outlets connected to side A and B respectively) bulb of 2 liters in the injection line and were well mixed before the chamber was divided. The contents of each side were blown into the other using two box fans located between them. Mixing fans were used to mix the reactants in the chamber during the injection period, but these were turned off prior to the irradiation. The sides were then separated by closing the ports which connected them, after turning all the fans off to allow their pressures to equalize. After that, reactants for specific sides (the test compound in the case of reactivity experiments) were injected and mixed. The irradiation began by turning on the lights and proceeded for 6 hours. After the run, the contents of the chamber were emptied by allowing the bag to collapse, and then was flushed with purified air. The contents of the reactors were vented into a fume hood.

The procedures for injecting the various types of reactants were as follows. The NO and NO_2 were prepared for injection using a high vacuum rack. Known pressure of NO, measured with MKS Baratron capacitance manometers, were expanded into Pyrex bulbs with known volumes, which were then filled with nitrogen (for NO) or oxygen (for NO2). The contents of the bulbs were then flushed into the chamber with AADCO air. The other gas reactants were prepared for injection either using a high vacuum rack or a gas-tight syringes whose amounts were calculated. The gas reactants in a gas-tight syringe was usually diluted to 100-ml with nitrogen in a syringe. The volatile liquid reactants were injected, using a micro syringe, into a 1-liter Pyrex bulb equipped with stopcocks on each end and a port for the injection of the liquid. The port was then closed and one end of the bulb was attached to the injection port of the chamber and the other to a dry air source. The stopcocks were then opened, and the contents of the bulb were flushed into the chamber with a combination of dry air and heat gun for approximately 5 minutes. Formaldehyde was prepared in a vacuum rack system by heating paraformaldehyde in an evacuated bulb until the pressure corresponded to the desired amount of formaldehyde. The bulb was then closed and detached from the vacuum system and its contents were flushed into the chamber with dry air through the injection port.

Since PTI has a high boiling point (70-72°C at 10 mmHg) and may condense in cold spots using usual liquid injection, a heated injection system was employed to inject this compound. This was done by placing the desired quantity of PTI in a three-way (one port for the liquid injection) glass tube which was surrounded with heat tape. The tube was then heated to around 200°C and its contents were flushed into chamber with purified dry air at 2 liters/minute for about 15 minutes.

6

Chamber Characterization Methods

Three thermocouples were used to monitor the temperature of the reaction chambers, two of which were located in the sampling line of continuous analyzers drawing sample from each side, and the third being located in the chamber between the reaction gabs. The temperature in these experiments was typically in the 21-25 C range.

The light intensity in the DTC chamber was monitored by periodic NO_2 actinometry experiments utilizing the quartz tube method of Zafonte et al (1977), with the data analysis method modified as discussed by Carter et al. (1995c). The results of these experiments were tracked over time, and indicated a gradual decrease in light intensity during the period these experiments were carried out. The results of actinometry experiments were fit by a line, which was used to derive an NO_2 photolysis rate for modeling each experiment. This line predicted the NO_2 photolysis rates declined from 0.18 min^{-1} to 0.16 min^{-1} during the course of this program.

The spectrum of the blacklight light source is periodically measured using a LiCor LI-1200 spectra radiometer, and found to be essentially the same as the general blacklight spectrum recommended by Carter et al (1995c) for use in modeling blacklight chamber experiments.

The dilution of the DTC chamber due to sampling is expected to be small because the flexible reaction bags can collapse as samples are withdrawn for analysis. However, some dilution occurs with the aging of reaction bags because of small leaks. Information concerning dilution in an experiment can be obtained from relative rates of decay of added VOCs which react with OH radicals with differing rate constants (Carter et al., 1993a; 1995c). Most experiments had a more reactive compounds such as m-xylene and n-octane present either as a reactant or added in trace amounts to monitor OH radical levels. Trace amounts (~0.1 ppm) of n-butane were also added to experiments if needed to provide a less reactive compound for monitoring dilution. In addition, specific dilution check experiments such as CO irradiations are periodically carried out. Based on these results, the dilution rates were found to average ~1% per hour on both sides during the period of these experiments.

Various characterization runs were carried out to measure the chamber radical source, background effects, and to test side equivalency. The results of these experiments are described in the Results and in the Environmental Chamber Modeling Methods sections.

OH Radical Rate Constant Measurements

The rate constant for the reaction of OH radicals with PTI was determined using the relative rate method where the rates of consumption of PTI relative to a reference compound with known OH radical rate constant were measured in the presence of an OH radical source. If it is assumed that reaction with

OH radicals is the only significant process causing consumption of PTI and the reference compound, then the ratio of OH radical rate constants can be determined as discussed below.

Three kinetic experiments were carried out, all using Side A of the DTC chamber. Hydroxyl radicals were generated by the photolysis of methyl nitrite, with NO also present to suppress formation of O3 or of NO3 radicals. Toluene was used as the primary reference compound in this study, though m-xylene was also present as a potential reference compound n the first experiment. Initial concentrations in the first experiment (DTC605) were ~200-250 ppb for PTI, toluene, and m-xylene, ~2 ppm methyl nitrite, and ~3 ppm NO. Initial concentrations of the other two experiments (DTC606 and DTC611) were similar except that m-xylene was not present and the initial methyl nitrite concentration was increased to 4 ppm.

Several measurements of PTI and the reference compound(s) were made prior to beginning the irradiation to determine the initial reactant concentrations and check for possible wall losses. The lights were then turned at 100% intensity (twice that used in the reactivity experiments) for ~10 minutes and the PTI and reference compound(s) were then monitored after the lights were turned off. This was repeated several times until there was no significant measured change in PTI or the reference compound, indicating that all the initially present methyl nitrite had been reacted. The total irradiation time was typical 30~40 minutes and the total experimental time was approximately 300-360 minutes. The experiments were carried out using purified air as the dilution gas. The analysis and injection procedures were the same as employed for the reactivity experiments, as discussed above and below.

The reactants and their stated purity levels were as follows: PTI (99%), toluene (99.5%) and m-xylene (99%), Aldrich Chemical Company; NO (99.0%) and Matheson Gas Company. The methyl nitrite was provided by the Statewide Air Pollution Research Center, who prepared it by drop-wise addition of 50% H2SO4 to a saturated solution of NaNO2 and methanol (Taylor et al, 1980), and purified it on a vacuum line using bulb-to-bulb distillations.

Analytical Methods

Ozone and nitrogen oxides (NO_x) were continuously monitored using commercially available continuous analyzers with Teflon sample lines inserted directly into the chambers. The sampling lines from each side of the chamber were connected to solenoids which switched from side to side every 10 minutes, so the instruments alternately collected data from each side. Ozone was monitored using a Dasibi 1003AH UV photometric ozone analyzer and NO and total oxides of nitrogen (the latter also responding to HNO_3 and organic nitrates) were monitored using a Teco Model 14B chemiluminescent NO/NO_x monitor. The output of these instruments, along with that from the temperature sensors and the formaldehyde instrument, were attached to a computer data acquisition system, which recorded the data at 10 minutes intervals for ozone, NO and temperature (and at 15 minutes for formaldehyde), using 30

second averaging times. This yielded a sampling interval of 20 minutes for taking data from each side.

The Teco instrument and Dasibi CO analyzer were calibrated with a certified NO and CO source and CSI gas-phase dilution system. This was done prior to chamber experiment for each run. The NO_2 converter efficiency check was carried out in regular intervals. The Dasibi ozone analyzer was calibrated against a transfer standard ozone analyzer approximately once every three months and it was checked with a CSI ozone generator (set to 400 ppb) prior to each experiment to assure that the instrument worked properly. The details were discussed elsewhere (Carter et al, 1995c)

Organic reactants other than formaldehyde and were measured by gas chromatography with FID or ECD detections as described elsewhere (Carter et al. 1993a; 1995c). GC samples were taken for analysis at intervals from 20 minutes to 30 minutes either using 100 ml gas-tight glass syringes or by collecting the 100 ml sample from the chamber onto Tenax-GC solid adsorbent cartridge. These samples were taken from ports directly connected to the chamber after injection and before irradiation and at regular intervals after irradiation. The sampling method employed for injecting the sample onto the GC column depended on the volatility or "stickiness" of the compound. For analysis of the more volatile species, the contents of the syringe were flushed through a 2 ml or 3 ml stainless steel or 1/8' Teflon tube loop and subsequently injected onto the column by turning a gas sample valve.

Unlike TDI, which we found could not be monitored by GC and required special analysis methods (Carter et al, 1997a), we found that PTI could be monitored by GC/FID using both the Tenax and loop sampling method. However, the compound was sufficiently "sticky" that the data using the Tenax method tended to be less scattered than those from the loop analysis. Therefore, the Tenax data were primary method in the PTI analysis for both the kinetic and reactivity experiments.

The calibrations for the GC analyses for most compounds were carried out by sampling from chambers or vessels of known volume into which known amounts of the reactants were injected, as described previously (Carter et al, 1995c).

Data Analysis Methods
Reactivity Data Analysis Methods
The results of the environmental chamber experiments are analyzed to yield two measures of reactivity for PTI. The first is the effect of PTI on the change in the quantity $[O_3]-[NO]$, or $([O_3]_t-[NO]_t)-([O_3]_0-[NO]_0)$, which is abbreviated as $d(O_3-NO)$ in the subsequent discussion. As discussed elsewhere (e.g., Johnson, 1983; Carter and Atkinson, 1987; Carter and Lurmann, 1990, 1991, Carter et al, 1993a, 1995a), this gives a direct measure of the amount of conversion of NO to NO_2 by peroxy radicals formed in the photooxidation reactions, which is the process that is directly responsible for ozone formation in

the atmosphere. (Johnson calls it "smog produced" or "SP".) The incremental reactivity of the compound relative to this quantity, which is calculated for each hour of the experiment, is given by

$$IR[d(O_3\text{-}NO)]_t^{VOC} = \frac{d(O_3\text{-}NO)_t^{test} - d(O_3\text{-}NO)_t^{base}}{[VOC]_0} \qquad (I)$$

where $d(O_3\text{-}NO)_t^{test}$ is the $d(O_3\text{-}NO)$ measured at time t from the experiment where the test compound was added, $d(O_3\text{-}NO)_t^{base}$ is the corresponding value from the corresponding base case run, and $[VOC]_0$ is the amount of test compound added. The units used are ppm for O_3, NO, and $[VOC]_0$, so the incremental reactivity units are moles of O_3 formed and NO oxidized per mole VOC sample added. An estimated uncertainty for $IR[d(O_3\text{-}NO)]$ is derived based on assuming an ~3% uncertainty or imprecision in the measured $d(O_3\text{-}NO)$ values. This is consistent with the results of the side equivalency tests, where equivalent base case mixtures are irradiated on each side of the chamber.

Note that reactivity relative to $d(O_3\text{-}NO)$ is essentially the same as reactivity relative to O_3 in experiments where O_3 levels are high, because under such conditions $[NO]_t^{base} \approx [NO]_t^{test} \approx 0$, so a change $d(O_3\text{-}NO)$ caused by the test compound is due to the change in O_3 alone. However, $d(O_3\text{-}NO)$ reactivity has the advantage that it provides a useful measure of the effect of the compound on processes responsible for O_3 formation even in experiments where O_3 formation is suppressed by relatively high NO levels.

The second measure of reactivity is the effect of the test compound on integrated hydroxyl (OH) radical concentrations in the experiment, which is abbreviated as "IntOH" in the subsequent discussion. This is an important factor affecting reactivity because radical levels affect how rapidly all VOCs present, including the ROG surrogate components, react to form ozone. If a compound is present in the experiment which reacts primarily with OH radicals, then the IntOH at time t can be estimated from

$$IntOH_t = \int_0^t [OH]_\tau \, d\tau = \frac{\ln \left(\dfrac{[tracer]_0}{[tracer]_t}\right) - D\,t}{kOH^{tracer}}, \qquad (II)$$

where $[tracer]_0$ and $[tracer]_t$ are the initial and time=t concentrations of the tracer compound, kOH^{tracer} is its OH rate constant, and D is the dilution rate in the experiments. The latter was found to be small and was neglected in our analysis. The concentration of tracer at each hourly interval was determined by linear interpolation of the experimentally measured values. M-xylene was used as the OH tracer in these experiments because it is a base case component present in all incremental reactivity experiments, its OH rate constant is known (the value used was 2.36×10^{-11} cm^3 $molec^{-1}$ s^{-1} [Atkinson, 1989]), and it reacts sufficiently rapidly that its consumption rate can be measured with reasonable precision.

The effect of PTI on OH radicals can thus be measured by its IntOH incremental reactivity, which is defined as

$$IR[IntOH]_t = \frac{IntOH_t^{test} - IntOH_t^{base}}{[VOC]_0} \qquad (III)$$

where $IntOH_t^{test}$ and $IntOH_t^{base}$ are the IntOH values measured at time t in the added compound and the base case experiment, respectively. The results are reported in units of 10^6 min per ppm. The uncertainties in IntOH and IR[IntOH] are estimated based on assuming an ~2% imprecision in the measurements of the m-xylene concentrations. This is consistent with the observed precision of results of replicate analyses of this compound.

Kinetic Data Analysis Methods

The kinetic experiments consisted of monitoring the consumption rates of both toluene and PTI in experiments where OH radicals are generated by the photolysis of methyl nitrite. Methyl nitrate photolyzes relatively rapidly in our environmental chamber experiments, forming OH radicals through the following sequence of reactions:

$$CH_3ONO + h\nu \rightarrow CH_3O\cdot + NO$$
$$CH_3O\cdot + O_2 \rightarrow HCHO + HO_2$$
$$HO_2 + NO \rightarrow NO_2 + OH$$
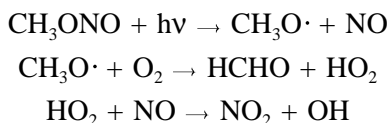
If toluene and PTI are present in the same experiment and are consumed significantly only by reaction with OH radicals or some unimolecular loss process such as dilution or wall decay, then their rates of consumption are given by

$$d \ln[PTI]/dt = kOH^{PTI} [OH]_t + D^{PTI}$$
$$d \ln[toluene]/dt = kOH^{toluene} [OH]_t + D^{toluene}$$

where $[PTI]t$ and $[toluene]_t$ are the PTI and toluene concentrations at time=t, kOH^{PTI} and $kOH^{toluene}$ are their respective OH radical rate constants, and D^{PTI} and $D^{toluene}$ are their respective first order loss rates. If first order loss processes are assumed to be negligible, then combining these equations and integrating yields

$$\ln([PTI]_0/[PTI]_t) = (kOH^{PTI}/kOH^{toluene}) \ln([toluene]_0/[toluene]_t) \qquad (IV)$$

In this case, plots of $\ln([PTI]_0/[PTI]_t)$ <u>vs</u> $\ln([toluene]_0/[toluene]_t)$ should yield a straight line with a slope of $kOH_{PTI}/kOH_{toluene}$ and an intercept near zero. If this plot is not linear, then it may indicate that other loss processes may be non-negligible. If this is assumed to be due dark decay processes such as wall losses, then the data should be fit by

$$\ln([PTI]_0/[PTI]_t)-D^{PTI} t = (kOH^{PTI}/kOH^{toluene}) \{\ln([toluene]_0/[toluene]_t)-D^{toluene} t\} \qquad (V)$$

11

where t refers to the time after the reactants were injected into the chamber. In this case, plots of $\ln([PTI]_0/[PTI]_t)-D^{PTI}$ t $\underline{vs}$ $kOH^{toluene}$ $[OH]_t + D^{toluene}$ t can be used to determine the OH radical rate constant ratio. The value of D^{PTI} and $D^{toluene}$ can be determined either in separate dark decay experiments or by least squares fits of the data to Equation (V).

Chemical Mechanisms Used in the Model Simulations
General Atmospheric Photooxidation Mechanism

Ozone formation in photochemical smog is due to the gas-phase reactions of oxides of nitrogen (NO_x) and various reactive organic gases (ROGs) in sunlight. Various reaction schemes have been developed to represent these processes (e.g., Gery et al., 1988; Carter, 1990; Stockwell et al., 1990), but the one used in this work was an updated version of the detailed SAPRC mechanism (Carter, 1990, 1995; Carter et al., 1993b, 1997b). This is detailed in the sense that it explicitly represents a large number of different types of organic compounds, but it uses a condensed representation for most of their reactive products. The major characteristics of this mechanism are described by Carter (1990). The reactions of inorganics, CO, formaldehyde, acetaldehyde, peroxyacetyl nitrate, propionaldehyde, peroxypropionyl nitrate, glyoxal and its PAN analog, methyl glyoxal, and several other product compounds are represented explicitly. The reactions of unknown photoreactive products formed in the reactions of aromatic hydrocarbons are represented by model species whose yields and photolysis rate are adjusted based on fits of model simulations to environmental chamber experiments. A "chemical operator" approach is used to represent peroxy radical reactions. Generalized reactions with variable rate constants and product yields are used to represent the primary emitted alkane, alkene, aromatic, and other VOCs (with rate constants and product yields appropriate for the individual compounds being represented in each simulation). Most of the higher molecular weight oxygenated product species are represented using the "surrogate species" approach, where simpler molecules such as propionaldehyde or 2-butanone are used to represent the reactions of higher molecular weight analogues that are assumed to react similarly.

The mechanism of Carter (1990) was updated several times prior to this work. A number of changes were made to account for new kinetic and mechanistic information for certain classes of compounds as described by Carter et. al. (1993b) and Carter (1995). Further modifications to the uncertain portions of the mechanisms for the aromatic hydrocarbons were made to satisfactorily simulate results of experiments carried out using differing light sources (Carter et al. 1997b). The latest version of the general mechanism is discussed by Carter et al. (1997b). A complete listing of this mechanism is given in Appendix A to this report.

Models for PTI Reactions

There is no information available concerning the atmospheric reactions of PTI and only relatively limited information concerning the atmospheric reactions of related compounds. The best studied compound in this class appears to be TDI, as discussed by Carter et al (1997a). The primary initial mode

of reaction of these compounds is believed to be with OH radicals, as is the case with the simpler aromatic hydrocarbons. Becker et al. (1988), measured the rate constant for the reaction of OH radicals with TDI to be 7.4 x 10^{-12} cm^3 molec^{-1} s^{-1} at room temperature, which is very close to the toluene OH rate constant of 5.96 x 10^{-12} cm^3 molec^{-1} s^{-1} at 298K (Atkinson, 1989). This suggests that isocyanate groups on the aromatic ring do not significantly affect the OH radical rate constant, implying that PTI may have a similar rate constant. As discussed below, this is in fact what was observed in our studies, where the OH rate constant was measured to be the same, within experimental error, as that for toluene.

Despite considerable study of the reactions of OH radicals with aromatic hydrocarbons (e.g., see Atkinson 1990, 1994 and references therein), the details of the aromatic photooxidation reactions are still highly uncertain. The reactions of the aromatic isocyanates, where mechanistic data are much more limited or nonexistent, are even more uncertain. Given this, in our study of the ozone reactivity of TDI we made no attempt to construct a detailed or explicit mechanism to model the data. Instead a parameterized mechanism, showing the overall processes in as simple a manner as is chemically reasonable and consistent with the data, was used, with the values of the adjusted to fit the chamber data. This is analogous to the approach used for representing the unknown ring-opening reactions of aromatic hydrocarbons, and for representing the atmospheric reactions of phenols, cresols, and the uncharacterized aromatic ring fragmentation products in the mechanisms currently used for air quality modeling (Carter, 1990; Gery et al, 1988; Stockwell et al, 1990). In all these cases, our current knowledge does not justify any greater level of detail, which may not give any more reliable predictions of ozone impacts than a simpler, parameterized approach. Therefore, this approach will also be used for PTI.

The parameterization we found fit the chamber data for TDI was used as the starting point when modeling the PTI experiments, though some minor refinements were made. The product yield parameters were as follows:

- The parameter y_{OH} is the amount of OH radicals regenerated in the overall reaction the overall reaction when PTI reacts in the presence of NO$_x$. Note that 1-y_{OH} is the amount of radical inhibition involved in the overall OH + PTI photooxidation process. The TDI data were best fit by assuming $y^{OH} \approx 0.3$, indicating that TDI had significant radical inhibition characteristics.

- The parameter $y_{NO \rightarrow NO2}$ is the number of NO to NO$_2$ conversions involved in the reactions of PTI. The conversion of NO to NO$_2$ is the process by which VOCs cause ozone formation. This is represented in the model in different ways, depending on the value of y_{OH} and the number of NO to NO$_2$ conversions involved. If $y_{NO \rightarrow NO2}$ is between 0 and y_{OH}, it is represented by replacing $y_{NO \rightarrow NO2}$ of the OH formed by HO$_2$. This is because in the presence of NO$_x$ most of the HO$_2$ forms reacts with NO to form NO$_2$ and OH, so formation of HO$_2$ involves the formation of OH plus one NO to NO$_2$ conversion. If $y_{NO \rightarrow NO2}$ is between y_{OH} and 2 y_{OH}, then all of the OH is replaced by HO$_2$ and $y_{NO \rightarrow NO2}$-y_{OH} of that HO$_2$ is replaced by the chemical "operator" RO2-R., which represents formation of peroxy radicals which react in the presence of NO$_x$ to form HO$_2$ after one NO to NO$_2$ conversion. If $y_{NO \rightarrow NO2}$ is greater than 2 y_{OH}, then all of the OH is replaced by RO2-R., and an

additional $y_{NO \to NO2}$ - 2 y_{OH} R2O2.'s are added, where the operator R2O2. represents additional NO to NO$_2$ conversion (see Tables A-1 and A-2). If $y_{NO \to NO2}$ is negative, then a new operator, "xNO2" is added, which represents NO$_2$ to NO conversions in the presence of NO$_2$. Its reactions were included in the mechanism for the purpose of examining all mechanistic options (with rate constants based on those assigned for phenoxy — see Table B-2), though it was not needed in the best fit mechanisms used for atmospheric reactivity assessment.

• The parameter y_{NO} is the amount of NO generated from the isocyanate group. (Formation of NO$_2$ from the isocyanate group could be modeled by a combination of y_{NO} and $y_{NO \to NO2}$. The TDI data are best fit by assuming this is negligible, i.e., the isocyanate group does not react to release NO$_x$ into the system.

• The parameter $y_{NO \to NPHE}$ is the yield of organic nitrates from the reactions of peroxy radicals with NO. In the case of aromatics, the organic nitrates are represented by the nitrophenol, or NPHE, model species (Carter, 1990). Organic nitrate formation from the peroxy + NO reaction is important in the photooxidations of the higher molecular weight alkanes (Carter and Atkinson, 1989b), though it is somewhat less important a factor in the current mechanisms assumed for aromatics (Carter, 1990). However, this possibility was considered for completeness. In the presence of NO$_x$ the operator RO2-NP. reacts with NO to form nitrophenols, while when NO$_x$ is absent it reacts with other peroxy radicals to form nothing. Some of the alternative mechanisms which fit the chamber data for TDI are based on assuming that this is important.

• The parameter y_{CRES} is the yield of products which react like phenols or cresols. These are represented by the model species "CRES" in the base mechanism. Formation of this product is an important factor affecting reactivity under NO$_x$-limited conditions, because in the presence of O$_3$ and NO$_x$ it reacts rapidly with NO$_3$ radicals via a mechanism which is assumed to remove NO$_x$ from the system. Some of the alternative mechanisms which fit the chamber data for TDI are based on assuming that this is important.

• The parameter y_{MGLY} is the yield of products which are highly photoreactive and tend to initiate radical formation. It is necessary to assume significant formation of such species in aromatic ring fragmentation processes in order to account for the relatively high reactivities of aromatic hydrocarbons such as toluene or the xylenes (Carter, 1990). Although the model species "AFG2" is the most reactive of the several model species used to represent photoreactive aromatic products, for this study we used the slightly less reactive methyl glyoxal model species, MGLY, for this purpose. The TDI data are best fit by assuming that no photoreactive products are formed, i.e., $y_{AFG2} \approx y_{MGLY} \approx 0$.

Several alternative mechanisms were employed in this study when determining the best fit parameters and for sensitivity and uncertainty analysis. The specific parameter values used in the various simulations discussed where applicable in the Results sections. The way they were represented in the model is shown in Table A-2 under the reactions of PTI or MDI. The rate constants used were those measured or estimated in this program, as discussed below.

Models for MDI Reactions

The MDI molecule can be thought of as two PTI molecules which are joined by sharing a methylene group. MDI is therefore represented by using the mechanism (or mechanisms) derived to fit the PTI chamber data, except that the initial OH radical rate constant is assumed to be twice that of PTI, to account for the fact that there are two rings which could be attacked. This is based on assuming that most of the reaction of OH radicals with PTI or MDI involves addition to the aromatic ring, that the subsequent reactions are independent of any substituents on the methyl (or methylene) group on that ring, and the reactivities of the products formed would be similar in both cases. Since MDI has two aromatic rings where the OH can react, the reaction is assumed to be twice as fast. However, if the other aromatic ring does not affect the reactions of the subsequently formed radicals, and the major reactivity characteristics of the most reactive products are assumed to be the same, then the overall product yield parameters should be the same. Note that the two aromatic rings in MDI are separated by the methylene group, so direct interaction of resonance structures involving the other aromatic ring is not expected. Although some of the products formed may be different, it is assumed that subsequent reactions of these products do not significantly affect the overall reactivity of the PTI or MDI.

These assumptions involved with deriving estimated MDI mechanisms from those derived for PTI are obviously not without uncertainty. The implication of these uncertainties with regard to the predictions of MDI reactivity will depend on the parameters of the PTI mechanisms which are derived, and how aromatic substitution on the alkyl group might affect these parameters. This will be discussed where appropriate in the Results and Conclusions sections of this report.

Environmental Chamber Modeling Methods

The ability of the chemical mechanisms to appropriately simulate the atmospheric impacts of PTI was evaluated by conducting model simulations of the environmental chamber experiments from this study. This requires including in the model appropriate representations of chamber-dependent effects such as wall reactions and characteristics of the light source. The methods used are based on those discussed in detail by Carter and Lurmann (1990, 1991), updated as discussed by Carter et al. (1995c,d 1997b). Tables A-1 in Appendix A show the reactions used to represent the chamber effects in the simulations of the experiments for this program, and Table A-4 show the values of the chamber-dependent parameters which were used, and indicate how they were derived.

Results of the characterization experiments carried out prior to this program indicated that Side A had a slightly higher chamber radical source, due to increased exposure to vehicle exhaust. This slight inequivalency, which had only minor effects on results of surrogate runs (see results) was taken into account when modeling these runs (see Table A-4). As was the case with TDI (Carter et al, 1997a), characterization runs indicated that PTI exposure increased the radical source in the chamber. This affected Side A experiments on and after DTC600, and Side B experiments on and after DTC604. This

was also taken into account when modeling the runs, as indicated on Table A-4. Side equivalency tests, were carried out to determine how these differences affected the results of the experiments, and to evaluate the ability of the model to take these effects into account. These are discussed in the Results section.

The photolysis rates were derived from results of NO_2 actinometry experiments and measurements of the relative spectra of the light source. In the case of the blacklight light source used in these experiments, where the spectrum of the light source appears to be relatively constant, the general blacklight spectrum derived by Carter et al (1995c,d) was used. During the period of these experiments the light intensity was found to decrease approximately linearly with time, and the NO_2 photolysis rates for modeling purposes were derived by fitting the results of the actinometry experiments to a straight line as a function of the DTC run number. For example, based on these data the first added PTI run, DTC600, was assigned an NO_2 photolysis rate of 0.166 min^{-1}, while the last run, DTC616, was modeled using an NO_2 photolysis rate of 0.156 min^{-1}.

The thermal rate constants were calculated using the temperatures measured during the experiments, with the small variations in temperature with time during the experiment being taken into account. The computer programs and modeling methods employed are discussed in more detail elsewhere (Carter et al, 1995c).

Atmospheric Reactivity Modeling Methods

To estimate the effects of MDI emissions on ozone formation under conditions more representative of polluted urban atmospheres, incremental reactivities, defined as the change in O_3 caused by adding small amounts of test compounds the emissions, were calculated for ethane, MDI and the mixture representing the VOCs emitted from all sources (the base ROG). The modeling approach and scenarios is the same as used in our previous study of TDI reactivity (Carter et al, 1997a) and is described in detail elsewhere (Carter, 1994a,b, Carter et al, 1993b). Therefore, it is only briefly summarized here.

Scenarios Used for Reactivity Assessment

The scenarios employed were those used by Carter (1994a,b) to develop various reactivity scales to quantify impacts of VOCs on ozone formation in various environments. These were based on a series of single-day EKMA box model scenarios (EPA, 1984) derived by the EPA for assessing how various ROG and NO_x control strategies would affect ozone nonattainment in various areas of the country (Baugues, 1990). The characteristics of these scenarios and the methods used to derive their input data are described in more detail elsewhere (Baugues, 1990; Carter, 1994b). Briefly, 39 urban areas in the United States were selected based on geographical representativeness of ozone nonattainment areas and data availability, and a representative high ozone episode was selected for each. The initial non-methane organic carbon (NMOC) and NO_x concentrations, the aloft O_3 concentrations, and the mixing height inputs were based on measurement data for the various areas, the hourly emissions in the scenarios were obtained

16

from the National Acid Precipitation Assessment Program emissions inventory (Baugues, 1990), and biogenic emissions were also included. Table 1 gives a summary of the urban areas represented and other selected characteristics of the scenarios.

Several changes to the scenario inputs were made based on discussions with the California ARB staff and others (Carter, 1994b). Two percent of the initial NO_x and 0.1% of the emitted NO_x in all the scenarios was assumed to be in the form of HONO. The photolysis rates were calculated using solar light intensities and spectra calculated by Jeffries (1991) for 640 meters, the approximate mid-point of the mixed layer during daylight hours. The composition of the VOCs entrained from aloft was based on the analysis of Jeffries et al. (1989). The composition of the initial and emitted reactive organics (referred to as the "base ROG" mixture) was derived based on analyses of air quality data (Carter, 1994a, Jeffries et al, 1989). Complete listings of the input data for the scenarios are given elsewhere (Carter, 1994b). These are referred to as "base case" scenarios, to distinguish them from those where NO_x inputs are adjusted as discussed below.

In addition to these 39 base case scenarios, three adjusted NO_x scenarios were developed to represent different conditions of NO_x availability. NO_x levels were found to be the most important factor affecting differences in relative ozone impacts among most VOCs (Carter and Atkinson, 1989a; Carter, 1994a), and for such compounds the ranges of relative reactivities under various conditions can be reasonably well represented by ranges in relative reactivities in three "averaged conditions" scenarios representing three different NO_x conditions. These scenarios were derived by averaging the inputs to the 39 EPA scenarios, except for the NO_x emissions. In the "Maximum Incremental Reactivity" (MIR) scenario, the NO_x inputs were adjusted such that the final O_3 level is most sensitive to changes in VOC emissions; in the "Maximum Ozone Incremental Reactivity" (MOIR) scenario the NO_x inputs were adjusted to yield the highest maximum O_3 concentration; and in the "Equal Benefit Incremental Reactivity" (EBIR) scenario the NO_x inputs were adjusted such that relative changes in VOC and NO_x emissions had equal effect on ozone formation. As discussed by Carter (1994a), there represent respectively the high, medium and low ranges of NO_x conditions which are of relevance when assessing VOC control strategies for reducing ozone.

Table 1. Summary of conditions of base case scenarios used for atmospheric reactivity assessment.

City, State	Calc. Max O_3 (ppb)	ROG /NO_x	NO_x /NO_x MOR	Final Height (km)	Init.+Emit Base ROG (mmol m^{-2})	Aloft O_3 (ppb)
Atlanta, GA	179	7.3	0.7	2.1	12	63
Austin, TX	175	9.3	0.5	2.1	11	85
Baltimore, MD	326	5.2	1.0	1.2	17	84
Baton Rouge, LA	247	6.8	0.8	1.0	11	62
Birmingham, AL	238	6.9	0.5	1.8	13	81
Boston, MA	195	6.5	0.6	2.6	14	105
Charlotte, NC	143	7.8	0.3	3.0	7	92
Chicago, IL	281	11.6	0.5	1.4	25	40
Cincinnati, OH	198	6.4	0.7	2.8	17	70
Cleveland, OH	251	6.6	0.9	1.7	16	89
Dallas, TX	213	4.7	1.2	2.3	18	75
Denver, CO	211	6.3	1.0	3.4	29	57
Detroit, MI	238	6.8	0.7	1.8	17	68
El Paso, TX	188	6.6	0.9	2.0	12	65
Hartford, CT	169	8.4	0.5	2.3	11	78
Houston, TX	307	6.1	0.9	1.7	25	65
Indianapolis, IN	211	6.6	0.8	1.7	12	52
Jacksonville, FL	156	7.6	0.6	1.5	8	40
Kansas City, MO	154	7.1	0.6	2.2	9	65
Lake Charles, LA	291	7.4	0.6	0.5	7	40
Los Angeles, CA	580	7.6	0.8	0.5	23	100
Louisville, KY	210	5.5	0.8	2.5	14	75
Memphis, TN	225	6.8	0.6	1.8	15	58
Miami, FL	133	9.6	0.4	2.7	9	57
Nashville, TN	166	8.1	0.4	1.6	7	50
New York, NY	363	8.1	0.7	1.5	39	103
Philadelphia, PA	242	6.2	0.9	1.8	19	53
Phoenix, AZ	275	7.6	0.8	3.3	40	60
Portland, OR	165	6.5	0.7	1.6	6	66
Richmond, VA	233	6.2	0.7	1.9	16	64
Sacramento, CA	202	6.6	0.8	1.1	7	60
St Louis, MO	322	6.1	1.0	1.6	26	82
Salt Lake City, UT	184	8.5	0.6	2.2	11	85
San Antonio, TX	132	3.9	1.0	2.3	6	60
San Diego, CA	196	7.1	0.9	0.9	8	90
San Francisco, CA	325	4.8	1.5	0.7	25	70
Tampa, FL	232	4.4	1.0	1.0	8	68
Tulsa, OK	225	5.3	0.9	1.8	15	70
Washington, DC	276	5.3	0.8	1.4	13	99

[a] Ratio of NO_x inputs to NO_x inputs which yield the highest ozone concentrations for the conditions of the scenario This provides a useful measure of NO_x availability (Carter, 1994a).

The use of averaged conditions, adjusted NO$_x$ scenarios in this work is slightly different than the approach used by Carter (1994a), where the MIR, MOIR, and EBIR scales were derived by adjusting NO$_x$ conditions separately for each of the 39 base case scenarios, and then averaging the reactivities derived from them. However, Carter (1994a) showed that both approaches yield essentially the same results.

Quantification of Atmospheric Reactivity

The reactivity of a VOC in an airshed scenario is measured by the change in ozone caused by adding the VOC to the emissions, divided by the amount of VOC added, calculated for sufficiently small amounts of added VOC that the incremental reactivity is independent of the amount added. The specific calculation procedure is discussed in detail elsewhere (Carter, 1994a,b). The incremental reactivities depend on how the amounts of VOC added and amounts of ozone formed are quantified. In this work, the amount of added VOC is quantified on a mass basis, since this is how VOCs are regulated. Two different ozone quantification methods were used, as follows:

- "Ozone Yield" incremental reactivities measure the effect of the VOC on the total amount of ozone formed in the scenario at the time of its maximum concentration. This is quantified as grams O$_3$ formed per gram VOC added. Most previous recent studies of incremental reactivity (Dodge, 1984; Carter and Atkinson, 1987, 1989a, Chang and Rudy, 1990; Jeffries and Crouse, 1991) have been based on this quantification method.

- "Max 8 Hour Average" incremental measure the effect of the VOC on the average ozone concentration during the 8-hour period when the average ozone concentration was the greatest. This provides a measure of ozone impact which is more closely related to the new Federal ozone standard, which is given in terms of an 8 hour average.

Since ratios of reactivities are generally more relevant to control strategy applications and are usually less sensitive to scenario conditions, the calculated atmospheric reactivity results in this work are given in terms of <u>relative reactivities</u>. This is defined as the incremental reactivity of the VOC divided by the incremental reactivity of the base ROG mixture, i.e., the mixture used to represent VOC emissions from all sources in the scenarios. These relative reactivities can also be thought of as the relative effect on O$_3$ of controlling emissions of the particular VOC by itself, compared to controlling emissions from all VOC sources equally.

In previous reports (e.g., see Carter et al, 1997a), we have reported reactivities in terms of integrated O$_3$ over the previous Federal standard of 0.12 ppm, referred to as "IntO$_3$>0.12". This is the sum of the hourly ozone concentrations for the hours when ozone 0.12 ppm in the base case scenarios (Carter 1994a), and provides a measure of the effect of the VOC on exposure to unacceptable levels of ozone. This is replaced by the Max 8 Hour Average reactivities because (1) it is more representative of the new ozone standard and (2) the IntO$_3$>0.12 relative reactivities were found to be between the Ozone Yield and the Max 8 Hour Average relative for those VOCs where they were different. Therefore, presenting both

ozone yield and maximum 8-hour average relative reactivities should be sufficient to provide information on how relative reactivities vary with quantification method.

Chemical Models and Mechanisms Used

The models used to represent the reactions of PTI and MDI in the atmospheric reactivity simulations were the same as used in modeling the chamber data, except that the unimolecular wall loss process was assumed to be negligible. All emitted MDI was assumed to be available for gas-phase reaction, and possible dry deposition processes, which may be non-negligible, were ignored. (It is likely that this approach will result in an overestimation of the MDI's actual ozone impact, since deposition may be significant for such a low volatility compound.) The mechanisms for the other species were also the same as employed in the chamber simulations, except that the reactions representing chamber effects were removed, and the reactions for the full variety of VOCs emitted into the scenarios (Carter, 1994a) were included. Most of the emitted VOCs are not represented in the model explicitly, but are represented using lumped model species whose rate constants and product yield parameters are derived based on the mixture of compounds they represent. The rate constants and mechanistic parameters for the emitted species in the scenarios were the same as those used previously (Carter et al, 1993b), except for the aromatics, whose unknown photoreactive product yields were reoptimized in a manner analogous to that discussed above for toluene and m-xylene (Carter et al. 1997b). The mechanism listing in Appendix A gives the reactions of the model species used in the atmospheric simulations to represent various types of anthropogenic and biogenic emissions, indicating the types of compounds each is used to represent, and giving their rate constants and product yield parameters.

RESULTS AND DISCUSSION

OH Radical Rate Constant Measurements

As discussed above, the kinetic experiments consisted of irradiating PTI - toluene - methyl nitrite - NO - air mixtures in the environmental chamber, and determining the ratio of OH radical rate constants for PTI and toluene from

$$\ln([\text{PTI}]_0/[\text{PTI}]_t) = (k\text{OH}^{\text{PTI}}/k\text{OH}^{\text{toluene}}) \ln([\text{toluene}]_0/[\text{toluene}]_t) \tag{IV}$$

if reaction with OH radicals is assumed to be the only loss process for both PTI and toluene, or by

$$\ln([\text{PTI}]_0/[\text{PTI}]_t)\text{-}D^{\text{PTI}} t = (k\text{OH}^{\text{PTI}}/k\text{OH}^{\text{toluene}}) \{\ln([\text{toluene}]_0/[\text{toluene}]_t)\text{-}D^{\text{toluene}} t\} \tag{V}$$

if unimolecular loss processes such as wall decay are non-negligible. Here, $[\text{PTI}]_0$, $[\text{PTI}]_t$, $[\text{toluene}]_0$, and $[\text{toluene}]_t$ are the initial and t=0 concentrations of PTI and toluene, respectively, $k\text{OH}^{\text{PTI}}$ and $k\text{OH}^{\text{tol}}$ are their respective OH radical rate constants, and D^{PTI} and D^{tol} are their respective unimolecular loss rates by other processes, which for these experiments should be primarily wall losses since dilution should be negligible.

Three kinetic experiments were carried out, designated runs DTC605, DTC609 and DTC611. Plots of Equation (IV) for these experiments are shown on Figure 1. Run DTC605 also contained non-negligible amounts of m-xylene, whose presence resulted on only small amounts of consumption of PTI and toluene. However, the data from all three experiments are reasonably consistent with each other, though some curvature can be seen in the plots of Equation (IV) on the figure. In particular, the amount of PTI consumption relative to toluene consumption was somewhat less during the initial periods of the experiments than was the case subsequently, though this may be due to scatter in the analytical data. However, within the likely uncertainty of the experimental measurements, the data from the three experiments are fit by Equation (IV) sufficiently well to obtain at least an approximate OH radical rate constant ratio of 1.0±0.08.

The curvature in Figure 1 cannot be due to wall losses for PTI, since in that case one would expect a positive rather than a slightly negative intercept. (The intercept for the least-squares fit using Equation (IV) is -0.08± 0.03.) On the other hand, the data are better fit using Equation (V) if a non-negligible unimolecular loss process for toluene, rather than PTI, is assumed. Least squares optimizations using Equation (V) yield D^{toluene} = 4.5 %/hour, $D^{\text{PTI}} \approx 0$, and a rate constant ratio of 1.08. This is shown on Figure 2, which gives a plot of the kinetic data using the optimized D^{tol} and D^{PTI} values and
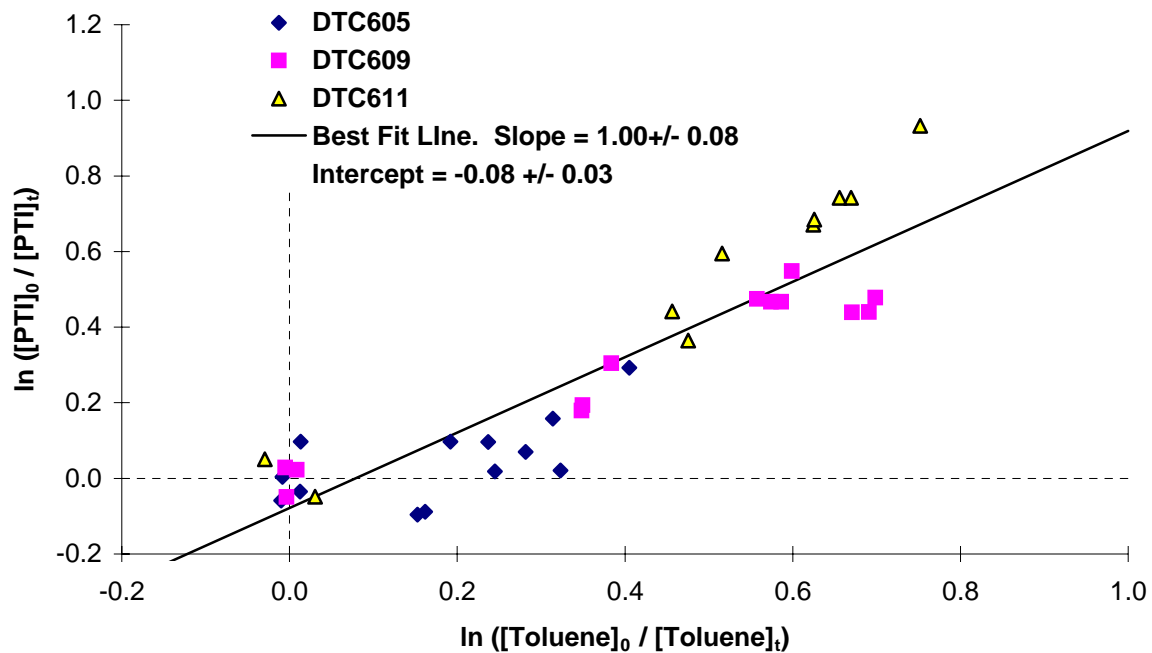
Figure 1.   Plot of Equation (IV) for the PTI vs toluene relative rate constant determination experiments.
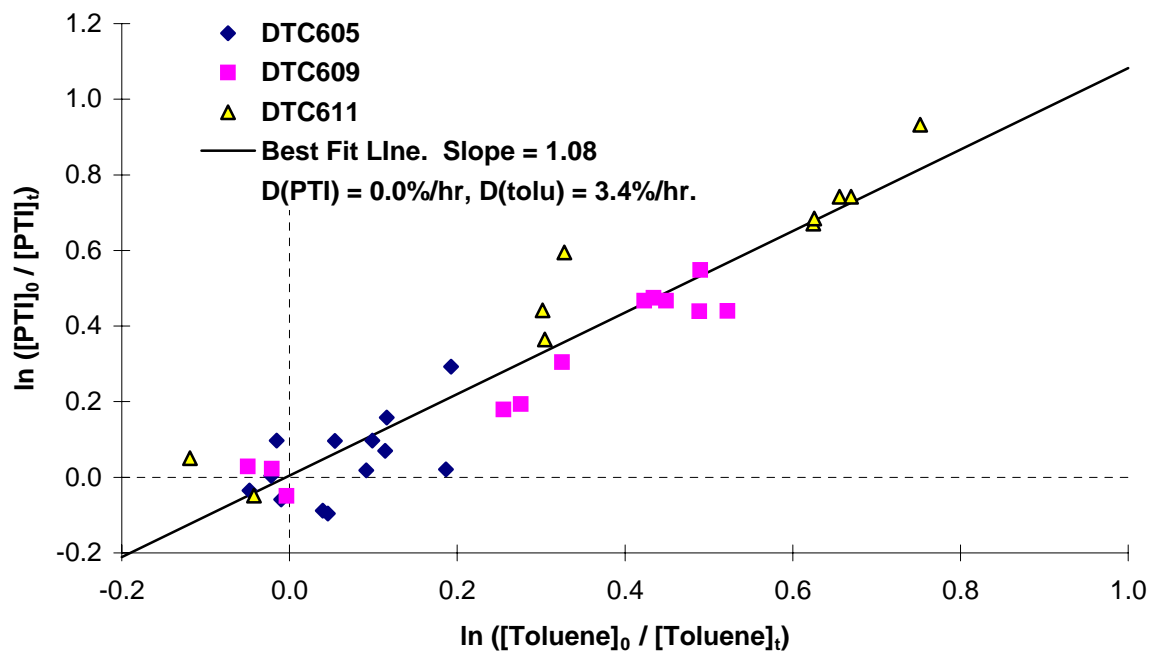
Figure 2.   Plot of Equation (V) for the PTI vs toluene relative rate constant determination experiments.

the best fit line for Equation (V) using the optimized rate constant ratio. Note that assuming the slightly nonzero $D^{toluene}$ completely removes the curvature in the plots. However, it is difficult to rationalize why there would be an apparent non-negligible loss rate for toluene but not for PTI. Toluene is used frequently in our chamber experiments, and there is no evidence for significant wall losses for this compound in our chamber.

In any case, the rate constant ratios derived using Equation (IV) and (V) give essentially the same rate constant ratio within experimental error, both indicating that PTI reacts with OH radicals with a rate constant which is nearly the same as that for toluene. Based on an extensive review of the literature, Atkinson (1989) recommended $kOH_{tol} = 5.95$ x 10^{-12} cm^3 $molec^{-1}$ s^{-1} at 298K, and this recommendation was not revised in subsequent reviews (Atkinson, 1994). Therefore, based on the results of these experiments, we conclude that

$$k (OH + PTI) = 5.9 \text{ x } 10^{-12} \text{ } cm^3 \text{ } molec^{-1} \text{ } s^{-1} \text{ at 298K,}$$

This was used when modeling the PTI experiments discussed in this report.

As discussed above, we assume that most of the reaction of OH with PTI and MDI are at the aromatic ring, and therefore kOH^{MDI} should approximately two times kOHPTI. Therefore, when estimating MDI's atmospheric reactivity, we assume that

$$k (OH + MDI) \approx 1.18 \text{ x } 10^{-11} \text{ } cm^3 \text{ } molec^{-1} \text{ } s^{-1}.$$

Any temperature dependence in this rate constant is likely to be small, so this rate constant was used for all scenarios.

Summary of Chamber Experiments and Characterization Results

Table 2 gives a chronological listing of all the experiments carried out for this program. In addition to the reactivity and kinetic experiments, characterization experiments were conducted to measure chamber wall effects, and side equivalency tests were conducted to determine differences between results of experiments in different chamber sides caused by PTI exposure. Table 2 includes characterization and control experiments carried out previously for other programs which are relevant to characterizing conditions of runs for this program. Relevant results of the control and characterization runs are summarized on the table, and are briefly discussed below.

The characterization and control runs consisted of NO_2 actinometry experiments to monitor light intensity, n-butane - NO_x experiments to measure the chamber radical source (see Carter et al, 1982, 1995c,d), a pure air irradiation to measure background effects, an ozone and CO dark decay experiment

Table 2.   Chronolological listing of the environmental chamber experiments carried out for this program during this reporting period.

RunID	Date	Title	Comments
DTC580	11/11/97	NO2 Actinometry	NO2 photolysis rate was 0.204 min^{-1}, suggesting a slight downward trend in light intensity due to ageing of the lights.
DTC587	11/21/97	n-Butane + NOx	Characterization run to measure the chamber radical source. NO oxidation rate was somewhat greater on Side A than Side B. Side A results in good agreement with predictions of standard chamber model. Side B results lower than normal range
DTC597	12/11/97	Propene - NOx	Standard control run for comparison with previous propene - NOx runs and side equivalency test run. Results comparable with other propene runs. Model gives good simulation of data. Slightly faster O3 formation rate on Side A.
DTC599	1/13/98	Pure Air Irradiation	Control run to test for background effects. O3 after 6 hours was 30 ppb on Side A and 23 ppb on Side B. These are within the range of the predictions of the standard chamber model.
DTC600	1/14/98	Mini Surrogate Side Equivalency Test	Control run to test side equivalency. Slightly more ozone formed on Side A, but results in normal range. See Figure 2 and Table 2.
DTC601	1/15/98	Mini Surrogate + PTI (A)	Mini-Surrogate - NOx mixture added to both sides of chamber and 0.4 ppm PTI added to Side A. Very little difference in ozone formation or IntOH. See Figure 3 and Table 2.
DTC602	1/22/98	Mini Surrogate + PTI (A)	Mini-surrogate - NOx mixture added to both sides and 3.8 PTI added to Side A. Very little difference in ozone formation and only a slight reduction in IntOH caused by added PTI. See Figure 4 and Table 2.

Table 2 (continued)

RunID	Date	Title	Comments
DTC603	1/23/98	Mini Surrogate Side Equivalency Test	Control run to measure side differences caused by PTI exposure. Equal mini-surrogate - NOx mixture added to both sides. Side differences somewhat greater than observed in Run DTC600. See Figure 2 and Table 2.
DTC604	1/27/98	Low NOx Full Surrogate + PTI (B)	Low NOx full surrogate mixture added to both sides of chamber and 3.8 ppm PTI added to Side B. Added PTI caused reduction in both O3 yield and IntOH. See Figure 7 and Table 2.
DTC605	1/29/98	Kinetic study of PTI	One of three experiments carried out to measure the OH radical rate constant of PTI relative to toluene. Experiments involved irriadiating PTI and toluene in the presence of methyl nitrite. Side A used. See text and Figure 1.
DTC606	1/30/98	Kinetic study of PTI	Second of three experiments to measure the OH radical rate constant of PTI relative to toluene. Procedure same as DTC605 except more methyl nitrate added to achieve greater conversions. See text and Figure 1.
DTC607	2/3/98	n-Butane + NOx	Characterization run to measure chamber radical source. Radical source in Side B was in normal range but radical source in Side A was about two times higher. Chamber characterization model modified to account for these differences.
DTC608	2/4/98	Low NOx Full Surrogate + PTI (A)	Low NOx full surrogate mixture added to both sides of chamber and 7.2 ppm PTI added to Side A. Added PTI caused reduction in both O3 yield and IntOH. See Figure 8 and Table 2.
DTC609	2/5/98	Low NOx Full Surrogate Side Equivalency Test	Low NOx full surrogate mixture added to both sides to determine side differences for this mixture. Very little difference in ozone formation and IntOH. See Table 2 and Figure 2.

Table 2 (continued)

RunID	Date	Title	Comments
DTC610	2/6/98	Full Surrogate + PTI (A)	Full surrogate - NOx mixture added to both sides of chamber and 10 ppm PTI added to Side A. Added PTI caused a slight increase in NO oxidation and ozone formation during the middle period of the run. See Figure 6 and Table 2.
DTC611	2/10/98	Kinetic study of PTI	Third of three experiments to measure the OH radical rate constant of PTI relative to toluene. Same procedure employed as previous kinetic run. See text and Figure 1.
DTC613	2/12/98	NO2 Actinometry	NO2 photolysis rate was approximately 0.15 min^{-1}, significantly lower than observed previously, and indicating a downward trend in light intensity.
DTC614	2/13/98	O3 and CO dark decay	Ozone and CO were monitored in the dark to measure both dilution and O3 dark decay. The CO data indicated no significant dilution. The O3 decay rates were 1.1 and 0.8%/hour on Sides A and B, respectively, somewhat higher than average for this chamber.
DTC616	2/19/98	Full Surrogate Side Equivalency Test	Same full surrogate - NOx mixture added to both sides. The amount of NOx added being higher than in usual full surrogate runs, and because of this no ozone was formed. NO oxidation was slightly faster on Side A. See Table 2 and Figure 2.
DTC617	2/20/98	NO2 actinometry	The measured NO2 photolysis rate was consistent with DTC613 and confirmed a decrease in the light intensity in the chamber. The chamber effects model was updated to take this into account.
DTC618	2/25/98	Mini-Surrogate + PTI (A)	Mini-surrogate - NOx mixture added to both sides and 10 ppm PTI added to Side A. Added PTI caused reduction in ozone formation rate and IntOH. See Figure 5 and Table 2.
DTC619	2/26/98 - 3/2/98	NO2 actinometry	The measured NO2 photolysis rate was consistent with previous actinometry results and indicated a decrease in total light intensity in the chamber.

to measure O_3 wall losses and dilution, a propene - NO_x control run and various side equivalency tests where the same surrogate - NO_x mixture is irradiated on both sides of the chamber. As indicated on Table 2, the results of the actinometry experiments indicated a gradual decline in overall light intensity in the chamber but are consistent with trends observed in previous runs (see also the modeling methods discussion, above), and the propene - NO_x and pure air irradiation were also within the normal range for this chamber, and consistent with standard model predictions. The other experiments indicated some side inequavalencies, as discussed below.

The experiments for this program followed a series of experiments where dilute auto exhaust was injected and irradiated in Side A and various control or synthetic surrogate mixtures were irradiated in Side B. Apparently because of this unequal treatment, the n-butane - NO_x characterization runs indicated that the chamber radical source (which is a parameter which needs to be specified when modeling chamber experiments for mechanism evaluation) was about 35% higher in Side A than Side B (e.g., see comments for DTC587 on Table 2). The radical source for both these sides are within the normal variability observed for this chamber, though the side-to-side difference is greater than normal. Following the experiments where both sides were exposed to PTI (though more with PTI in Side A than Side B), the apparent radical source increased in both sides, but with the radical source still being higher in Side A than Side B. The ozone decay experiment carried out around the end of this program indicated a slight increase in the ozone decay rate as well, though in this case the difference may not be outside of the normal variability observed in this type of chamber. As indicated on Table A-4, the side differences in the radical source was taken into account when modeling these experiments, but the standard model for the ozone dark decay was not modified. The ozone decay in these chambers is relatively small and this degree of variability will not significantly affect results of modeling the reactivity experiments.

To evaluate the effect of this apparent side inequivalency on the reactivity experiments, and the ability of the model to take this into account when simulating these runs, several side equivalency tests were carried out; two with the mini-surrogate and two with the full surrogate. The experimental and calculated concentration-time profiles for $d(O_3$-NO) and m-xylene, and the side-by-side differences between them, are shown on Figure 3. Note that in all cases the differences plotted are values for Side B - values for Side A.

The mini-surrogate runs are expected to be the most sensitive to the chamber radical source, so some side inequivalency is expected based on the results of the n-butane runs. Only small side differences are seen in run DTC600 which was carried out prior to PTI exposure, but a larger difference is seen in run DTC603, which was carried out after Side A (but not Side B) was exposed to PTI. A smaller but still non-negligible side difference was observed in the full surrogate run DTC616 which was carried out after both sides were exposed to PTI. The figure shows that the model, using radical source
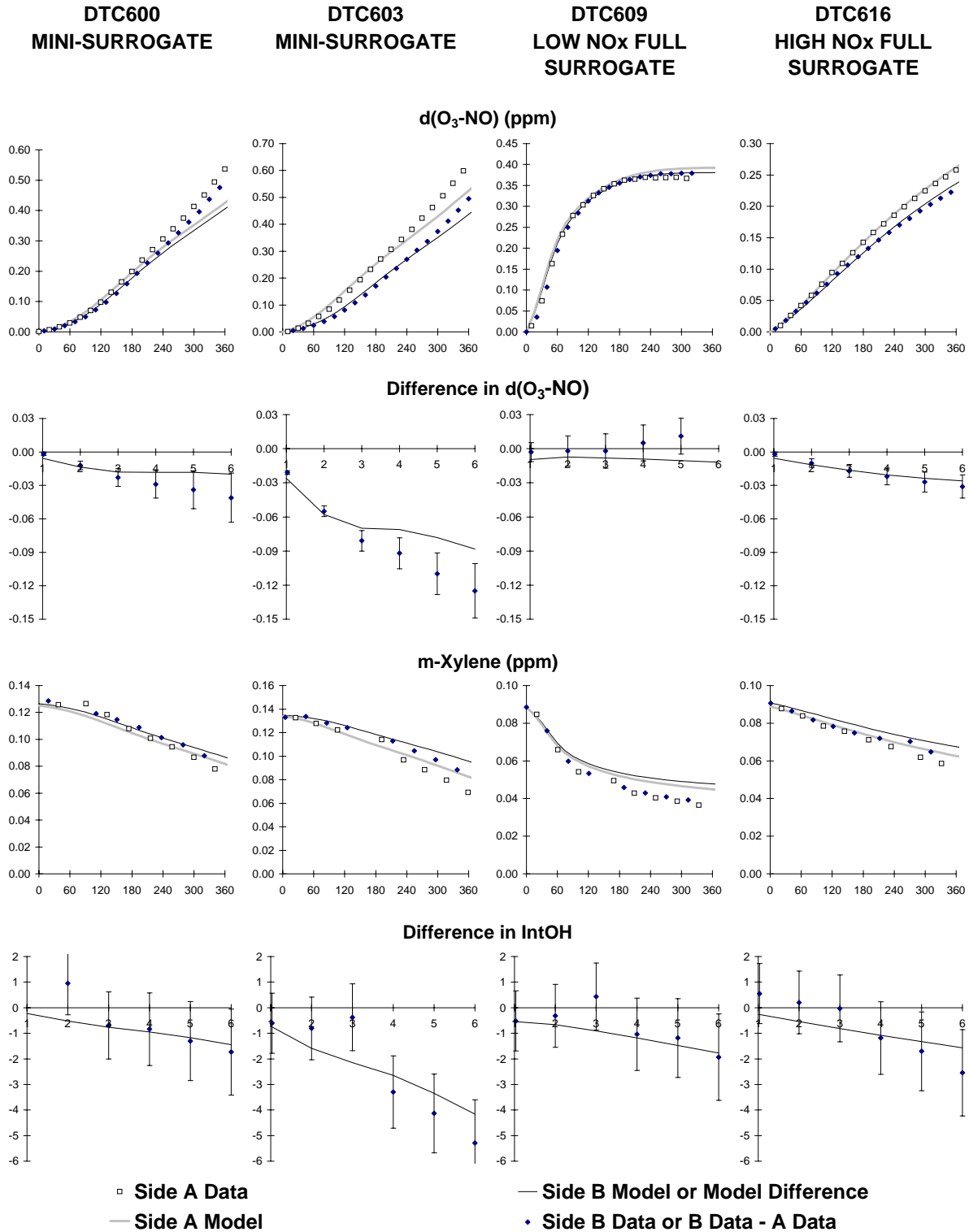
Figure 3.   Plots of selected results of the side comparison test experiments.

28

differences derived from the results of the n-butane runs (see Table A-4), gives reasonably good predictions of these side differences. Low NO_x full surrogate experiments are expected to be much less sensitive to the chamber radical source, and consistent with this the low NO_x full surrogate side equivalency test (DTC609) had only small differences between the sides. This also was consistent with model prediction.

The side differences would be expected to affect the results of the incremental reactivity experiments, tending to increase the apparent incremental reactivity when the test compound is in Side A and reduce it when it is in Side B. However, if the model can account for these differences as caused by chamber effects, the results of model evaluation of these experiments, i.e., determination whether there are consistent biases caused by errors in the mechanism's ability to simulate the effects of the added PTI, should not be affected. The results of the simulations of the side equivalency tests, which are also shown on Figure 3, indicate that the model is reasonably successful in accounting for these differences.

Results of The Reactivity Experiments

A total of six reactivity experiments, three with the mini-surrogate, one with the high NO_x full surrogate, and two with the low NO_x full surrogate, were carried out for this program. Table 3 summarizes the conditions and selected results of these experiments, and also shows the results of the side equivalency tests for comparison purposes. Figures 4-9 show concentration-time plots of their major experimental and calculated results.

The addition of the 0.4 and ~4 ppm PTI to the mini-surrogate mixture had almost no effect on the results (see Figures 4 and 5), though addition of ~10 ppm caused a slight inhibition in O_3 and IntOH (see Figure 6). The addition of ~10 ppm PTI in the high NO_x full surrogate run had relatively little effect on $d(O_3\text{-}NO)$, with the slightly higher $d(O_3\text{-}NO)$ on the added PTI side (A) during the first half of the experiment being of comparable magnitude to that observed in the side equivalency tests (Figure 7). However, there was indications that the PTI was beginning to slightly inhibit the peak ozone around the end of the experiment, and it was clearly suppressing the IntOH levels. The largest effect of PTI was observed in the low NO_x full surrogate experiments (Figures 8 and 9), where significant inhibition in the peak $d(O_3\text{-}NO)$ (i.e, peak O_3) was observed even in the run with less than 4 ppm added PTI. The IntOH inhibition also appeared to be somewhat greater in the low NO_x full surrogate runs than observed in the higher NO_x experiments.

Results of model simulations of these experiments are also shown on Figures 4-9. The model for the base case experiments tended to underpredict somewhat the $d(O_3\text{-}NO)$ formation rate in the mini-surrogate runs, though the full surrogate base case experiments were reasonably well simulated. (Similar model performance is seen in the simulations of the side equivalency tests in Figure 2). These results are within the variability observed in the base case simulations using this mechanism. The discrepancy

Table 3. Summary of conditions and results of the incremental reactivity and side equivalency test experiments.

Run	Initial Reactants (ppm)			t=3 d(O_3-NO) (ppm)			t=6 d(O_3-NO) (ppm)			t=5 IntOH (10^{-6} min)		
	NO_x	Surg [a]	PTI	Base	Test	IR [b]	Base	Test	IR [b]	Base	Test	IR [b]
Mini-Surrogate +PTI												
DTC-601 (A)	0.39	3.5	0.42	0.20	0.22	0.05	0.52	0.57	0.11	11	12	2.0
DTC-602 (A)	0.42	3.8	3.79	0.20	0.17	-0.007	0.54	0.50	-0.011	10	7	-0.7
DTC-618 (A)	0.28	2.8	10.18	0.36	0.38	0.002	0.54	0.53	-0.002	21	13	-0.7
Full Surrogate + PTI												
DTC-610 (A)	0.31	2.6	10.47	0.17	0.14	-0.003	0.48	0.41	-0.007	9	4	-0.5
Low NOx Full Surrogate + PTI												
DTC-604 (B)	0.17	2.6	3.83	0.37	0.33	-0.012	0.41	0.32	-0.025	26	11	-3.8
DTC-608 (A)	0.15	2.9	7.17	0.38	0.33	-0.007	0.41	0.30	-0.015	24	11	-1.8
Side Equivalency Tests [c]												
DTC-600 (A)	0.37	3.3		0.20	0.18	-0.004	0.50	0.54	0.007	9	11	0.2
DTC-603 (A)	0.37	3.6		0.25	0.17	-0.014	0.50	0.62	0.021	10	14	0.7
DTC-609 (A) [d]	0.14	2.9		0.36	0.36	0.000	0.38	0.37	-0.002	23	24	0.2
DTC-616 (A)	0.82	2.7		0.14	0.13	-0.003	0.23	0.26	0.005	9	11	0.3

[a] Total base ROG surrogate in ppmC.

[b] Incremental reactivity. For Side Equivalency tests, this is the difference between the sides divided by the average PTI concentration in the added PTI runs, or 5.14 ppm. In other words, the incremental reactivity shown for the side equivalency runs is the incremental reactivity corresponding to the d(O3-NO) or IntOH change if 5.14 ppm of PTI were added to Side A.

[c] Side A data tabulated under "Test" columns, Side B under "Base" columns.

[d] d(O3-NO) data for t=5 hours.

DTC601A: 0.4 ppm PTI
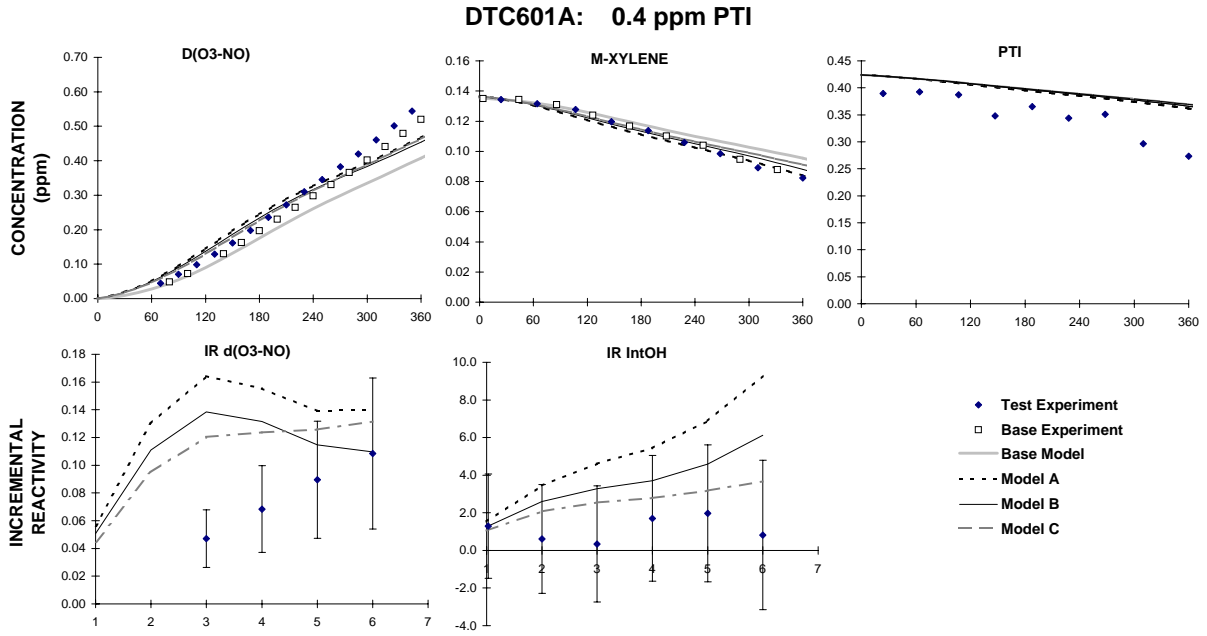
Figure 4.   Plots of selected results of the mini-surrogate + PTI run DTC601..

DTC602A: 3.8 ppm PTI
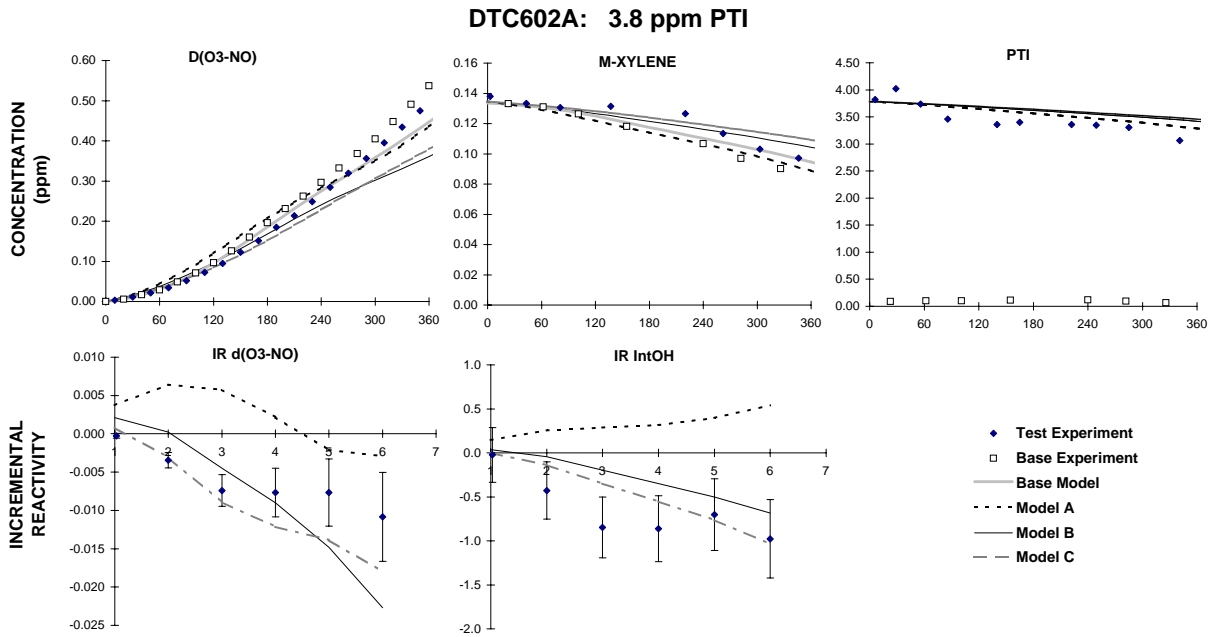
Figure 5.   Plots of selected results of the mini-surrogate + PTI experiment DTC602.
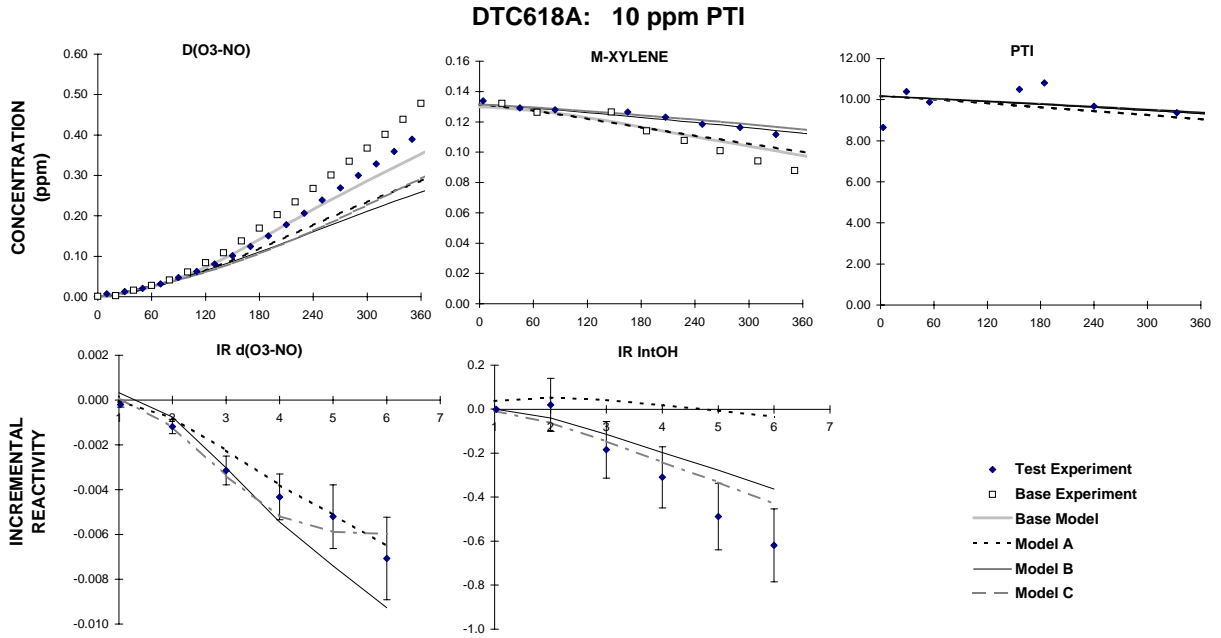
Figure 6.   Plots of selected results of the mini-surrogate + PTI run DTC618..
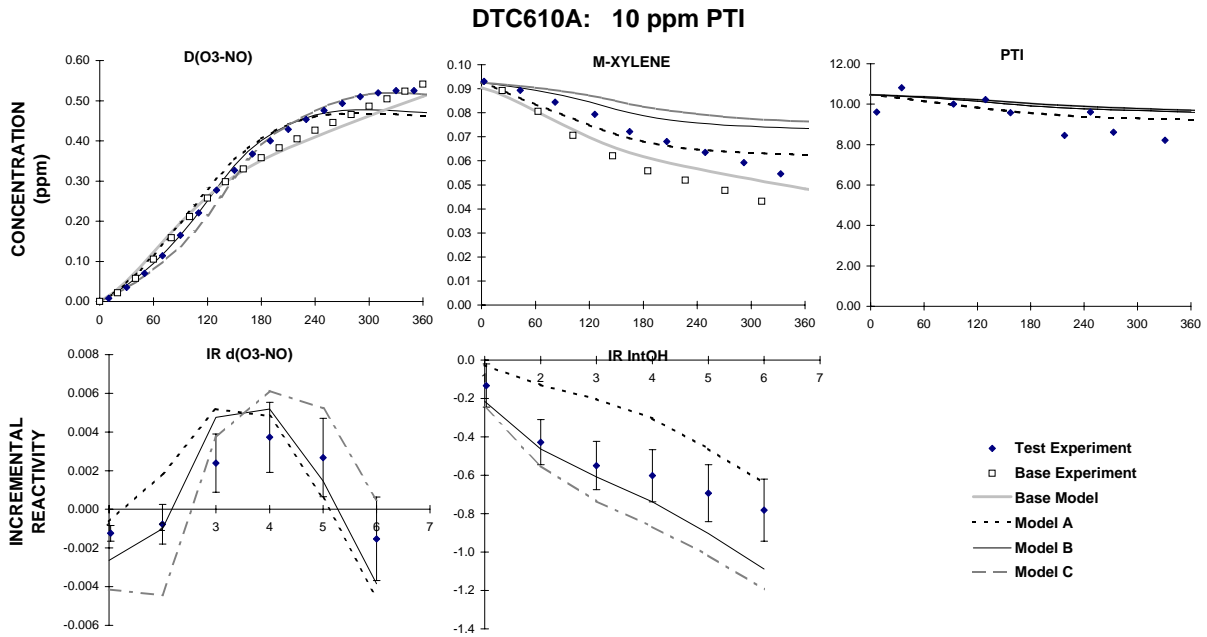
Figure 7.   Plots of selected results of the full surrogate + PTI experiment DTC610.

DTC604B: 3.8 ppm PTI
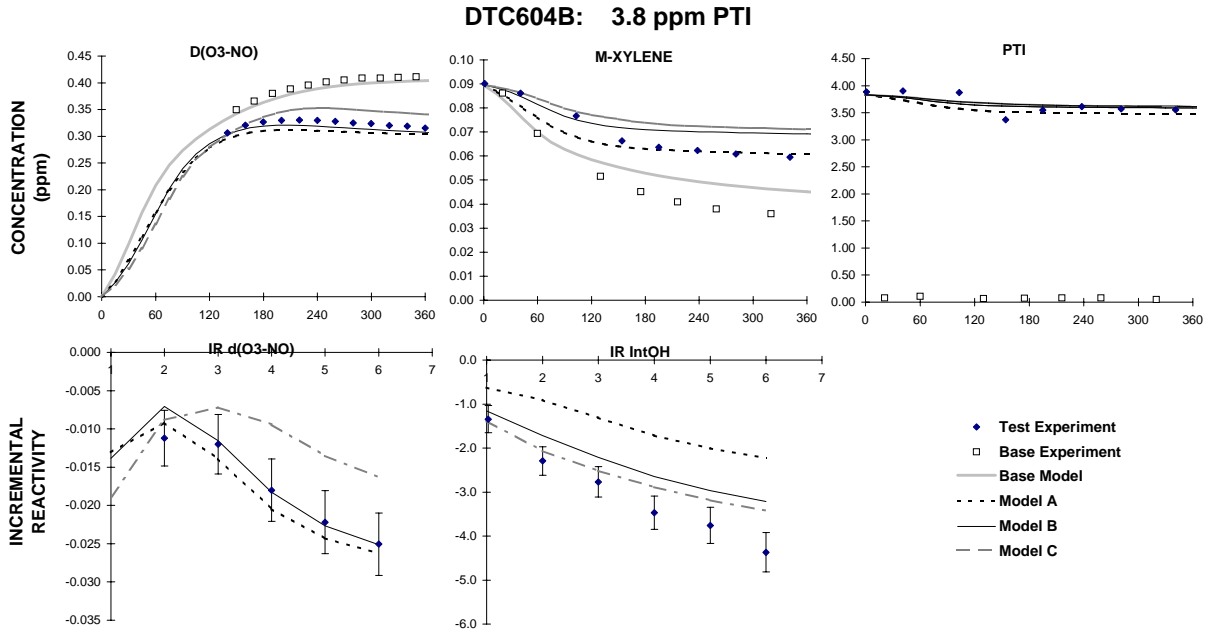
Figure 8.   Plots of selected results of the low NOx full surrogate + PTI run DTC604..

DTC608A: 7 ppm PTI
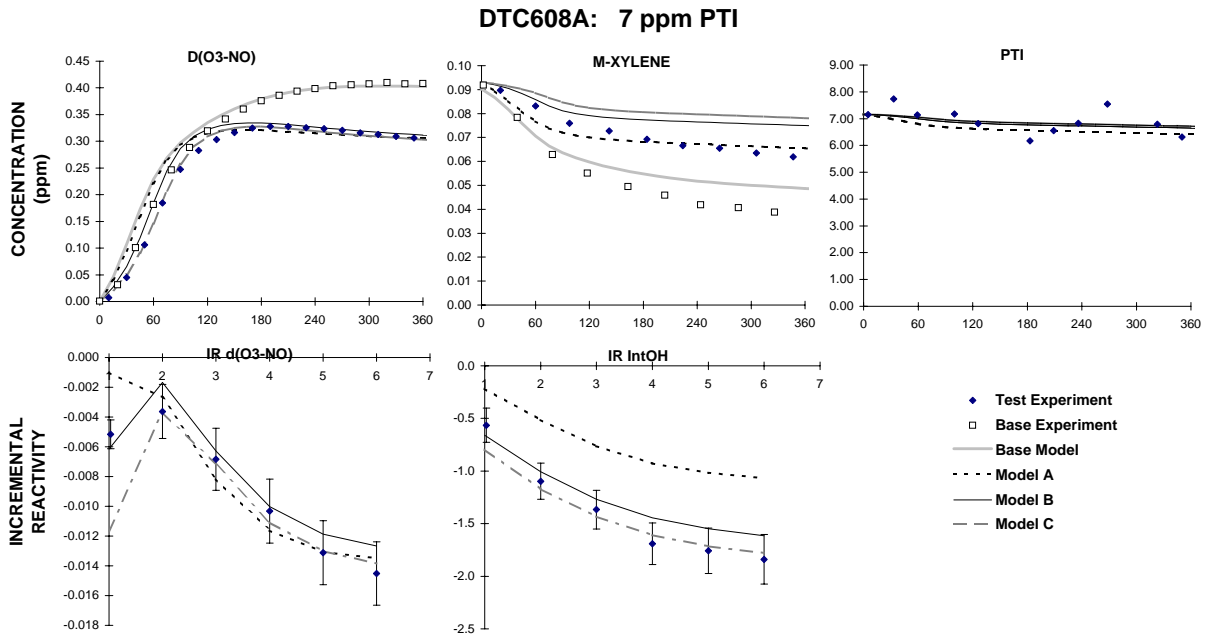
Figure 9.   Plots of selected results of the low NOx full surrogate + PTI experiment DTC608.

33

in the case of the simulations of the base case runs is not considered a significant problem in evaluating reactivity effects, since the quantity of interest is the difference between the simulation of the base case and added test compound experiments. If the model for the test compound is approximately correct, the simulation of the added test compound experiment would have a similar underprediction, so the predicted difference between the base case and added test compound experiments should be about the same.

As discussed above, because the details of the atmospheric chemistry of aromatic isocyanates are unknown, the reactions of PTI were modeled using a highly simplified parameterized mechanism, with the various parameters adjusted to achieve the best fits to the chamber data. Although a number of alternative mechanisms with different sets of parameter values examined, we will present the results for three alternative mechanisms, designated Models A, B, and C, which gave the best fits to most of the data. These are discussed below.

Model "A" is the simplest parameterized mechanism which could fit the $d(O_3$-NO) reactivities in all the types of experiments. It is based on the assumption that the negative $d(O_3$-NO) reactivities in the low NO_x experiments is due to the formation of cresol-like products, whose reaction with NO_3 radicals remove NO_x from the system and thus reduce O_3 yields in systems which are NO_x-limited. If it is assumed that no other reactive products are formed in significant yields, then the $d(O_3$-NO) data in the various types of experiments can be fit if it is assumed that $y_{CRES} \approx 1$, $y_{OH} \approx 1$ and $y_{NO \rightarrow NO2} \approx -0.12$. Note that this model assumes that PTI has no radical inhibition characteristics, but that it involves net NO_2 to NO conversions. This can be compared to TDI Model A, which also assumes that $y_{CRES} \approx 1$, but where $y_{OH} \approx 0.3$ and $y_{NO \rightarrow NO2} \approx 0$ gives best fits to the data.

Figures 4-9 show that Model A gives reasonably good simulations of the $d(O_3$-NO) reactivities in the various types of experiments, agreeing with the data within the experimental variability in most cases. However, this mechanism significantly underpredicts the IntOH reactivities in essentially all experiments. The generally negative IntOH reactivities observed in the PTI experiments indicates that this compound has some radical termination characteristics which are not being represented in this model, which assumes that 100% of the OH radicals reacting with the PTI are regenerated.

The IntOH reactivity data can only be fit if it is assumed that y_{OH} is in the 0.8 to 0.9 range, i.e., that 10-20% radical inhibition is occurring. However, if this is assumed, then it is necessary to assume either significantly positive $y_{NO \rightarrow NO2}$ values, or to assume significant yields of a highly reactive product such as MGLY, in order to counteract this inhibition to the extent needed to fit the $d(O_3$-NO) reactivity data

in the mini-surrogate runs. If no reactive product is assumed (i.e, assuming $y_{MGLY} \approx 0$), then the $y_{NO \rightarrow NO2}$ needed to fit the mini-surrogate $d(O_3\text{-NO})$ reactivity data is so high that the $d(O_3\text{-NO})$ reactivities in the full surrogate runs, which are more sensitive to $y_{NO \rightarrow NO2}$, is significantly overpredicted. However, the $d(O_3\text{-NO})$ and IntOH reactivity data for the various types of runs can be fit if both $y_{NO \rightarrow NO2}$ and y_{MGLY} are adjusted.

Model "B" is similar to Model A in that it assumes that the inhibition in the low NO_x experiments is due to the formation of cresol-like products (i.e., that $y_{CRES} \approx 1$), but allows y_{OH}, $y_{NO \rightarrow NO2}$ and y_{MGLY} to be optimized to fit both the $d(O_3\text{-NO})$ and the IntOH reactivities in the runs. The best fits are obtained using $y_{OH} \approx 0.9$, $y_{NO \rightarrow NO2} \approx 0.7$, and $y_{MGLY} \approx 0.3$. Thus this model assumes ~10% radical inhibition, some NO to NO_2 conversions, and non-negligible formation of highly photoreactive products. This contrasts with the corresponding TDI mechanisms, which assume 70% inhibition, no NO to NO_2 conversions, and no significant formation of photoreactive products. Figures 4-9 shows that this mechanism gives reasonably good fits to $d(O_3\text{-NO})$ and IntOH reactivity data, in most cases to within the estimated experimental uncertainty. No obvious systematic biases are seen in the simulations using this mechanism.

The formation of cresol-like products is not the only route by which PTI's reactions could cause inhibition in the low NO_x experiments. Another possibility is formation of alkyl nitrates in the reactions of peroxy radicals with NO, which is a NO_x and radical sink process which is important in the photooxidations of the higher alkanes (Carter and Atkinson, 1989b), and which is assumed in the alternative TDI model "B" (Carter et al, 1997a). Since this is a significantly different mechanism for NO_x removal than that assumed in Models A and B, mechanisms based on this may yield different results when models adjusted to fit chamber data are extrapolated to atmospheric conditions.

In Model "C" it is assumed that the NO_x sink in the PTI mechanism is due to such a nitrate-forming peroxy reaction rather than formation of cresol-like products. This is represented in the model by assuming non-negligible values for $y_{NO \rightarrow NPHE}$, which is adjusted, along with y_{OH}, $y_{NO \rightarrow NO2}$ and y_{MGLY} to fit the $d(O_3\text{-NO})$ and IntOH reactivity data. Best fits to the data for the high NO_x mini- and full surrogate runs and for the low NO_x full surrogate run with the highest amount of added PTI is obtained if $y_{NO \rightarrow NPHE} \approx 0.2$, $y_{OH} = 1 - y_{NO \rightarrow NPHE}$, $y_{NO \rightarrow NO2} \approx 1$, and $y_{MGLY} \approx 1$. The results of the model simulations using this mechanism are shown on Figures 4-9.

Although Figures 4-7 and 9 show that Model "C" gives generally good fits to the $d(O_3\text{-NO})$ and IntOH reactivity data for the high NO_x mini- and full surrogate runs and for the low NO_x full surrogate run with the highest amount of added PTI (run DTC608), Figure 8 shows that has a definite bias towards underpredicting the $d(O_3\text{-NO})$ inhibition in the low NO_x full surrogate run with the lower amount of added PTI (run DTC604). Thus this model apparently does not correctly predict the dependence of the extent of low NO_x inhibition on the amount of PTI that is added. If this is the case, the discrepancy may be even

greater for more atmospherically representative simulations when the amount of added VOC is much lower.

Atmospheric Reactivity Calculations

The PTI mechanisms which were derived from the chamber data can be used as a basis for estimating mechanisms for MDI for the purpose of estimating its atmospheric ozone impacts. For this purpose, three estimated MDI mechanisms were derived, corresponding to each of the three PTI models which were derived from the chamber data as discussed above. These are referred to as MDI models "A", "B", and "C", to indicate the corresponding PTI model from which they were derived. The corresponding reactions used in the model simulations are given in Table A-2. Note that the predictions of the MDI Model B is considered to be our best estimate because of the superior performance of the corresponding PTI model in simulating the chamber data, and is therefore referred to as the "best estimate" mechanism. However, calculations using Models A and C are also shown, to give an indication of the sensitivity of the model predictions to alternative assumptions concerning the mechanism.

The relative ozone impacts of ethane and of MDI as predicted using the three mechanisms are shown on Table 4. The impacts are given as relative reactivities (see above), derived in terms of ozone formed per unit mass of ethane or MDI emitted, relative to ozone formed per unit mass for the total (or weighted average) of all VOC emissions into the scenarios. The ozone impacts are quantified both in terms of peak ozone (ozone yield) and in terms of maximum 8-hour average ozone. Since the ozone impacts are shown relative to the ozone impact caused by increasing the mass emissions of all VOCs, the numbers on the table can be considered to be an estimate of the relative effects of controlling emissions of MDI or ethane, compared to controlling emissions of VOCs from all sources equally. The data are shown for each of the 39 "base case" EKMA scenarios, together with the corresponding averages and standard deviations, and for the three adjusted NO_x scenarios. The predictions for ethane is shown for comparison with those MDI because ethane is the compound the EPA has used as the basis for determining VOC exemptions (Dimitriades, 1996).

The results on Table 4 show that the relative reactivities of MDI calculated using the best estimate model B are highly dependent on scenario conditions. Negative reactivities are calculated for most base case and the lower NO_x adjusted NO_x scenarios, but with positive reactivities for a few of the higher NO_x scenarios, including MIR. When ozone yields are considered, MDI is predicted to be an inhibitor under all but three of the 39 base case scenarios, and is predicted to be more reactive than ethane in only one of these scenarios. The results are similar for the 8-hour average reactivities, though the variability with scenario conditions appears to be somewhat less. MDI is predicted to inhibit the 8-hour average ozone in all but four of the base case scenarios, and is predicted to form more average ozone in only one of those cases. The results with the adjusted NO_x MIR, MOIR, and EBIR scenarios suggest that NO_x

36

Table 4. Summary of calculated incremental reactivities (gram basis) for ethane and the best fit
PTI model for MDI, relative to the average of all VOC emissions.

	Scenario	O₃ Yield Relative Reactivities				Max 8 Hour Avg Relative. Reactivities			
		Ethane	MDI			Ethane	MDI		
			A	B (best)	C		A	B (best)	C
Adj'd	Max React	0.08	0.14	0.29	0.49	0.06	0.10	0.24	0.45
NOx	Max Ozone	0.15	-0.44	-0.29	0.30	0.09	-0.08	0.06	0.40
	Equal Benefit	0.19	-1.45	-1.27	0.06	0.11	-0.68	-0.54	0.21
Base	**Average**	**0.18**	**-1.13**	**-0.96**	**0.15**	**0.10**	**-0.52**	**-0.37**	**0.26**
Case	**St.Dev**	**0.04**	**1.03**	**1.01**	**0.19**	**0.03**	**0.60**	**0.59**	**0.13**
	Maximum	**0.28**	**0.10**	**0.25**	**0.49**	**0.18**	**0.07**	**0.21**	**0.45**
	ATL GA	0.17	-0.73	-0.57	0.17	0.10	-0.32	-0.17	0.28
	AUS TX	0.20	-1.62	-1.42	0.00	0.12	-0.96	-0.80	0.11
	BAL MD	0.16	-0.76	-0.60	0.28	0.08	-0.18	-0.04	0.38
	BAT LA	0.16	-0.70	-0.54	0.23	0.10	-0.32	-0.17	0.31
	BIR AL	0.24	-2.33	-2.13	-0.05	0.13	-1.22	-1.05	0.14
	BOS MA	0.21	-1.08	-0.92	0.10	0.13	-0.56	-0.41	0.22
	CHA NC	0.21	-1.58	-1.38	-0.05	0.14	-0.97	-0.80	0.09
	CHI IL	0.28	-5.65	-5.36	-0.54	0.18	-3.50	-3.27	-0.26
	CIN OH	0.20	-1.00	-0.83	0.15	0.10	-0.36	-0.22	0.29
	CLE OH	0.15	-0.89	-0.73	0.23	0.09	-0.27	-0.12	0.34
	DAL TX	0.12	-0.05	0.10	0.43	0.08	0.02	0.16	0.41
	DEN CO	0.11	-0.48	-0.31	0.32	0.07	-0.09	0.05	0.39
	DET MI	0.20	-1.12	-0.96	0.13	0.11	-0.38	-0.25	0.29
	ELP TX	0.12	-0.51	-0.35	0.32	0.07	-0.17	-0.02	0.37
	HAR CT	0.21	-1.28	-1.10	0.01	0.13	-0.66	-0.51	0.18
	HOU TX	0.19	-0.84	-0.69	0.22	0.11	-0.35	-0.21	0.32
	IND IN	0.16	-0.64	-0.48	0.23	0.09	-0.20	-0.06	0.34
	JAC FL	0.17	-0.66	-0.49	0.14	0.10	-0.30	-0.14	0.26
	KAN MO	0.20	-0.74	-0.57	0.14	0.11	-0.31	-0.16	0.27
	LAK LA	0.23	-1.67	-1.50	-0.05	0.14	-1.11	-0.95	0.08
	LOS CA	0.15	-2.16	-1.99	0.15	0.09	-0.82	-0.68	0.30
	LOU KY	0.19	-0.51	-0.37	0.23	0.11	-0.22	-0.08	0.31
	MEM TN	0.21	-1.15	-0.98	0.10	0.12	-0.55	-0.40	0.24
	MIA FL	0.19	-1.43	-1.23	-0.06	0.12	-0.82	-0.65	0.09
	NAS TN	0.24	-1.31	-1.14	-0.03	0.17	-1.00	-0.83	0.06
	NEW NY	0.18	-3.97	-3.76	-0.23	0.09	-1.35	-1.20	0.14
	PHI PA	0.17	-0.69	-0.53	0.21	0.10	-0.22	-0.08	0.32
	PHO AZ	0.17	-1.24	-1.07	0.21	0.09	-0.42	-0.28	0.34
	POR OR	0.18	-0.61	-0.45	0.17	0.11	-0.26	-0.11	0.28
	RIC VA	0.19	-1.06	-0.89	0.13	0.10	-0.33	-0.20	0.29
	SAC CA	0.18	-0.58	-0.42	0.23	0.10	-0.20	-0.05	0.35
	SAI MO	0.14	-0.90	-0.73	0.25	0.08	-0.24	-0.10	0.35
	SAL UT	0.19	-1.52	-1.34	0.08	0.11	-0.67	-0.51	0.25
	SAN TX	0.13	-0.09	0.07	0.39	0.08	0.00	0.13	0.39
	SDO CA	0.12	-0.72	-0.55	0.23	0.08	-0.28	-0.14	0.32
	SFO CA	0.06	0.10	0.25	0.49	0.05	0.07	0.21	0.45
	TAM FL	0.14	-0.22	-0.08	0.35	0.08	-0.04	0.09	0.39
	TUL OK	0.18	-0.59	-0.44	0.23	0.10	-0.17	-0.04	0.34
	WAS DC	0.20	-1.08	-0.92	0.16	0.10	-0.42	-0.28	0.29

conditions is a major factor affecting whether MDI is calculated to inhibit or enhance O_3 formation, and by how much.

To examine the extent to which variations in NO_x conditions explain the differences in MDI relative reactivities among the various scenarios, Figure 10 shows a plot of the best estimate (Model B) relative MDI reactivities against relative NO_x levels in the various scenarios. The latter is quantified by the ratio of NO_x inputs (sum of initially present and emitted NO_x) in the scenarios divided by the NO_x inputs which give the highest peak ozone concentrations, i.e., the NO_x inputs of the corresponding MOIR scenario (referred to as NO_x^{MO}). This quantity is believed to be a good indicator of relative NO_x levels in scenarios as they affect VOC reactivity (Carter, 1994a). Figure 10 shows that although relative NO_x levels is clearly a major factor determining whether this model predicts MDI will inhibit or enhance ozone formation, the degree of inhibition under the lower NO_x conditions can be significantly affected by other factors as well. This dependence on NO_x conditions and variability of low NO_x inhibition is somewhat less when O_3 is quantified by the 8-hour average, with results being similar to ozone yield reactivities under high NO_x (e.g., MIR) conditions, but the inhibition being less extreme under low NO_x conditions.

Table 4 also shows the relative MDI reactivities calculated with the other MDI models. Model A gives qualitatively similar results to the best estimate Model B, though it calculates somewhat lower positive reactivities under MIR conditions (though still slightly higher than ethane), and somewhat greater inhibition when NO_x is low. However, Model C, which is based on assuming a different mechanism for NO_x removal than the other mechanisms, gives quite different results. Not only is the MIR reactivity calculated to be over 50% higher than for Model B, positive reactivities, often greater than that for ethane, are calculated even for most of the low NO_x scenarios. This indicates the sensitivity of the reactivity predictions to the type of mechanism used to extrapolate from chamber data to atmospheric conditions.
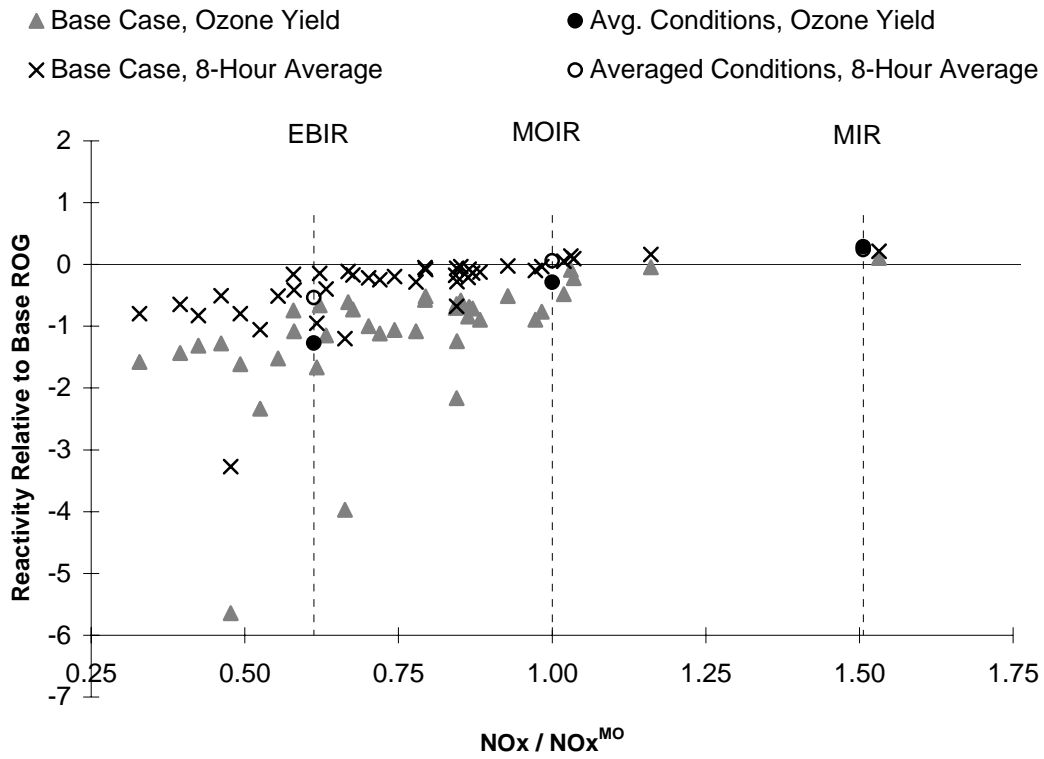
Figure 10. Plots relative ozone yield reactivities for MDI calculated using the "best estimate" Model B against the NO_x / NO_x^{MO} ratio for the base case and the adjusted NO_x averaged conditions scenarios.

CONCLUSIONS

The decision whether it is appropriate to regulate a compound as an ozone precursor requires a qualitative assessment of its ozone impacts under a variety of environmental conditions, taking into account the uncertainties involved. This involves developing a chemical mechanism or model for the compound's atmospheric reactions which can be used in airshed models to predict its atmospheric reactivity. Until this study, the only information concerning isocyanate reactivity was an experimental and modeling study which indicated that TDI probably inhibited ozone formation under most tropospheric conditions. There was no information available to indicate whether this was the case for other aromatic isocyanate species such as MDI. Our lack of knowledge of the details of aromatic atmospheric reaction mechanisms made extrapolations from one compound to another highly unreliable. The objective of this study was to provide data concerning whether the tendency of TDI to strongly inhibit ozone may be a characteristic of aromatic isocyanates in general, and of MDI in particular. This project was successful in obtaining kinetic and reactivity data for the model compound PTI, allowing atmospheric reactivity estimates to be made for it and related compounds. However, the project was not successful in the obtaining information needed to make unambiguous conclusions concerning the atmospheric ozone impacts of aromatic isocyanates as a class.

In particular, although PTI, like TDI, was found to inhibit ozone formation under most conditions, PTI was found to be a much less strong radical inhibitor than TDI, and was also predicted to have a small but positive impact on ozone formation in the higher NO_x scenarios where ozone is most sensitive to VOC emissions. Therefore, it cannot be concluded that all aromatic isocyanates will necessarily be like TDI in being probable ozone inhibitor under all conditions. Different types of aromatic isocyanates apparently differ in their radical inhibiting characteristics. On the other hand, since both TDI and PTI are shown to be inhibitors under low NO_x conditions, it is likely that this is the case for other aromatic isocyanates as well. However, these results indicate that the aromatic isocyanates can be much more variable in their effects on ozone formation under the higher NO_x conditions which are sensitive to radical inhibition or initiation effects.

Nevertheless, the data obtained from PTI can be used to make conclusions concerning the likely ozone impacts of MDI. The MDI molecule can be thought of as two PTI molecules joined at the methylene group, which isolates the two rings so that they should not significantly interact. It is reasonable to expect that reactions at the aromatic ring should occur with similar mechanisms, and also that most of the reaction will occur at the aromatic ring, which has a similar environment for both compounds. The fact that the rate constant for the reaction of OH radicals with PTI was found to be almost exactly the same as that for toluene is consistent with this.

The rate constant for the reaction of PTI with OH radicals was measured to be approximately 5.9 x 10^{-12} cm^3 molec^{-1} s^{-1} at ~300K, from which we estimate an OH + MDI rate constant of ~1.2 x 10^{-11} cm^3 molec^{-1} s^{-1}. This indicates that MDI reacts relatively rapidly in the atmosphere. Based on the reactivity parameters which fit the chamber data for PTI, MDI is calculated to have a positive effect on O$_3$ formation under high NO$_x$, maximum incremental reactivity (MIR) conditions, but to inhibit ozone formation under most lower NO$_x$ scenarios, which includes most of the "base case" EKMA scenarios designed to represent worst case or typical episodes in various ozone exceedence areas.

These ozone impact estimates for MDI are not without uncertainties. The best fit mechanism for PTI which was used to derive the MDI mechanism is a highly simplified parameterization of the actual chemistry which is occurring, which is unknown and may be quite complex. Since the best estimate model fit the chamber data under a variety of conditions reasonably well, it is assumed that it can be extrapolated to the range of conditions in the atmosphere. However, the isocyanate and NO$_x$ concentrations in the atmosphere will be much lower than the range of conditions in the experiments, so the extrapolation is uncertain. An alternative mechanism which assumes that the inhibition of peak O$_3$ in the low NO$_x$ experiments was due to nitrate formation from peroxy + NO reactions rather than to formation of cresol-like products as assumed in the best estimate mechanism gives quite different predictions of atmospheric reactivities, especially under low NO$_x$ conditions. Although we think that the best estimate mechanism is much more likely to give correct predictions in the atmosphere because it gave better predictions of the effects of changing PTI levels in the low NO$_x$ experiments and because it is also more chemically reasonable, the difference in model predictions indicate that mechanism formulation is important in affecting how mechanisms which fit chamber data extrapolate to atmospheric conditions. That is why it is important to know as much as possible about the details of a VOC's actual mechanism when developing models to extrapolate from chamber data to atmospheric conditions.

There are also uncertainties involved in estimating the MDI mechanism from that derived from reactivity data for PTI. Reaction of OH radicals at the methylene group in MDI might be somewhat more likely than reaction at the methyl group in PTI, though it is probably still not important compared to reaction at an aromatic ring. In addition, the product expected to be formed after reaction at the methylene group, diphenyl ketone, is probably not highly reactive. Perhaps more significantly, any phenyl-substituted products formed in the photooxidation of MDI may have quite reactivity characteristics than the corresponding methyl-substituted products from PTI. The best fit PTI mechanism predicts a significantly reactivity contribution from highly photoreactive products represented by methyl glyoxal. The corresponding phenyl-substituted product may be less photoreactive, or have other photolysis routes which do not form radicals, thus giving correspondingly less reactivity to MDI than predicted in the mechanism derived from that for PTI. The reactive product(s) from MDI may also have a greater tendency to condense into the aerosol phase and thus not participate in O$_3$ formation. For these reasons, we think that modeling MDI reactions using a PTI-derived mechanism is more likely to cause overestimations of MDI's

ozone impacts than the other way around. Thus, the actual ozone impact of MDI is likely to be lower than estimated in this work.

Therefore, it is concluded that MDI will probably negative impacts on ozone formation under atmospheric conditions where NO_x is limited, including most of the "base case" scenarios designed to represent high ozone episodes in 39 urban areas in the United States. On the other hand, MDI was predicted to have positive impacts on ozone under high NO_x conditions where ozone is more sensitive to VOC emissions, and its ozone impact in the MIR scenario was calculated to be somewhat higher than that for ethane. Therefore, MDI is not expected to be as general and effective an ozone inhibitor as TDI, which appears to be a strong ozone inhibitor under all conditions relevant to ozone control. However, the conclusions for MDI are based on that for a surrogate compound, and it is possible that we are overestimating its atmospheric ozone impacts. More information concerning the atmospheric reactions mechanisms for aromatic isocyanates is needed to improve our ability to estimate impacts of compounds which cannot be studied directly.

Of course, these conclusions about the effects of MDI on ozone formation are only relevant to ozone control strategies if the use of MDI actually results in its being emitted into the open atmosphere, as opposed to being deposited on surfaces, or oxidized or converted to other substances before it is emitted. Given its very low vapor pressure and probable affinity to surfaces (based on the high surface affinity for the much less volatile TDI), it cannot necessarily be assumed that use of MDI will result in its reacting in the atmosphere. Our analysis also neglects any deposition processes MDI may undergo once it is emitted. If these are taken into account, the actual ozone impact of MDI may be considerably less than estimated in this work.

REFERENCES

Atkinson, R. (1989): "Kinetics and Mechanisms of the Gas-Phase Reactions of the Hydroxyl Radical with Organic Compounds," J. Phys. Chem. Ref. Data, Monograph no 1.

Atkinson, R. (1990): "Gas-Phase Tropospheric Chemistry of Organic Compounds: A Review," Atmos. Environ., 24A, 1-24.

Atkinson, R. (1994): "Gas-Phase Tropospheric Chemistry of Organic Compounds," J. Phys. Chem. Ref. Data, Monograph No. 2.

Baugues, K. (1990): "Preliminary Planning Information for Updating the Ozone Regulatory Impact Analysis Version of EKMA," Draft Document, Source Receptor Analysis Branch, Technical Support Division, U. S. Environmental Protection Agency, Research Triangle Park, NC, January.

Becker, K. H., V. Bastian, and Th. Klein (1988): "The Reactions of OH Radicals with Toluene Diisocyanate, Toluenediamine and Methylenedianiline Under Simulated Atmospheric Conditions," J. Photochem. Photobiol A., 45 195-205.

Carter, W. P. L. (1990): "A Detailed Mechanism for the Gas-Phase Atmospheric Reactions of Organic Compounds," Atmos. Environ., 24A, 481-518.

Carter, W. P. L. (1994a): "Development of Ozone Reactivity Scales for Volatile Organic Compounds," J. Air & Waste Manage. Assoc., 44, 881-899.

Carter, W. P. L. (1994b): "Calculation of Reactivity Scales Using an Updated Carbon Bond IV Mechanism," Report Prepared for Systems Applications International Under Funding from the Auto/Oil Air Quality Improvement Research Program, April 12.

Carter, W. P. L. (1995): "Computer Modeling of Environmental Chamber Measurements of Maximum Incremental Reactivities of Volatile Organic Compounds," Atmos. Environ., 29, 2513-2517.

Carter, W. P. L., R. Atkinson, A. M. Winer, and J. N. Pitts, Jr. (1982): "Experimental Investigation of Chamber-Dependent Radical Sources," Int. J. Chem. Kinet., 14, 1071.

Carter, W. P. L. and R. Atkinson (1987): "An Experimental Study of Incremental Hydrocarbon Reactivity," Environ. Sci. Technol., 21, 670-679

Carter, W. P. L. and R. Atkinson (1989a): "A Computer Modeling Study of Incremental Hydrocarbon Reactivity", Environ. Sci. Technol., 23, 864.

Carter, W. P. L. and R. Atkinson (1989b): "Alkyl Nitrate Formation from the Atmospheric Photooxidation of Alkanes; a Revised Estimation Method," J. Atm. Chem. 8, 165-173.

Carter, W. P. L., and F. W. Lurmann (1990): "Evaluation of the RADM Gas-Phase Chemical Mechanism," Final Report, EPA-600/3-90-001.

Carter, W. P. L. and F. W. Lurmann (1991): "Evaluation of a Detailed Gas-Phase Atmospheric Reaction Mechanism using Environmental Chamber Data," Atm. Environ. 25A, 2771-2806.

Carter, W. P. L., J. A. Pierce, I. L. Malkina, and D. Luo (1992): "Investigation of the Ozone Formation Potential of Selected Volatile Silicone Compounds," Final Report to Dow Corning Corporation, Midland, MI, November.

Carter, W. P. L., J. A. Pierce, I. L. Malkina, D. Luo and W. D. Long (1993a): "Environmental Chamber Studies of Maximum Incremental Reactivities of Volatile Organic Compounds," Report to Coordinating Research Council, Project No. ME-9, California Air Resources Board Contract No. A032-0692; South Coast Air Quality Management District Contract No. C91323, United States Environmental Protection Agency Cooperative Agreement No. CR-814396-01-0, University Corporation for Atmospheric Research Contract No. 59166, and Dow Corning Corporation. April 1.

Carter, W. P. L, D. Luo, I. L. Malkina, and J. A. Pierce (1993b): "An Experimental and Modeling Study of the Photochemical Ozone Reactivity of Acetone," Final Report to Chemical Manufacturers Association Contract No. KET-ACE-CRC-2.0. December 10.

Carter, W. P. L., J. A. Pierce, D. Luo, and I. L. Malkina (1995a): "Environmental Chamber Study of Maximum Incremental Reactivities of Volatile Organic Compounds," Atmos. Environ. 29, 2499-2511.

Carter, W. P. L., D. Luo, I. L. Malkina, and J. A. Pierce (1995b): "Environmental Chamber Studies of Atmospheric Reactivities of Volatile Organic Compounds. Effects of Varying ROG Surrogate and NO_x," Final report to Coordinating Research Council, Inc., Project ME-9, California Air Resources Board, Contract A032-0692, and South Coast Air Quality Management District, Contract C91323. March 24.

Carter, W. P. L., D. Luo, I. L. Malkina, and D. Fitz (1995c): "The University of California, Riverside Environmental Chamber Data Base for Evaluating Oxidant Mechanism. Indoor Chamber Experiments through 1993," Report submitted to the U. S. Environmental Protection Agency, EPA/AREAL, Research Triangle Park, NC., March 20..

Carter, W. P. L., D. Luo, I. L. Malkina, and J. A. Pierce (1995d): "Environmental Chamber Studies of Atmospheric Reactivities of Volatile Organic Compounds. Effects of Varying Chamber and Light Source," Final report to National Renewable Energy Laboratory, Contract XZ-2-12075, Coordinating Research Council, Inc., Project M-9, California Air Resources Board, Contract A032-0692, and South Coast Air Quality Management District, Contract C91323, March 26.

W. P. L. Carter, D. Luo and I. L. Malkina (1997a): "Investigation of the Atmospheric Ozone Formation Potential of Toluene Diisocyanate," Final Report to The Society for the Plastics Industry, Inc., December 2.

Carter, W. P. L., D. Luo, and I. L. Malkina (1997b): "Environmental Chamber Studies for Development of an Updated Photochemical Mechanism for VOC Reactivity Assessment," Draft final report to California Air Resources Board Contract 92-345, Coordinating Research Council Project M-9, and National Renewable Energy Laboratory Contract ZF-2-12252-07. March 10.

Chang, T. Y. and S. J. Rudy (1990): "Ozone-Forming Potential of Organic Emissions from Alternative-Fueled Vehicles," Atmos. Environ., 24A, 2421-2430.

Dimitriades, B. (1996): "Scientific Basis for the VOC Reactivity Issues Raised by Section 183(e) of the Clean Air Act Amendments of 1990," J. Air Waste Manage. Assoc. 46, 963-970.

Dodge, M. C. (1984): "Combined effects of organic reactivity and NMHC/NOx ratio on photochemical oxidant formation -- a modeling study," Atmos. Environ., 18, 1657.

Duff, P. B. (1984): "Fate of Toluene Diisocyanate in Air. Phase II Study," Proceedings of the SPI 29th Annual Technical/Marketing Conference. 9-24.

EPA (1984): "Guideline for Using the Carbon Bond Mechanism in City-Specific EKMA," EPA-450/4-84-005, February.

Gery, M. W., G. Z. Whitten, and J. P. Killus (1988): "Development and Testing of the CBM-IV For Urban and Regional Modeling,", EPA-600/ 3-88-012, January.

Johnson, G. M. (1983): "Factors Affecting Oxidant Formation in Sydney Air," in "The Urban Atmosphere -- Sydney, a Case Study." Eds. J. N. Carras and G. M. Johnson (CSIRO, Melbourne), pp. 393-408.

Jeffries, H. E. (1991): "UNC Solar Radiation Models," unpublished draft report for EPA Cooperative Agreements CR813107, CR813964 and CR815779". Undated.

Jeffries, H. E., K. G. Sexton, J. R. Arnold, and T. L. Kale (1989): "Validation Testing of New Mechanisms with Outdoor Chamber Data. Volume 2: Analysis of VOC Data for the CB4 and CAL Photochemical Mechanisms," Final Report, EPA-600/3-89-010b.

Jeffries, H. E. and R. Crouse (1991): "Scientific and Technical Issues Related to the Application of Incremental Reactivity. Part II: Explaining Mechanism Differences," Report prepared for Western States Petroleum Association, Glendale, CA, October.

Pitts, J. N., Jr., E. Sanhueza, R. Atkinson, W. P. L. Carter, A. M. Winer, G. W. Harris, and C. N. Plum (1984): "An Investigation of the Dark Formation of Nitrous Acid in Environmental Chambers," Int. J. Chem. Kinet., 16, 919-939.

Stockwell, W. R., P. Middleton, J. S. Chang, and X. Tang (1990): "The Second Generation Regional Acid Deposition Model Chemical Mechanism for Regional Air Quality Modeling," J. Geophys. Res. 95, 16343- 16376.

Taylor, W. D., T. D. Allison, M. J. Moscato, G. B. Fazekas, R. Kozlowski, and G. A. Takacs (1980): Int. J. Chem. Kinet. 12, 231-240.

Tuazon, E. C., R. Atkinson, C. N. Plum, A. M. Winer, and J. N. Pitts, Jr. (1983): "The Reaction of Gas-Phase N_2O_5 with Water Vapor," Geophys. Res. Lett. <u>10</u>, 953-956.

Zafonte, L., P. L. Rieger, and J. R. Holmes (1977): "Nitrogen Dioxide Photolysis in the Los Angeles Atmosphere," Environ. Sci. Technol. <u>11</u>, 483-487.

LISTING OF THE CHEMICAL MECHANISM

The chemical mechanism used in the environmental chamber and atmospheric model simulations discussed in this report is given in Tables A-1 through A-4. Table A-1 lists the species used in the mechanism, Table A-2 gives the reactions and rate constants, Table A-3 gives the parameters used to calculate the rates of the photolysis reactions, and Table A-4 gives the values and derivations of the chamber-dependent parameters used when modeling the environmental chamber experiments. Footnotes to Table A-2 indicate the format used for the reaction listing.

Table A-1.   List of species in the chemical mechanism used in the model simulations for this study.

Name	Description
Constant Species.	
O2	Oxygen
M	Air
H2O	Water
Active Inorganic Species.	
O3	Ozone
NO	Nitric Oxide
NO2	Nitrogen Dioxide
NO3	Nitrate Radical
N2O5	Nitrogen Pentoxide
HONO	Nitrous Acid
HNO3	Nitric Acid
HNO4	Peroxynitric Acid
HO2H	Hydrogen Peroxide
Active Radical Species and Operators.	
HO2.	Hydroperoxide Radicals
RO2.	Operator to Calculate Total Organic Peroxy Radicals
RCO3.	Operator to Calculate Total Acetyl Peroxy Radicals
Active Reactive Organic Product Species.	
CO	Carbon Monoxide
HCHO	Formaldehyde
CCHO	Acetaldehyde
RCHO	Lumped C3+ Aldehydes
ACET	Acetone
MEK	Lumped Ketones
PHEN	Phenol

Name	Description
CRES	Cresols
BALD	Aromatic aldehydes (e.g., benzaldehyde)
GLY	Glyoxal
MGLY	Methyl Glyoxal
BACL	Biacetyl or other lumped α-dicarbonyls, including α-keto esters
AFG1	Reactive Aromatic Fragmentation Products from benzene and naphthalene
AFG2	Other Reactive Aromatic Fragmentation Products
AFG3	Aromatic Fragmentation Products used in adjusted m-xylene mechanism
RNO3	Organic Nitrates
NPHE	Nitrophenols
ISOPROD	Lumped isoprene product species
PAN	Peroxy Acetyl Nitrate
PPN	Peroxy Propionyl Nitrate
GPAN	PAN Analogue formed from Glyoxal
PBZN	PAN Analogues formed from Aromatic Aldehydes
-OOH	Operator Representing Hydroperoxy Groups

Non-Reacting Species

CO2	Carbon Dioxide
-C	"Lost Carbon"
-N	"Lost Nitrogen"
H2	Hydrogen

Steady State Species and Operators.

HO.	Hydroxyl Radicals
O	Ground State Oxygen Atoms
O*1D2	Excited Oxygen Atoms
RO2-R.	Peroxy Radical Operator representing NO to NO_2 conversion with HO_2 formation.
RO2-N.	Peroxy Radical Operator representing NO consumption with organic nitrate formation.
RO2-NP.	Peroxy Radical Operator representing NO consumption with nitrophenol formation
R2O2.	Peroxy Radical Operator representing NO to NO_2 conversion.
CCO-O2.	Peroxy Acetyl Radicals
C2CO-O2.	Peroxy Propionyl Radicals
HCOCO-O2.	Peroxyacyl Radical formed from Glyoxal
BZ-CO-O2.	Peroxyacyl Radical formed from Aromatic Aldehydes
HOCOO.	Intermediate formed in Formaldehyde + HO_2 reaction
BZ-O.	Phenoxy Radicals
BZ(NO2)-O.	Nitratophenoxy Radicals
HOCOO.	Radical Intermediate formed in the HO_2 + Formaldehyde system.
(HCHO2)	Excited Criegee biradicals formed from $=CH_2$ groups
(CCHO2)	Excited Criegee biradicals formed from $=CHCH_3$ groups
(RCHO2)	Excited Criegee biradicals formed from $=CHR$ groups, where R not CH_3
(C(C)CO2)	Excited Criegee biradicals formed from $=C(CH_3)_2$ groups
(C(R)CO2)	Excited Criegee biradicals formed from $=C(CH_3)R$ or CR_2 groups
(BZCHO2)	Excited Criegee biradicals formed from styrenes
(C:CC(C)O2)	Excited Criegee biradicals formed from isoprene
(C:C(C)CHO2)	Excited Criegee biradicals formed from isoprene
(C2(O2)CHO)	Excited Criegee biradicals formed from isoprene products

Table A-1, (continued)

Name	Description
(HOCCHO2)	Excited Criegee biradicals formed from isoprene products
(HCOCHO2)	Excited Criegee biradicals formed from isoprene products
(C2(O2)COH)	Excited Criegee biradicals formed from isoprene products
xNO2	Operator causing NO_2 to NO conversions in the presence of NO_x

Primary Organics Represented explicitly

Name	Description
CH4	Methane
ETHANE	Ethane
N-C4	n-Butane
N-C6	n-Hexane
N-C8	n-Octane
TOLUENE	Toluene
M-XYLENE	m-Xylene
ETHE	Ethene
PROPENE	Propene
T-2-BUTE	trans-2-Butene
ISOP	Isoprene
APIN	α-Pinene
UNKN	Unknown biogenics.
PTI	para Toluene Isocyanate
MDI	Methylene Diphenylene Diisocyanate

Lumped species used to represent the Base ROG mixture in the EKMA model simulations.

Name	Description
ALK1	Alkanes and other saturated compounds with $k_{OH} < 10^4$ ppm^{-1} min^{-1}.
ALK2	Alkanes and other saturated compounds with $k_{OH} \geq 10^4$ ppm^{-1} min^{-1}.
ARO1	Aromatics with $k_{OH} < 2 \times 10^4$ ppm^{-1} min^{-1}.
ARO2	Aromatics with $k_{OH} \geq 2 \times 10^4$ ppm^{-1} min^{-1}.
OLE2	Alkenes (other than ethene) with $k_{OH} < 7 \times 10^4$ ppm^{-1} min^{-1}.
OLE3	Alkenes with $k_{OH} \geq 7 \times 10^4$ ppm^{-1} min^{-1}.

Table A-2.   List of reactions in the chemical mechanism used in the model simulations for this study.

```
——————————————————————————————————————————————————————————————————————
Rxn.         Kinetic Parameters [a]
         ———————————————————————————————    Reactions [b]
Label  k(300)     A         Ea     B
——————————————————————————————————————————————————————————————————————

Inorganic Reactions

1         (Phot. Set = NO2     )     NO2 + HV = NO + O
2      6.00E-34  6.00E-34  0.00 -2.30  O + O2 + M = O3 + M
3A     9.69E-12  6.50E-12 -0.24  0.00  O + NO2 = NO + O2
3B     1.55E-12   (Falloff Kinetics)  O + NO2 = NO3 + M
       k0   =   9.00E-32  0.00 -2.00
       kINF =   2.20E-11  0.00  0.00
                F= 0.60  n= 1.00
4      1.88E-14  2.00E-12  2.78  0.00  O3 + NO = NO2 + O2
5      3.36E-17  1.40E-13  4.97  0.00  O3 + NO2 = O2 + NO3
6      2.80E-11  1.70E-11 -0.30  0.00  NO + NO3 = 2 NO2
7      1.92E-38  3.30E-39 -1.05  0.00  NO + NO + O2 = 2 NO2
8      1.26E-12   (Falloff Kinetics)  NO2 + NO3 = N2O5
       k0   =   2.20E-30  0.00 -4.30
       kINF =   1.50E-12  0.00 -0.50
                F= 0.60  n= 1.00
9      5.53E+10  9.09E+26 22.26  0.00  N2O5 + #RCON8 = NO2 + NO3
10     1.00E-21   (No T Dependence)   N2O5 + H2O = 2 HNO3
11     4.17E-16  2.50E-14  2.44  0.00  NO2 + NO3 = NO + NO2 + O2
12A       (Phot. Set = NO3NO   )     NO3 + HV = NO + O2
12B       (Phot. Set = NO3NO2  )     NO3 + HV = NO2 + O
13A       (Phot. Set = O3O3P   )     O3 + HV = O + O2
13B       (Phot. Set = O3O1D   )     O3 + HV = O*1D2 + O2
14     2.20E-10   (No T Dependence)   O*1D2 + H2O = 2 HO.
15     2.92E-11  1.92E-11 -0.25  0.00  O*1D2 + M = O + M
16     4.81E-12   (Falloff Kinetics)  HO. + NO = HONO
       k0   =   7.00E-31  0.00 -2.60
       kINF =   1.50E-11  0.00 -0.50
                F= 0.60  n= 1.00
17        (Phot. Set = HONO    )     HONO + HV = HO. + NO
18     1.13E-11   (Falloff Kinetics)  HO. + NO2 = HNO3
       k0   =   2.60E-30  0.00 -3.20
       kINF =   2.40E-11  0.00 -1.30
                F= 0.60  n= 1.00
19     1.03E-13  6.45E-15 -1.65  0.00  HO. + HNO3 = H2O + NO3
21     2.40E-13   (No T Dependence)   HO. + CO = HO2. + CO2
22     6.95E-14  1.60E-12  1.87  0.00  HO. + O3 = HO2. + O2
23     8.28E-12  3.70E-12 -0.48  0.00  HO2. + NO = HO. + NO2
24     1.37E-12   (Falloff Kinetics)  HO2. + NO2 = HNO4
       k0   =   1.80E-31  0.00 -3.20
       kINF =   4.70E-12  0.00 -1.40
                F= 0.60  n= 1.00
25     7.92E+10  4.76E+26 21.66  0.00  HNO4 + #RCON24 = HO2. + NO2
27     4.61E-12  1.30E-12 -0.75  0.00  HNO4 + HO. = H2O + NO2 + O2
28     2.08E-15  1.10E-14  0.99  0.00  HO2. + O3 = HO. + 2 O2
29A    1.73E-12  2.20E-13 -1.23  0.00  HO2. + HO2. = HO2H + O2
29B    5.00E-32  1.90E-33 -1.95  0.00  HO2. + HO2. + M = HO2H + O2
29C    3.72E-30  3.10E-34 -5.60  0.00  HO2. + HO2. + H2O = HO2H + O2 + H2O
29D    2.65E-30  6.60E-35 -6.32  0.00  HO2. + HO2. + H2O = HO2H + O2 + H2O
30A    1.73E-12  2.20E-13 -1.23  0.00  NO3 + HO2. = HNO3 + O2
30B    5.00E-32  1.90E-33 -1.95  0.00  NO3 + HO2. + M = HNO3 + O2
30C    3.72E-30  3.10E-34 -5.60  0.00  NO3 + HO2. + H2O = HNO3 + O2 + H2O
30D    2.65E-30  6.60E-35 -6.32  0.00  NO3 + HO2. + H2O = HNO3 + O2 + H2O
31        (Phot. Set = H2O2    )     HO2H + HV = 2 HO.
32     1.70E-12  3.30E-12  0.40  0.00  HO2H + HO. = HO2. + H2O
33     9.90E-11  4.60E-11 -0.46  0.00  HO. + HO2. = H2O + O2

Peroxy Radical Operators

B1     7.68E-12  4.20E-12 -0.36  0.00  RO2. + NO = NO
B2     2.25E-11   (Falloff Kinetics)  RCO3. + NO = NO
       k0   =   5.65E-28  0.00 -7.10
       kINF =   2.64E-11  0.00 -0.90
                F= 0.27  n= 1.00
B4     1.04E-11   (Falloff Kinetics)  RCO3. + NO2 = NO2
       k0   =   2.57E-28  0.00 -7.10
       kINF =   1.20E-11  0.00 -0.90
                F= 0.30  n= 1.00
B5     4.90E-12  3.40E-13 -1.59  0.00  RO2. + HO2. = HO2. + RO2-HO2-PROD
B6     4.90E-12  3.40E-13 -1.59  0.00  RCO3. + HO2. = HO2. + RO2-HO2-PROD
B8     1.00E-15   (No T Dependence)   RO2. + RO2. = RO2-RO2-PROD
```

Rxn.	Kinetic Parameters [a]				Reactions [b]
Label	k(300)	A	Ea	B	
B9	1.09E-11	1.86E-12	-1.05	0.00	RO2. + RCO3. = RO2-RO2-PROD
B10	1.64E-11	2.80E-12	-1.05	0.00	RCO3. + RCO3. = RO2-RO2-PROD
B11	(Same k as for RO2.		)		RO2-R. + NO = NO2 + HO2.
B12	(Same k as for RO2.		)		RO2-R. + HO2. = -OOH
B13	(Same k as for RO2.		)		RO2-R. + RO2. = RO2. + 0.5 HO2.
B14	(Same k as for RO2.		)		RO2-R. + RCO3. = RCO3. + 0.5 HO2.
B19	(Same k as for RO2.		)		RO2-N. + NO = RNO3
B20	(Same k as for RO2.		)		RO2-N. + HO2. = -OOH + MEK + 1.5 -C
B21	(Same k as for RO2.		)		RO2-N. + RO2. = RO2. + 0.5 HO2. + MEK + 1.5 -C
B22	(Same k as for RO2.		)		RO2-N. + RCO3. = RCO3. + 0.5 HO2. + MEK + 1.5 -C
B15	(Same k as for RO2.		)		R2O2. + NO = NO2
B16	(Same k as for RO2.		)		R2O2. + HO2. =
B17	(Same k as for RO2.		)		R2O2. + RO2. = RO2.
B18	(Same k as for RO2.		)		R2O2. + RCO3. = RCO3.
B23	(Same k as for RO2.		)		RO2-XN. + NO = -N
B24	(Same k as for RO2.		)		RO2-XN. + HO2. = -OOH
B25	(Same k as for RO2.		)		RO2-XN. + RO2. = RO2. + 0.5 HO2.
B26	(Same k as for RO2.		)		RO2-XN. + RCO3. = RCO3. + HO2.
G2	(Same k as for RO2.		)		RO2-NP. + NO = NPHE
G3	(Same k as for RO2.		)		RO2-NP. + HO2. = -OOH + 6 -C
G4	(Same k as for RO2.		)		RO2-NP. + RO2. = RO2. + 0.5 HO2. + 6 -C
G5	(Same k as for RO2.		)		RO2-NP. + RCO3. = RCO3. + HO2. + 6 -C

Operator Added to Represent Possible NO$_2$ to NO Conversions

	(Same k as for BZ-O.		)		xNO2 + NO2 = NO
	(Same k as for BZ-O.		)		xNO2 + HO2. =
	(Same k as for BZ-O.		)		xNO2 =

Excited Criegee Biradicals

RZ1	(fast)				(HCHO2) = 0.7 HCOOH + 0.12 "HO. + HO2. + CO" + 0.18 "H2 + CO2"
RZ2	(fast)				(CCHO2) = 0.25 CCOOH + 0.15 "CH4 + CO2" + 0.6 HO. + 0.3 "CCO-O2. + RCO3." + 0.3 "RO2-R. + HCHO + CO + RO2."
RZ3	(fast)				(RCHO2) = 0.25 CCOOH + 0.15 CO2 + 0.6 HO. + 0.3 "C2CO-O2. + RCO3." + 0.3 "RO2-R. + CCHO + CO + RO2." + 0.55 -C
RZ4	(fast)				(C(C)CO2) = HO. + R2O2. + HCHO + CCO-O2. + RCO3. + RO2.
RZ5	(fast)				(C(R)CO2) = HO. + CCO-O2. + CCHO + R2O2. + RCO3. + RO2.
RZ6	(fast)				(CYCCO2) = 0.3 "HO. + C2CO-O2. + R2O2. + RCO3. + RO2." + 0.3 RCHO + 4.2 -C
RZ8	(fast)				(BZCHO2) = 0.5 "BZ-O. + R2O2. + CO + HO."
ISZ1	(fast)				(C:CC(C)O2) = HO. + R2O2. + HCHO + C2CO-O2. + RO2. + RCO3.
ISZ2	(fast)				(C:C(C)CHO2) = 0.75 RCHO + 0.25 ISOPROD + 0.5 -C
MAZ1	(fast)				(C2(O2)CHO) = HO. + R2O2. + HCHO + HCOCO-O2. + RO2. + RCO3.
M1Z1	(fast)				(HOCCHO2) = 0.6 HO. + 0.3 "CCO-O2. + RCO3." + 0.3 "RO2-R. + HCHO + CO + RO2." + 0.8 -C
M2Z1	(fast)				(HCOCHO2) = 0.12 "HO2. + 2 CO + HO." + 0.74 -C + 0.51 "CO2 + HCHO"
M2Z2	(fast)				(C2(O2)COH) = HO. + MGLY + HO2. + R2O2. + RO2.

Organic Product Species

B7	(Phot. Set = CO2H		)		-OOH + HV = HO2. + HO.
B7A	1.81E-12	1.18E-12	-0.25	0.00	HO. + -OOH = HO.
B7B	3.71E-12	1.79E-12	-0.44	0.00	HO. + -OOH = RO2-R. + RO2.
C1	(Phot. Set = HCHONEWR		)		HCHO + HV = 2 HO2. + CO
C2	(Phot. Set = HCHONEWM		)		HCHO + HV = H2 + CO
C3	9.76E-12	1.13E-12	-1.29	2.00	HCHO + HO. = HO2. + CO + H2O
C4	7.79E-14	9.70E-15	-1.24	0.00	HCHO + HO2. = HOCOO.
C4A	1.77E+02	2.40E+12	13.91	0.00	HOCOO. = HO2. + HCHO
C4B	(Same k as for RO2.		)		HOCOO. + NO = -C + NO2 + HO2.
C9	6.38E-16	2.80E-12	5.00	0.00	HCHO + NO3 = HNO3 + HO2. + CO
C10	1.57E-11	5.55E-12	-0.62	0.00	CCHO + HO. = CCO-O2. + H2O + RCO3.
C11A	(Phot. Set = CCHOR		)		CCHO + HV = CO + HO2. + HCHO + RO2-R. + RO2.

Table A-2 (continued)

───

Rxn.	Kinetic Parameters [a]				Reactions [b]
Label	k(300)	A	Ea	B	

───

```
C12    2.84E-15  1.40E-12  3.70  0.00    CCHO + NO3 = HNO3 + CCO-O2. + RCO3.

C25    1.97E-11  8.50E-12 -0.50  0.00    RCHO + HO. = C2CO-O2. + RCO3.
C26        (Phot. Set = RCHO    )        RCHO + HV = CCHO + RO2-R. + RO2. + CO + HO2.
C27    2.84E-15  1.40E-12  3.70  0.00    NO3 + RCHO = HNO3 + C2CO-O2. + RCO3.

C38    2.23E-13  4.81E-13  0.46  2.00    ACET + HO. = R2O2. + HCHO + CCO-O2. + RCO3. + RO2.
C39        (Phot. Set = ACET-93C)        ACET + HV = CCO-O2. + HCHO + RO2-R. + RCO3. + RO2.

C44    1.16E-12  2.92E-13 -0.82  2.00    MEK + HO. = H2O + 0.5 "CCHO + HCHO + CCO-O2. + C2CO-O2." +
                                             RCO3. + 1.5 "R2O2. + RO2."
C57        (Phot. Set = KETONE  )        MEK + HV + #0.1 = CCO-O2. + CCHO + RO2-R. + RCO3. + RO2.

C95    2.07E-12  2.19E-11  1.41  0.00    RNO3 + HO. = NO2 + 0.155 MEK + 1.05 RCHO + 0.48 CCHO +
                                             0.16 HCHO + 0.11 -C + 1.39 "R2O2. + RO2."

C58A       (Phot. Set = GLYOXAL1)        GLY + HV  = 0.8 HO2. + 0.45 HCHO + 1.55 CO
C58B       (Phot. Set = GLYOXAL2)        GLY + HV + #0.029 = 0.13 HCHO + 1.87 CO
C59    1.14E-11    (No T Dependence)     GLY + HO. = 0.6 HO2. + 1.2 CO + 0.4 "HCOCO-O2. + RCO3."
C60        (Same k as for CCHO    )      GLY + NO3 = HNO3 + 0.6 HO2. + 1.2 CO + 0.4 "HCOCO-O2. +
                                             RCO3."

C68A       (Phot. Set = MEGLYOX1)        MGLY + HV = HO2. + CO + CCO-O2. + RCO3.
C68B       (Phot. Set = MEGLYOX2)        MGLY + HV + 0.107 = HO2. + CO + CCO-O2. + RCO3.
C69    1.72E-11    (No T Dependence)     MGLY + HO. = CO + CCO-O2. + RCO3.
C70        (Same k as for CCHO    )      MGLY + NO3 = HNO3 + CO + CCO-O2. + RCO3.

G7     1.14E-11    (No T Dependence)     HO. + AFG1 = HCOCO-O2. + RCO3.
G8         (Phot. Set = ACROLEIN)        AFG1 + HV + #0.029 = HO2. + HCOCO-O2. + RCO3.

U2OH   1.72E-11    (No T Dependence)     HO. + AFG2 = C2CO-O2. + RCO3.
U2HV       (Phot. Set = ACROLEIN)        AFG2 + HV = HO2. + CO + CCO-O2. + RCO3.

G46    2.63E-11    (No T Dependence)     HO. + PHEN = 0.15 RO2-NP. + 0.85 RO2-R. + 0.2 GLY +
                                             4.7 -C + RO2.
G51    3.60E-12    (No T Dependence)     NO3 + PHEN = HNO3 + BZ-O.
G52    4.20E-11    (No T Dependence)     HO. + CRES = 0.15 RO2-NP. + 0.85 RO2-R. + 0.2 MGLY +
                                             5.5 -C + RO2.
G57    2.10E-11    (No T Dependence)     NO3 + CRES = HNO3 + BZ-O. + -C
G30    1.29E-11    (No T Dependence)     BALD + HO. = BZ-CO-O2. + RCO3.
G31        (Phot. Set = BZCHO   )        BALD + HV + #0.05 = 7 -C
G32    2.61E-15  1.40E-12  3.75  0.00    BALD + NO3 = HNO3 + BZ-CO-O2.

G58    3.60E-12    (No T Dependence)     NPHE + NO3 = HNO3 + BZ(NO2)-O.
G59        (Same k as for BZ-O.   )      BZ(NO2)-O. + NO2 = 2 -N + 6 -C
G60        (Same k as for RO2.    )      BZ(NO2)-O. + HO2. = NPHE
G61        (Same k as for BZ-O.   )      BZ(NO2)-O. = NPHE

C13        (Same k as for RCO3.    )     CCO-O2. + NO = CO2 + NO2 + HCHO + RO2-R. + RO2.
C14        (Same k as for RCO3.    )     CCO-O2. + NO2 = PAN
C15        (Same k as for RCO3.    )     CCO-O2. + HO2. = -OOH + CO2 + HCHO
C16        (Same k as for RCO3.    )     CCO-O2. + RO2. = RO2. + 0.5 HO2. + CO2 + HCHO
C17        (Same k as for RCO3.    )     CCO-O2. + RCO3. = RCO3. + HO2. + CO2 + HCHO
C18    6.50E-04   (Falloff Kinetics)     PAN = CCO-O2. + NO2 + RCO3.
        k0   =   4.90E-03 23.97  0.00
        kINF =   4.00E+16 27.08  0.00
                 F= 0.30  n= 1.00

C28        (Same k as for RCO3.    )     C2CO-O2. + NO = CCHO + RO2-R. + CO2 + NO2 + RO2.
C29    8.40E-12    (No T Dependence)     C2CO-O2. + NO2 = PPN
C30        (Same k as for RCO3.    )     C2CO-O2. + HO2. = -OOH + CCHO + CO2
C31        (Same k as for RCO3.    )     C2CO-O2. + RO2. = RO2. + 0.5 HO2. + CCHO + CO2
C32        (Same k as for RCO3.    )     C2CO-O2. + RCO3. = RCO3. + HO2. + CCHO + CO2
C33    6.78E-04  1.60E+17 27.97  0.00    PPN = C2CO-O2. + NO2 + RCO3.

C62        (Same k as for RCO3.    )     HCOCO-O2. + NO = NO2 + CO2 + CO + HO2.
C63        (Same k as for RCO3.    )     HCOCO-O2. + NO2 = GPAN
C65        (Same k as for RCO3.    )     HCOCO-O2. + HO2. = -OOH + CO2 + CO
C66        (Same k as for RCO3.    )     HCOCO-O2. + RO2. = RO2. + 0.5 HO2. + CO2 + CO
C67        (Same k as for RCO3.    )     HCOCO-O2. + RCO3. = RCO3. + HO2. + CO2 + CO
C64        (Same k as for PAN      )     GPAN = HCOCO-O2. + NO2 + RCO3.
```

Table A-2 (continued)

───

Rxn.	Kinetic Parameters [a]				Reactions [b]
Label	k(300)	A	Ea	B	

───

G33	(Same k as for RCO3.)				BZ-CO-O2. + NO = BZ-O. + CO2 + NO2 + R2O2. + RO2.
G43	3.53E-11	1.30E-11	-0.60	0.00	BZ-O. + NO2 = NPHE
G44	(Same k as for RO2.)				BZ-O. + HO2. = PHEN
G45	1.00E-03	(No T Dependence)			BZ-O. = PHEN
G34	8.40E-12	(No T Dependence)			BZ-CO-O2. + NO2 = PBZN
G36	(Same k as for RCO3.)				BZ-CO-O2. + HO2. = -OOH + CO2 + PHEN
G37	(Same k as for RCO3.)				BZ-CO-O2. + RO2. = RO2. + 0.5 HO2. + CO2 + PHEN
G38	(Same k as for RCO3.)				BZ-CO-O2. + RCO3. = RCO3. + HO2. + CO2 + PHEN
G35	2.17E-04	1.60E+15	25.90	0.00	PBZN = BZ-CO-O2. + NO2 + RCO3.

IPOH 3.36E-11 (No T Dependence) ISOPROD + HO. = 0.293 CO + 0.252 CCHO + 0.126 HCHO + 0.041 GLY + 0.021 RCHO + 0.168 MGLY + 0.314 MEK + 0.503 RO2-R. + 0.21 CCO-O2. + 0.288 C2CO-O2. + 0.21 R2O2. + 0.713 RO2. + 0.498 RCO3. + -0.112 -C

IPO3 7.11E-18 (No T Dependence) ISOPROD + O3 = 0.02 CCHO + 0.04 HCHO + 0.01 GLY + 0.84 MEK + 0.09 (HCHO2) + 0.09 (HCOCHO2) + 0.18 (HOCCHO2) + 0.06 (C2(O2)CHO) + 0.01 (C2(O2)COH) + -0.39 -C

IPHV (Phot. Set = ACROLEIN) ISOPROD + HV + 0.0036 = 0.333 CO + 0.067 CCHO + 0.9 HCHO + 0.033 MEK + 0.333 HO2. + 0.7 RO2-R. + 0.267 CCO-O2. + 0.7 C2CO-O2. + 0.7 RO2. + 0.967 RCO3. + -0.133 -C

IPN3 1.00E-15 (No T Dependence) ISOPROD + NO3 = 0.643 CO + 0.282 HCHO + 0.85 RNO3 + 0.357 RCHO + 0.925 HO2. + 0.075 C2CO-O2. + 0.075 R2O2. + 0.925 RO2. + 0.075 RCO3. + 0.075 HNO3 + -2.471 -C

Hydrocarbon Species Represented Explicitly

8.71E-15	6.25E-13	2.55	2.00	METHANE + HO. = RO2-R. + HCHO + RO2.
2.74E-13	1.28E-12	0.92	2.00	ETHANE + HO. = RO2-R. + CCHO + RO2.

2.56E-12 1.36E-12 -0.38 2.00 N-C4 + HO. = 0.076 RO2-N. + 0.924 RO2-R. + 0.397 R2O2. + 0.001 HCHO + 0.571 CCHO + 0.14 RCHO + 0.533 MEK + -0.076 -C + 1.397 RO2.

5.63E-12 1.35E-11 0.52 0.00 N-C6 + HO. = 0.185 RO2-N. + 0.815 RO2-R. + 0.738 R2O2. + 0.02 CCHO + 0.105 RCHO + 1.134 MEK + 0.186 -C + 1.738 RO2.

8.76E-12 3.15E-11 0.76 0.00 N-C8 + HO. = 0.333 RO2-N. + 0.667 RO2-R. + 0.706 R2O2. + 0.002 RCHO + 1.333 MEK + 0.998 -C + 1.706 RO2.

5.91E-12 1.81E-12 -0.70 0.00 TOLUENE + HO. = 0.085 BALD + 0.26 CRES + 0.118 GLY + 0.964 MGLY + 0.259 AFG2 + 0.74 RO2-R. + 0.26 HO2. + 0.681 -C + 0.74 RO2.

2.36E-11 (No T Dependence) M-XYLENE + HO. = 0.04 BALD + 0.18 CRES + 0.108 GLY + 1.599 MGLY + 0.461 AFG2 + 0.82 RO2-R. + 0.18 HO2. + 0.063 -C + 0.82 RO2. 0.82 RO2.

8.43E-12	1.96E-12	-0.87	0.00	ETHENE + HO. = RO2-R. + RO2. + 1.56 HCHO + 0.22 CCHO
1.68E-18	9.14E-15	5.13	0.00	ETHENE + O3 = HCHO + (HCHO2)
2.18E-16	4.39E-13	4.53	2.00	ETHENE + NO3 = R2O2. + RO2. + 2 HCHO + NO2
7.42E-13	1.04E-11	1.57	0.00	ETHENE + O = RO2-R. + HO2. + RO2. + HCHO + CO

2.60E-11 4.85E-12 -1.00 0.00 PROPENE + HO. = RO2-R. + RO2. + HCHO + CCHO
1.05E-17 5.51E-15 3.73 0.00 PROPENE + O3 = 0.6 HCHO + 0.4 CCHO + 0.4 (HCHO2) + 0.6 (CCHO2)
9.74E-15 4.59E-13 2.30 0.00 PROPENE + NO3 = R2O2. + RO2. + HCHO + CCHO + NO2
4.01E-12 1.18E-11 0.64 0.00 PROPENE + O = 0.4 HO2. + 0.5 RCHO + 0.5 MEK + -0.5 -C

6.30E-11 1.01E-11 -1.09 0.00 T-2-BUTE + HO. = RO2-R. + RO2. + 2 CCHO
1.95E-16 6.64E-15 2.10 0.00 T-2-BUTE + O3 = CCHO + (CCHO2)
3.92E-13 1.10E-13 -0.76 2.00 T-2-BUTE + NO3 = R2O2. + RO2. + 2 CCHO + NO2
2.34E-11 2.26E-11 -0.02 0.00 T-2-BUTE + O = 0.4 HO2. + 0.5 RCHO + 0.5 MEK + 0.5 -C

9.88E-11 2.54E-11 -0.81 0.00 ISOP + HO. = 0.088 RO2-N. + 0.912 RO2-R. + 0.629 HCHO + 0.912 ISOPROD + 0.079 R2O2. + 1.079 RO2. + 0.283 -C
1.34E-17 7.86E-15 3.80 0.00 ISOP + O3 = 0.4 HCHO + 0.6 ISOPROD + 0.55 (HCHO2) + 0.2 (C:CC(C)O2) + 0.05 (C:C(C)CHO2)
3.60E-11 (No T Dependence) ISOP + O = 0.75 "ISOPROD + -C "+ 0.25 "C2CO-O2. + RCO3. + 2 HCHO + RO2-R. + RO2."
6.81E-13 3.03E-12 0.89 0.00 ISOP + NO3 = 0.8 "RCHO + RNO3 + RO2-R." + 0.2 "ISOPROD + R2O2. + NO2" + RO2. + -2.2 -C

Table A-2 (continued)

───

Rxn.	Kinetic Parameters [a]				Reactions [b]
Label	k(300)	A	Ea	B	

───

```
        1.50E-19   (No T Dependence)   ISOP + NO2 = 0.8 "RCHO + RNO3 + RO2-R." + 0.2 "ISOPROD +
                                         R2O2. + NO" + RO2. + -2.2 -C

        5.31E-11  1.21E-11 -0.88  0.00  APIN + HO. = RO2-R. + RCHO + RO2. + 7 -C
        1.00E-16  9.90E-16  1.37  0.00  APIN + O3 = 0.05 HCHO + 0.2 CCHO + 0.5 RCHO + 0.61 MEK +
                                         0.075 CO + 0.1 O3OL-SB + 0.05 CCO-O2. + 0.05 C2CO-O2. +
                                         0.1 RCO3. + 0.105 HO2. + 0.16 HO. + 0.135 RO2-R. +
                                         0.15 R2O2. + 0.285 RO2. + 5.285 -C
        6.10E-12  1.19E-12 -0.97  0.00  APIN + NO3 = NO2 + R2O2. + RCHO + RO2. + 7 -C

        3.00E-11   (No T Dependence)   APIN + O = 0.4 HO2. + 0.5 MEK + 0.5 RCHO + 6.5 -C
        6.57E-11   (No T Dependence)   UNKN + HO. = RO2-R. + RO2. + 0.5 HCHO + RCHO + 6.5 -C
        5.85E-17   (No T Dependence)   UNKN + O3 = 0.135 RO2-R. + 0.135 HO2. + 0.075 R2O2. +
                                         0.21 RO2. + 0.025 CCO-O2. + 0.025 C2CO-O2. + 0.05 RCO3. +
                                         0.275 HCHO + 0.175 CCHO + 0.5 RCHO + 0.41 MEK + 0.185 CO +
                                         5.925 -C + 0.11 HO. + 0.192 O3OL-SB
        4.30E-12   (No T Dependence)   UNKN + NO3 = R2O2. + RO2. + 0.5 HCHO + RCHO + 6.5 -C + NO2
        2.90E-11   (No T Dependence)   UNKN + O = 0.4 HO2. + 0.5 RCHO + 0.5 MEK + 6.5 -C
```

Models for PTI and MDI Reactions [c]

```
  A     5.90E-12   (No T Dependence)   PTI + HO. = HO. + CRES + 0.12 xNO2
  B     5.90E-12   (No T Dependence)   PTI + HO. = 0.2 HO. + 0.7 HO2. + CRES + 0.3 MGLY
  C     5.90E-12   (No T Dependence)   PTI + HO. = 0.6 HO2. + 0.2 (RO2-R. + RO2.) + 0.2 (RO2-NP. +
                                         RO2.) + MGLY


  A     1.18E-12   (No T Dependence)   MDI + HO. = HO. + CRES + 0.12 xNO2
  B     1.18E-12   (No T Dependence)   MDI + HO. = 0.2 HO. + 0.7 HO2. + CRES + 0.3 MGLY
  C     1.18E-12   (No T Dependence)   MDI + HO. = 0.6 HO2. + 0.2 (RO2-R. + RO2.) + 0.2 (RO2-NP. +
                                         RO2.) + MGLY
```

Lumped Species used in EKMA Simulations [d]

```
A1OH  3.46E-12  2.56E-12 -0.18  0.00  ALK1 + HO. = 0.911 RO2-R. + 0.074 RO2-N. + 0.005 RO2-XN. +
                                        0.011 HO2. + 0.575 R2O2. + 1.564 RO2. + 0.065 HCHO +
                                        0.339 CCHO + 0.196 RCHO + 0.322 ACET + 0.448 MEK +
                                        0.024 CO + 0.025 GLY + 0.051 -C

A2OH  9.14E-12  5.12E-12 -0.35  0.00  ALK2 + HO. = 0.749 RO2-R. + 0.249 RO2-N. + 0.002 RO2-XN. +
                                        0.891 R2O2. + 1.891 RO2. + 0.029 HCHO + 0.048 CCHO +
                                        0.288 RCHO + 0.028 ACET + 1.105 MEK + 0.043 CO +
                                        0.018 CO2 + 1.268 -C

B1OH  5.87E-12   (No T Dependence)   ARO1 + HO. = 0.742 RO2-R. + 0.258 HO2. + 0.742 RO2. +
                                        0.015 PHEN + 0.244 CRES + 0.08 BALD + 0.124 GLY +
                                        0.681 MGLY + 0.11 AFG1 + 0.244 AFG2 + 1.857 -C

B2OH  3.22E-11  1.20E-11 -0.59  0.00  ARO2 + HO. = 0.82 RO2-R. + 0.18 HO2. + 0.82 RO2. +
                                        0.18 CRES + 0.036 BALD + 0.068 GLY + 1.02 MGLY +
                                        0.532 AFG2 + 2.588 -C

O2OH  3.17E-11  2.22E-12 -1.59  0.00  OLE2 + HO. = 0.858 RO2-R. + 0.142 RO2-N. + RO2. +
                                        0.858 HCHO + 0.252 CCHO + 0.606 RCHO + 1.267 -C
O2O3  1.08E-17  1.42E-15  2.91  0.00  OLE2 + O3 = 0.6 HCHO + 0.635 RCHO + 0.981 -C + 0.4 (HCHO2) +
                                        0.529 (CCHO2) + 0.071 (RCHO2)
O2N3  1.16E-14  1.99E-13  1.69  0.00  OLE2 + NO3 = R2O2. + RO2. + HCHO + 0.294 CCHO + 0.706 RCHO +
                                        1.451 -C + NO2
O2OA  4.11E-12  4.51E-12  0.06  0.00  OLE2 + O = 0.4 HO2. + 0.5 RCHO + 0.5 MEK + 1.657 -C

O3OH  6.23E-11  4.54E-12 -1.56  0.00  OLE3 + HO. = 0.861 RO2-R. + 0.139 RO2-N. + RO2. +
                                        0.24 HCHO + 0.661 CCHO + 0.506 RCHO + 0.113 ACET +
                                        0.086 MEK + 0.057 BALD + 0.848 -C
O3O3  1.70E-16  1.77E-15  1.40  0.00  OLE3 + O3 = 0.203 HCHO + 0.358 CCHO + 0.309 RCHO +
                                        0.061 MEK + 0.027 BALD + 0.976 -C + 0.076 (HCHO2) +
                                        0.409 (CCHO2) + 0.279 (RCHO2) + 0.158 (C(C)CO2 +
                                        0.039 (C(R)CO2 + 0.04 (BZCHO2)
O3N3  1.07E-12  3.19E-13 -0.72  0.00  OLE3 + NO3 = R2O2. + RO2. + 0.278 HCHO + 0.767 CCHO +
                                        0.588 RCHO + 0.131 ACET + 0.1 MEK + 0.066 BALD +
                                        0.871 -C + NO2
O3OA  2.52E-11  8.66E-12 -0.64  0.00  OLE3 + O = 0.4 HO2. + 0.5 RCHO + 0.5 MEK + 2.205 -C
```

Table A-2 (continued)
_____

```
Rxn.        Kinetic Parameters [a]
        _____       Reactions [b]
Label  k(300)     A        Ea    B
```
_____

```
                                      0.001 RCHO + 1.223 MEK + 5.004 -C + 1.644 RO2.
```

Reactions used to Represent Chamber-Dependent Processes [e]

```
O3W    (varied)  (No T Dependence)   O3 =
N25I   (varied)  (No T Dependence)   N2O5 = 2 NOX-WALL
N25S   (varied)  (No T Dependence)   N2O5 + H2O = 2 NOX-WALL
NO2W   (varied)  (No T Dependence)   NO2 = (yHONO) HONO + (1-yHONO) NOX-WALL
XSHC   (varied)  (No T Dependence)   HO. = HO2.
RSI      (Phot. Set = NO2    )       HV + #RS/K1 = HO.
ONO2     (Phot. Set = NO2    )       HV + #E-NO2/K1 = NO2 + #-1 NOX-WALL
```

_____

[a] Except as noted, the expression for the rate constant is $k = A\ e^{Ea/RT}\ (T/300)^B$. Rate constants and
     A factor are in cm, molecule, sec. units. Units of Ea is kcal mole^{-1}. "Phot Set" means this is
     a photolysis reaction, with the absorption coefficients and quantum yields given in Table A-3. In
     addition, if "#(number)" or "#(parameter)" is given as a reactant, then the value of that number
     or parameter is multiplied by the result in the "rate constant expression" columns to obtain the
     rate constant used. Furthermore, "#RCONnn" as a reactant means that the rate constant for the
     reaction is obtained by multiplying the rate constant given by that for reaction "nn". Thus, the
     rate constant given is actually an equilibrium constant.
[b] The format of the reaction listing is the same as that used in the documentation of the detailed
     mechanism (Carter 1990).
[c] First column gives model designation for alternative PTI or MDI mechanisms which were examined.
     See text.
[d] The rate constants and product yield parameters are based on the mixture of species in the base ROG
     mixture which are being represented.
[e] See Table A-4 for the values of the parameters used for the specific chambers modeled in this study.

Table A-3.   Absorption cross sections and quantum yields for photolysis reactions.

WL (nm)	Abs (cm^2)	QY	WL (nm)	Abs (cm^2)	QY	WL (nm)	Abs (cm^2)	QY	WL (nm)	Abs (cm^2)	QY	WL (nm)	Abs (cm^2)	QY

Photolysis File = NO2

WL	Abs	QY	WL	Abs	QY	WL	Abs	QY	WL	Abs	QY	WL	Abs	QY
250.0	2.83E-20	1.000	255.0	1.45E-20	1.000	260.0	1.90E-20	1.000	265.0	2.05E-20	1.000	270.0	3.13E-20	1.000
275.0	4.02E-20	1.000	280.0	5.54E-20	1.000	285.0	6.99E-20	1.000	290.0	8.18E-20	0.999	295.0	9.67E-20	0.998
300.0	1.17E-19	0.997	305.0	1.66E-19	0.996	310.0	1.76E-19	0.995	315.0	2.25E-19	0.994	320.0	2.54E-19	0.993
325.0	2.79E-19	0.992	330.0	2.99E-19	0.991	335.0	3.45E-19	0.990	340.0	3.88E-19	0.989	345.0	4.07E-19	0.988
350.0	4.10E-19	0.987	355.0	5.13E-19	0.986	360.0	4.51E-19	0.984	365.0	5.78E-19	0.983	370.0	5.42E-19	0.981
375.0	5.35E-19	0.979	380.0	5.99E-19	0.975	381.0	5.98E-19	0.974	382.0	5.97E-19	0.973	383.0	5.96E-19	0.972
384.0	5.95E-19	0.971	385.0	5.94E-19	0.969	386.0	5.95E-19	0.967	387.0	5.96E-19	0.966	388.0	5.98E-19	0.964
389.0	5.99E-19	0.962	390.0	6.00E-19	0.960	391.0	5.98E-19	0.959	392.0	5.96E-19	0.957	393.0	5.93E-19	0.953
394.0	5.91E-19	0.950	395.0	5.89E-19	0.942	396.0	6.06E-19	0.922	397.0	6.24E-19	0.870	398.0	6.41E-19	0.820
399.0	6.59E-19	0.760	400.0	6.76E-19	0.695	401.0	6.67E-19	0.635	402.0	6.58E-19	0.560	403.0	6.50E-19	0.485
404.0	6.41E-19	0.425	405.0	6.32E-19	0.350	406.0	6.21E-19	0.290	407.0	6.10E-19	0.225	408.0	5.99E-19	0.185
409.0	5.88E-19	0.153	410.0	5.77E-19	0.130	411.0	5.88E-19	0.110	412.0	5.98E-19	0.094	413.0	6.09E-19	0.083
414.0	6.19E-19	0.070	415.0	6.30E-19	0.059	416.0	6.29E-19	0.048	417.0	6.27E-19	0.039	418.0	6.26E-19	0.030
419.0	6.24E-19	0.023	420.0	6.23E-19	0.018	421.0	6.18E-19	0.012	422.0	6.14E-19	0.008	423.0	6.09E-19	0.004
424.0	6.05E-19	0.000	425.0	6.00E-19	0.000									

Photolysis File = NO3NO

WL	Abs	QY	WL	Abs	QY	WL	Abs	QY	WL	Abs	QY
585.0	2.77E-18	0.000	590.0	5.14E-18	0.250	595.0	4.08E-18	0.400	600.0	2.83E-18	0.250	605.0	3.45E-18	0.200
610.0	1.48E-18	0.200	615.0	1.96E-18	0.100	620.0	3.58E-18	0.100	625.0	9.25E-18	0.050	630.0	5.66E-18	0.050
635.0	1.45E-18	0.030	640.0	1.11E-18	0.000									

Photolysis File = NO3NO2

WL	Abs	QY	WL	Abs	QY	WL	Abs	QY	WL	Abs	QY	WL	Abs	QY
400.0	0.00E+00	1.000	405.0	3.00E-20	1.000	410.0	4.00E-20	1.000	415.0	5.00E-20	1.000	420.0	8.00E-20	1.000
425.0	1.00E-19	1.000	430.0	1.30E-19	1.000	435.0	1.80E-19	1.000	440.0	1.90E-19	1.000	445.0	2.20E-19	1.000
450.0	2.80E-19	1.000	455.0	3.30E-19	1.000	460.0	3.70E-19	1.000	465.0	4.30E-19	1.000	470.0	5.10E-19	1.000
475.0	6.00E-19	1.000	480.0	6.40E-19	1.000	485.0	6.90E-19	1.000	490.0	8.80E-19	1.000	495.0	9.50E-19	1.000
500.0	1.01E-18	1.000	505.0	1.10E-18	1.000	510.0	1.32E-18	1.000	515.0	1.40E-18	1.000	520.0	1.45E-18	1.000
525.0	1.48E-18	1.000	530.0	1.94E-18	1.000	535.0	2.04E-18	1.000	540.0	1.81E-18	1.000	545.0	1.81E-18	1.000
550.0	2.36E-18	1.000	555.0	2.68E-18	1.000	560.0	3.07E-18	1.000	565.0	2.53E-18	1.000	570.0	2.54E-18	1.000
575.0	2.74E-18	1.000	580.0	3.05E-18	1.000	585.0	2.77E-18	1.000	590.0	5.14E-18	0.750	595.0	4.08E-18	0.600
600.0	2.83E-18	0.550	605.0	3.45E-18	0.400	610.0	1.45E-18	0.300	615.0	1.96E-18	0.250	620.0	3.58E-18	0.200
625.0	9.25E-18	0.150	630.0	5.66E-18	0.050	635.0	1.45E-18	0.000						

Photolysis File = O3O3P

WL	Abs	QY	WL	Abs	QY	WL	Abs	QY	WL	Abs	QY	WL	Abs	QY
280.0	3.97E-18	0.100	281.0	3.60E-18	0.100	282.0	3.24E-18	0.100	283.0	3.01E-18	0.100	284.0	2.73E-18	0.100
285.0	2.44E-18	0.100	286.0	2.21E-18	0.100	287.0	2.01E-18	0.100	288.0	1.76E-18	0.100	289.0	1.58E-18	0.100
290.0	1.41E-18	0.100	291.0	1.26E-18	0.100	292.0	1.10E-18	0.100	293.0	9.89E-19	0.100	294.0	8.59E-19	0.100
295.0	7.70E-19	0.100	296.0	6.67E-19	0.100	297.0	5.84E-19	0.100	298.0	5.07E-19	0.100	299.0	4.52E-19	0.100
300.0	3.92E-19	0.100	301.0	3.42E-19	0.100	302.0	3.06E-19	0.100	303.0	2.60E-19	0.100	304.0	2.37E-19	0.100
305.0	2.01E-19	0.112	306.0	1.79E-19	0.149	307.0	1.56E-19	0.197	308.0	1.38E-19	0.259	309.0	1.25E-19	0.339
310.0	1.02E-19	0.437	311.0	9.17E-20	0.546	312.0	7.88E-20	0.652	313.0	6.77E-20	0.743	314.0	6.35E-20	0.816
315.0	5.10E-20	0.872	316.0	4.61E-20	0.916	317.0	4.17E-20	0.949	318.0	3.72E-20	0.976	319.0	2.69E-20	0.997
320.0	3.23E-20	1.000	330.0	6.70E-21	1.000	340.0	1.70E-21	1.000	350.0	4.00E-22	1.000	355.0	0.00E+00	1.000
400.0	0.00E+00	1.000	450.0	1.60E-22	1.000	500.0	1.34E-21	1.000	550.0	3.32E-21	1.000	600.0	5.06E-21	1.000
650.0	2.45E-21	1.000	700.0	8.70E-22	1.000	750.0	3.20E-22	1.000	800.0	1.60E-22	1.000	900.0	0.00E+00	1.000

Photolysis File = O3O1D

WL	Abs	QY	WL	Abs	QY	WL	Abs	QY	WL	Abs	QY	WL	Abs	QY
280.0	3.97E-18	0.900	281.0	3.60E-18	0.900	282.0	3.24E-18	0.900	283.0	3.01E-18	0.900	284.0	2.73E-18	0.900
285.0	2.44E-18	0.900	286.0	2.21E-18	0.900	287.0	2.01E-18	0.900	288.0	1.76E-18	0.900	289.0	1.58E-18	0.900
290.0	1.41E-18	0.900	291.0	1.26E-18	0.900	292.0	1.10E-18	0.900	293.0	9.89E-19	0.900	294.0	8.59E-19	0.900
295.0	7.70E-19	0.900	296.0	6.67E-19	0.900	297.0	5.84E-19	0.900	298.0	5.07E-19	0.900	299.0	4.52E-19	0.900
300.0	3.92E-19	0.900	301.0	3.42E-19	0.900	302.0	3.06E-19	0.900	303.0	2.60E-19	0.900	304.0	2.37E-19	0.900
305.0	2.01E-19	0.888	306.0	1.79E-19	0.851	307.0	1.56E-19	0.803	308.0	1.38E-19	0.741	309.0	1.25E-19	0.661
310.0	1.02E-19	0.563	311.0	9.17E-20	0.454	312.0	7.88E-20	0.348	313.0	6.77E-20	0.257	314.0	6.35E-20	0.184
315.0	5.10E-20	0.128	316.0	4.61E-20	0.084	317.0	4.17E-20	0.051	318.0	3.72E-20	0.024	319.0	2.69E-20	0.003
320.0	3.23E-20	0.000												

Photolysis File = HONO

WL	Abs	QY	WL	Abs	QY	WL	Abs	QY	WL	Abs	QY	WL	Abs	QY
311.0	0.00E+00	1.000	312.0	2.00E-21	1.000	313.0	4.20E-21	1.000	314.0	4.60E-21	1.000	315.0	4.20E-21	1.000
316.0	3.00E-21	1.000	317.0	4.60E-21	1.000	318.0	3.60E-20	1.000	319.0	6.10E-20	1.000	320.0	2.10E-20	1.000
321.0	4.27E-20	1.000	322.0	4.01E-20	1.000	323.0	3.93E-20	1.000	324.0	4.01E-20	1.000	325.0	4.04E-20	1.000
326.0	3.13E-20	1.000	327.0	4.12E-20	1.000	328.0	7.55E-20	1.000	329.0	6.64E-20	1.000	330.0	7.29E-20	1.000
331.0	8.70E-20	1.000	332.0	1.38E-19	1.000	333.0	5.91E-20	1.000	334.0	5.91E-20	1.000	335.0	6.45E-20	1.000
336.0	5.91E-20	1.000	337.0	4.58E-20	1.000	338.0	1.91E-19	1.000	339.0	1.63E-19	1.000	340.0	1.05E-19	1.000
341.0	8.70E-20	1.000	342.0	3.35E-19	1.000	343.0	2.01E-19	1.000	344.0	1.02E-19	1.000	345.0	8.54E-20	1.000
346.0	8.32E-20	1.000	347.0	8.20E-20	1.000	348.0	7.49E-20	1.000	349.0	7.13E-20	1.000	350.0	6.83E-20	1.000
351.0	1.74E-19	1.000	352.0	1.14E-19	1.000	353.0	3.71E-19	1.000	354.0	4.96E-19	1.000	355.0	2.46E-19	1.000
356.0	1.19E-19	1.000	357.0	9.35E-20	1.000	358.0	7.78E-20	1.000	359.0	7.29E-20	1.000	360.0	6.83E-20	1.000
361.0	6.90E-20	1.000	362.0	7.32E-20	1.000	363.0	9.00E-20	1.000	364.0	1.21E-19	1.000	365.0	1.33E-19	1.000
366.0	2.13E-19	1.000	367.0	3.52E-19	1.000	368.0	4.50E-19	1.000	369.0	2.93E-19	1.000	370.0	1.19E-19	1.000
371.0	9.46E-20	1.000	372.0	8.85E-20	1.000	373.0	7.44E-20	1.000	374.0	4.77E-20	1.000	375.0	2.70E-20	1.000
376.0	1.90E-20	1.000	377.0	1.50E-20	1.000	378.0	1.90E-20	1.000	379.0	5.80E-20	1.000	380.0	7.78E-20	1.000
381.0	1.14E-19	1.000	382.0	1.40E-19	1.000	383.0	1.72E-19	1.000	384.0	1.99E-19	1.000	385.0	1.90E-19	1.000
386.0	1.19E-19	1.000	387.0	5.65E-20	1.000	388.0	3.20E-20	1.000	389.0	1.90E-20	1.000	390.0	1.20E-20	1.000
391.0	5.00E-21	1.000	392.0	0.00E+00	1.000									

Photolysis File = H2O2

WL	Abs	QY	WL	Abs	QY	WL	Abs	QY	WL	Abs	QY	WL	Abs	QY
250.0	8.30E-20	1.000	255.0	6.70E-20	1.000	260.0	5.20E-20	1.000	265.0	4.20E-20	1.000	270.0	3.20E-20	1.000
275.0	2.50E-20	1.000	280.0	2.00E-20	1.000	285.0	1.50E-20	1.000	290.0	1.13E-20	1.000	295.0	8.70E-21	1.000
300.0	6.60E-21	1.000	305.0	4.90E-21	1.000	310.0	3.70E-21	1.000	315.0	2.80E-21	1.000	320.0	2.00E-21	1.000
325.0	1.50E-21	1.000	330.0	1.20E-21	1.000	335.0	9.00E-22	1.000	340.0	7.00E-22	1.000	345.0	5.00E-22	1.000
350.0	3.00E-22	1.000	355.0	0.00E+00	1.000									

Table A-3. (continued)

WL (nm)	Abs (cm^2)	QY	WL (nm)	Abs (cm^2)	QY	WL (nm)	Abs (cm^2)	QY	WL (nm)	Abs (cm^2)	QY	WL (nm)	Abs (cm^2)	QY

Photolysis File = CO2H

WL (nm)	Abs (cm^2)	QY	WL (nm)	Abs (cm^2)	QY	WL (nm)	Abs (cm^2)	QY	WL (nm)	Abs (cm^2)	QY	WL (nm)	Abs (cm^2)	QY
210.0	3.75E-19	1.000	220.0	2.20E-19	1.000	230.0	1.38E-19	1.000	240.0	8.80E-20	1.000	250.0	5.80E-20	1.000
260.0	3.80E-20	1.000	270.0	2.50E-20	1.000	280.0	1.50E-20	1.000	290.0	9.00E-21	1.000	300.0	5.80E-21	1.000
310.0	3.40E-21	1.000	320.0	1.90E-21	1.000	330.0	1.10E-21	1.000	340.0	6.00E-22	1.000	350.0	4.00E-22	1.000
360.0	0.00E+00	1.000												

Photolysis File = HCHONEWR

WL (nm)	Abs (cm^2)	QY	WL (nm)	Abs (cm^2)	QY	WL (nm)	Abs (cm^2)	QY	WL (nm)	Abs (cm^2)	QY	WL (nm)	Abs (cm^2)	QY
280.0	2.49E-20	0.590	280.5	1.42E-20	0.596	281.0	1.51E-20	0.602	281.5	1.32E-20	0.608	282.0	9.73E-21	0.614
282.5	6.76E-21	0.620	283.0	5.82E-21	0.626	283.5	9.10E-21	0.632	284.0	3.71E-20	0.638	284.5	4.81E-20	0.644
285.0	3.95E-20	0.650	285.5	2.87E-20	0.656	286.0	2.24E-20	0.662	286.5	1.74E-20	0.668	287.0	1.13E-20	0.674
287.5	1.10E-20	0.680	288.0	2.62E-20	0.686	288.5	4.00E-20	0.692	289.0	3.55E-20	0.698	289.5	2.12E-20	0.704
290.0	1.07E-20	0.710	290.5	1.35E-20	0.713	291.0	1.99E-20	0.717	291.5	1.56E-20	0.721	292.0	8.65E-21	0.724
292.5	5.90E-21	0.727	293.0	1.11E-20	0.731	293.5	6.26E-20	0.735	294.0	7.40E-20	0.738	294.5	5.36E-20	0.741
295.0	4.17E-20	0.745	295.5	3.51E-20	0.749	296.0	2.70E-20	0.752	296.5	1.75E-20	0.755	297.0	1.16E-20	0.759
297.5	1.51E-20	0.763	298.0	3.69E-20	0.766	298.5	4.40E-20	0.769	299.0	3.44E-20	0.773	299.5	2.02E-20	0.776
300.0	1.06E-20	0.780	300.4	7.01E-21	0.780	300.6	8.63E-21	0.779	300.8	1.47E-20	0.779	301.0	2.01E-20	0.779
301.2	2.17E-20	0.779	301.4	1.96E-20	0.779	301.6	1.54E-20	0.778	301.8	1.26E-20	0.778	302.0	1.03E-20	0.778
302.2	8.53E-21	0.778	302.4	7.13E-21	0.778	302.6	6.61E-21	0.777	302.8	1.44E-20	0.777	303.0	3.18E-20	0.777
303.2	3.81E-20	0.777	303.4	5.57E-20	0.777	303.6	6.91E-20	0.776	303.8	6.58E-20	0.776	304.0	6.96E-20	0.776
304.2	5.79E-20	0.776	304.4	5.24E-20	0.776	304.6	4.30E-20	0.775	304.8	3.28E-20	0.775	305.0	3.60E-20	0.775
305.2	5.12E-20	0.775	305.4	4.77E-20	0.775	305.6	4.43E-20	0.774	305.8	4.60E-20	0.774	306.0	4.01E-20	0.774
306.2	3.28E-20	0.774	306.4	2.66E-20	0.774	306.6	2.42E-20	0.773	306.8	1.95E-20	0.773	307.0	1.58E-20	0.773
307.2	1.37E-20	0.773	307.4	1.19E-20	0.773	307.6	1.01E-20	0.772	307.8	9.01E-21	0.772	308.0	8.84E-21	0.772
308.2	2.08E-20	0.772	308.4	2.39E-20	0.772	308.6	3.08E-20	0.771	308.8	3.39E-20	0.771	309.0	3.18E-20	0.771
309.2	3.06E-20	0.771	309.4	2.84E-20	0.771	309.6	2.46E-20	0.770	309.8	1.95E-20	0.770	310.0	1.57E-20	0.770
310.2	1.26E-20	0.767	310.4	9.26E-21	0.764	310.6	7.71E-21	0.761	310.8	6.05E-21	0.758	311.0	5.13E-21	0.755
311.2	4.82E-21	0.752	311.4	4.54E-21	0.749	311.6	6.81E-21	0.746	311.8	1.04E-20	0.743	312.0	1.43E-20	0.740
312.2	1.47E-20	0.737	312.4	1.35E-20	0.734	312.6	1.13E-20	0.731	312.8	9.86E-21	0.728	313.0	7.82E-21	0.725
313.2	6.48E-21	0.722	313.4	1.07E-20	0.719	313.6	2.39E-20	0.716	313.8	3.80E-20	0.713	314.0	5.76E-20	0.710
314.2	6.14E-20	0.707	314.4	7.45E-20	0.704	314.6	5.78E-20	0.701	314.8	5.59E-20	0.698	315.0	4.91E-20	0.695
315.2	4.37E-20	0.692	315.4	3.92E-20	0.689	315.6	2.89E-20	0.686	315.8	2.82E-20	0.683	316.0	2.10E-20	0.680
316.2	1.66E-20	0.677	316.4	2.05E-20	0.674	316.6	4.38E-20	0.671	316.8	5.86E-20	0.668	317.0	6.28E-20	0.665
317.2	5.07E-20	0.662	317.4	4.33E-20	0.659	317.6	4.17E-20	0.656	317.8	3.11E-20	0.653	318.0	2.64E-20	0.650
318.2	2.24E-20	0.647	318.4	1.70E-20	0.644	318.6	1.24E-20	0.641	318.8	1.11E-20	0.638	319.0	7.70E-21	0.635
319.2	6.36E-21	0.632	319.4	5.36E-21	0.629	319.6	4.79E-21	0.626	319.8	6.48E-21	0.623	320.0	1.48E-20	0.620
320.2	1.47E-20	0.614	320.4	1.36E-20	0.608	320.6	1.69E-20	0.601	320.8	1.32E-20	0.595	321.0	1.49E-20	0.589
321.2	1.17E-20	0.583	321.4	1.15E-20	0.577	321.6	9.64E-21	0.570	321.8	7.26E-21	0.564	322.0	5.94E-21	0.558
322.2	4.13E-21	0.552	322.4	3.36E-21	0.546	322.6	2.39E-21	0.539	322.8	2.01E-21	0.533	323.0	1.76E-21	0.527
323.2	2.82E-21	0.521	323.4	4.65E-21	0.515	323.6	7.00E-21	0.508	323.8	7.80E-21	0.502	324.0	7.87E-21	0.496
324.2	6.59E-21	0.490	324.4	5.60E-21	0.484	324.6	4.66E-21	0.477	324.8	4.21E-21	0.471	325.0	7.77E-21	0.465
325.2	2.15E-20	0.459	325.4	3.75E-20	0.453	325.6	4.10E-20	0.446	325.8	6.47E-20	0.440	326.0	7.59E-20	0.434
326.2	6.51E-20	0.428	326.4	5.53E-20	0.422	326.6	5.76E-20	0.415	326.8	4.43E-20	0.409	327.0	3.44E-20	0.403
327.2	3.22E-20	0.397	327.4	2.13E-20	0.391	327.6	1.91E-20	0.384	327.8	1.42E-20	0.378	328.0	9.15E-21	0.372
328.2	6.79E-21	0.366	328.4	4.99E-21	0.360	328.6	4.77E-21	0.353	328.8	1.75E-20	0.347	329.0	3.27E-20	0.341
329.2	3.99E-20	0.335	329.4	5.13E-20	0.329	329.6	4.00E-20	0.322	329.8	3.61E-20	0.316	330.0	3.38E-20	0.310
330.2	3.08E-20	0.304	330.4	2.16E-20	0.298	330.6	2.09E-20	0.291	330.8	1.41E-20	0.285	331.0	9.95E-21	0.279
331.2	7.76E-21	0.273	331.4	6.16E-21	0.267	331.6	4.06E-21	0.260	331.8	3.03E-21	0.254	332.0	2.41E-21	0.248
332.2	1.74E-21	0.242	332.4	1.33E-21	0.236	332.6	2.70E-21	0.229	332.8	1.65E-21	0.223	333.0	1.17E-21	0.217
333.2	9.84E-22	0.211	333.4	8.52E-22	0.205	333.6	6.32E-22	0.198	333.8	5.21E-22	0.192	334.0	1.46E-21	0.186
334.2	1.80E-21	0.180	334.4	1.43E-21	0.174	334.6	1.03E-21	0.167	334.8	7.19E-22	0.161	335.0	4.84E-22	0.155
335.2	2.73E-22	0.149	335.4	1.34E-22	0.143	335.6	-1.62E-22	0.136	335.8	1.25E-22	0.130	336.0	4.47E-22	0.124
336.2	1.23E-21	0.118	336.4	2.02E-21	0.112	336.6	3.00E-21	0.105	336.8	2.40E-21	0.099	337.0	3.07E-21	0.093
337.2	2.29E-21	0.087	337.4	2.46E-21	0.081	337.6	2.92E-21	0.074	337.8	8.10E-21	0.068	338.0	1.82E-20	0.062
338.2	3.10E-20	0.056	338.4	3.24E-20	0.050	338.6	4.79E-20	0.043	338.8	5.25E-20	0.037	339.0	5.85E-20	0.031
339.2	4.33E-20	0.025	339.4	4.20E-20	0.019	339.6	3.99E-20	0.012	339.8	3.11E-20	0.006	340.0	2.72E-20	0.000

Photolysis File = HCHONEWM

WL (nm)	Abs (cm^2)	QY	WL (nm)	Abs (cm^2)	QY	WL (nm)	Abs (cm^2)	QY	WL (nm)	Abs (cm^2)	QY	WL (nm)	Abs (cm^2)	QY
280.0	2.49E-20	0.350	280.5	1.42E-20	0.346	281.0	1.51E-20	0.341	281.5	1.32E-20	0.336	282.0	9.73E-21	0.332
282.5	6.76E-21	0.327	283.0	5.82E-21	0.323	283.5	9.10E-21	0.319	284.0	3.71E-20	0.314	284.5	4.81E-20	0.309
285.0	3.95E-20	0.305	285.5	2.87E-20	0.301	286.0	2.24E-20	0.296	286.5	1.74E-20	0.291	287.0	1.13E-20	0.287
287.5	1.10E-20	0.282	288.0	2.62E-20	0.278	288.5	4.00E-20	0.273	289.0	3.55E-20	0.269	289.5	2.12E-20	0.264
290.0	1.07E-20	0.260	290.5	1.35E-20	0.258	291.0	1.99E-20	0.256	291.5	1.56E-20	0.254	292.0	8.65E-21	0.252
292.5	5.90E-21	0.250	293.0	1.11E-20	0.248	293.5	6.26E-20	0.246	294.0	7.40E-20	0.244	294.5	5.36E-20	0.242
295.0	4.17E-20	0.240	295.5	3.51E-20	0.238	296.0	2.70E-20	0.236	296.5	1.75E-20	0.234	297.0	1.16E-20	0.232
297.5	1.51E-20	0.230	298.0	3.69E-20	0.228	298.5	4.40E-20	0.226	299.0	3.44E-20	0.224	299.5	2.02E-20	0.222
300.0	1.06E-20	0.220	300.4	7.01E-21	0.220	300.6	8.63E-21	0.221	300.8	1.47E-20	0.221	301.0	2.01E-20	0.221
301.2	2.17E-20	0.221	301.4	1.96E-20	0.221	301.6	1.54E-20	0.222	301.8	1.26E-20	0.222	302.0	1.03E-20	0.222
302.2	8.53E-21	0.222	302.4	7.13E-21	0.222	302.6	6.61E-21	0.223	302.8	1.44E-20	0.223	303.0	3.18E-20	0.223
303.2	3.81E-20	0.223	303.4	5.57E-20	0.223	303.6	6.91E-20	0.224	303.8	6.58E-20	0.224	304.0	6.96E-20	0.224
304.2	5.79E-20	0.224	304.4	5.24E-20	0.224	304.6	4.30E-20	0.225	304.8	3.28E-20	0.225	305.0	3.60E-20	0.225
305.2	5.12E-20	0.225	305.4	4.77E-20	0.225	305.6	4.43E-20	0.226	305.8	4.60E-20	0.226	306.0	4.01E-20	0.226
306.2	3.28E-20	0.226	306.4	2.66E-20	0.226	306.6	2.42E-20	0.227	306.8	1.95E-20	0.227	307.0	1.58E-20	0.227
307.2	1.37E-20	0.227	307.4	1.19E-20	0.227	307.6	1.01E-20	0.228	307.8	9.01E-21	0.228	308.0	8.84E-21	0.228
308.2	2.08E-20	0.228	308.4	2.39E-20	0.228	308.6	3.08E-20	0.229	308.8	3.39E-20	0.229	309.0	3.18E-20	0.229
309.2	3.06E-20	0.229	309.4	2.84E-20	0.229	309.6	2.46E-20	0.230	309.8	1.95E-20	0.230	310.0	1.57E-20	0.230
310.2	1.26E-20	0.233	310.4	9.26E-21	0.236	310.6	7.71E-21	0.239	310.8	6.05E-21	0.242	311.0	5.13E-21	0.245
311.2	4.82E-21	0.248	311.4	4.54E-21	0.251	311.6	6.81E-21	0.254	311.8	1.04E-20	0.257	312.0	1.43E-20	0.260
312.2	1.47E-20	0.263	312.4	1.35E-20	0.266	312.6	1.13E-20	0.269	312.8	9.86E-21	0.272	313.0	7.82E-21	0.275
313.2	6.48E-21	0.278	313.4	1.07E-20	0.281	313.6	2.39E-20	0.284	313.8	3.80E-20	0.287	314.0	5.76E-20	0.290
314.2	6.14E-20	0.293	314.4	7.45E-20	0.296	314.6	5.78E-20	0.299	314.8	5.59E-20	0.302	315.0	4.91E-20	0.305
315.2	4.37E-20	0.308	315.4	3.92E-20	0.311	315.6	2.89E-20	0.314	315.8	2.82E-20	0.317	316.0	2.10E-20	0.320
316.2	1.66E-20	0.323	316.4	2.05E-20	0.326	316.6	4.38E-20	0.329	316.8	5.86E-20	0.332	317.0	6.28E-20	0.335
317.2	5.07E-20	0.338	317.4	4.33E-20	0.341	317.6	4.17E-20	0.344	317.8	3.11E-20	0.347	318.0	2.64E-20	0.350
318.2	2.24E-20	0.353	318.4	1.70E-20	0.356	318.6	1.24E-20	0.359	318.8	1.11E-20	0.362	319.0	7.70E-21	0.365

WL (nm)	Abs (cm^2)	QY	WL (nm)	Abs (cm^2)	QY	WL (nm)	Abs (cm^2)	QY	WL (nm)	Abs (cm^2)	QY	WL (nm)	Abs (cm^2)	QY
319.2	6.36E-21	0.368	319.4	5.36E-21	0.371	319.6	4.79E-21	0.374	319.8	6.48E-21	0.377	320.0	1.48E-20	0.380
320.2	1.47E-20	0.386	320.4	1.36E-20	0.392	320.6	1.69E-20	0.399	320.8	1.32E-20	0.405	321.0	1.49E-20	0.411
321.2	1.17E-20	0.417	321.4	1.15E-20	0.423	321.6	9.64E-21	0.430	321.8	7.26E-21	0.436	322.0	5.94E-21	0.442
322.2	4.13E-21	0.448	322.4	3.36E-21	0.454	322.6	2.39E-21	0.461	322.8	2.01E-21	0.467	323.0	1.76E-21	0.473
323.2	2.82E-21	0.479	323.4	4.65E-21	0.485	323.6	7.00E-21	0.492	323.8	7.80E-21	0.498	324.0	7.87E-21	0.504
324.2	6.59E-21	0.510	324.4	5.60E-21	0.516	324.6	4.66E-21	0.523	324.8	4.21E-21	0.529	325.0	7.77E-21	0.535
325.2	2.15E-20	0.541	325.4	3.75E-20	0.547	325.6	4.10E-20	0.554	325.8	6.47E-20	0.560	326.0	7.59E-20	0.566
326.2	6.51E-20	0.572	326.4	5.53E-20	0.578	326.6	5.76E-20	0.585	326.8	4.43E-20	0.591	327.0	3.44E-20	0.597
327.2	3.22E-20	0.603	327.4	2.13E-20	0.609	327.6	1.91E-20	0.616	327.8	1.42E-20	0.622	328.0	9.15E-21	0.628
328.2	6.79E-21	0.634	328.4	4.99E-21	0.640	328.6	4.77E-21	0.647	328.8	1.75E-20	0.653	329.0	3.27E-20	0.659
329.2	3.99E-20	0.665	329.4	5.13E-20	0.671	329.6	4.00E-20	0.678	329.8	3.61E-20	0.684	330.0	3.38E-20	0.690
330.2	3.08E-20	0.694	330.4	2.16E-20	0.699	330.6	2.09E-20	0.703	330.8	1.41E-20	0.708	331.0	9.95E-21	0.712
331.2	7.76E-21	0.717	331.4	6.16E-21	0.721	331.6	4.06E-21	0.726	331.8	3.03E-21	0.730	332.0	2.41E-21	0.735
332.2	1.74E-21	0.739	332.4	1.33E-21	0.744	332.6	2.70E-21	0.748	332.8	1.65E-21	0.753	333.0	1.17E-21	0.757
333.2	9.84E-22	0.762	333.4	8.52E-22	0.766	333.6	6.32E-22	0.771	333.8	5.21E-22	0.775	334.0	1.46E-21	0.780
334.2	1.80E-21	0.784	334.4	1.43E-21	0.789	334.6	1.03E-21	0.793	334.8	7.19E-22	0.798	335.0	4.84E-22	0.802
335.2	2.73E-22	0.798	335.4	1.34E-22	0.794	335.6	0.00E+00	0.790	335.8	1.25E-22	0.786	336.0	4.47E-22	0.782
336.2	1.23E-21	0.778	336.4	2.02E-21	0.773	336.6	3.00E-21	0.769	336.8	2.40E-21	0.764	337.0	3.07E-21	0.759
337.2	2.29E-21	0.754	337.4	2.46E-21	0.749	337.6	2.92E-21	0.745	337.8	8.10E-21	0.740	338.0	1.82E-20	0.734
338.2	3.10E-20	0.729	338.4	3.24E-20	0.724	338.6	4.79E-20	0.719	338.8	5.25E-20	0.714	339.0	5.85E-20	0.709
339.2	4.33E-20	0.703	339.4	4.20E-20	0.698	339.6	3.99E-20	0.693	339.8	3.11E-20	0.687	340.0	2.72E-20	0.682
340.2	1.99E-20	0.676	340.4	1.76E-20	0.671	340.6	1.39E-20	0.666	340.8	1.01E-20	0.660	341.0	6.57E-21	0.655
341.2	4.83E-21	0.649	341.4	3.47E-21	0.643	341.6	2.23E-21	0.638	341.8	1.55E-21	0.632	342.0	3.70E-21	0.627
342.2	4.64E-21	0.621	342.4	1.08E-20	0.616	342.6	1.14E-20	0.610	342.8	1.79E-20	0.604	343.0	2.33E-20	0.599
343.2	1.72E-20	0.593	343.4	1.55E-20	0.588	343.6	1.46E-20	0.582	343.8	1.38E-20	0.576	344.0	1.00E-20	0.571
344.2	8.26E-21	0.565	344.4	6.32E-21	0.559	344.6	4.28E-21	0.554	344.8	3.22E-21	0.548	345.0	2.54E-21	0.542
345.2	1.60E-21	0.537	345.4	1.15E-21	0.531	345.6	8.90E-22	0.525	345.8	6.50E-22	0.520	346.0	5.09E-22	0.514
346.2	5.15E-22	0.508	346.4	3.45E-22	0.503	346.6	3.18E-22	0.497	346.8	3.56E-22	0.491	347.0	3.24E-22	0.485
347.2	3.34E-22	0.480	347.4	2.88E-22	0.474	347.6	2.88E-22	0.468	347.8	9.37E-22	0.463	348.0	9.70E-22	0.457
348.2	7.60E-22	0.451	348.4	6.24E-22	0.446	348.6	4.99E-22	0.440	348.8	4.08E-22	0.434	349.0	3.39E-22	0.428
349.2	1.64E-22	0.423	349.4	1.49E-22	0.417	349.6	8.30E-23	0.411	349.8	2.52E-23	0.406	350.0	2.57E-23	0.400
350.2	0.00E+00	0.394	350.4	5.16E-23	0.389	350.6	0.00E+00	0.383	350.8	2.16E-23	0.377	351.0	7.07E-23	0.371
351.2	3.45E-23	0.366	351.4	1.97E-22	0.360	351.6	4.80E-22	0.354	351.8	3.13E-21	0.349	352.0	6.41E-21	0.343
352.2	8.38E-21	0.337	352.4	1.55E-20	0.331	352.6	1.86E-20	0.326	352.8	1.94E-20	0.320	353.0	2.78E-20	0.314
353.2	1.96E-20	0.309	353.4	1.67E-20	0.303	353.6	1.75E-20	0.297	353.8	1.63E-20	0.291	354.0	1.36E-20	0.286
354.2	1.07E-20	0.280	354.4	9.82E-21	0.274	354.6	8.66E-21	0.269	354.8	6.44E-21	0.263	355.0	4.84E-21	0.257
355.2	3.49E-21	0.251	355.4	2.41E-21	0.246	355.6	1.74E-21	0.240	355.8	1.11E-21	0.234	356.0	7.37E-22	0.229
356.2	4.17E-22	0.223	356.4	1.95E-22	0.217	356.6	1.50E-22	0.211	356.8	8.14E-23	0.206	357.0	0.00E+00	0.200

Photolysis File = CCHOR

WL (nm)	Abs (cm^2)	QY	WL (nm)	Abs (cm^2)	QY	WL (nm)	Abs (cm^2)	QY	WL (nm)	Abs (cm^2)	QY	WL (nm)	Abs (cm^2)	QY
260.0	2.00E-20	0.310	270.0	3.40E-20	0.390	280.0	4.50E-20	0.580	290.0	4.90E-20	0.530	295.0	4.50E-20	0.480
300.0	4.30E-20	0.430	305.0	3.40E-20	0.370	315.0	2.10E-20	0.170	320.0	1.80E-20	0.100	325.0	1.10E-20	0.040
330.0	6.90E-21	0.000												

Photolysis File = RCHO

WL (nm)	Abs (cm^2)	QY	WL (nm)	Abs (cm^2)	QY	WL (nm)	Abs (cm^2)	QY	WL (nm)	Abs (cm^2)	QY	WL (nm)	Abs (cm^2)	QY
280.0	5.26E-20	0.960	290.0	5.77E-20	0.910	300.0	5.05E-20	0.860	310.0	3.68E-20	0.600	320.0	1.66E-20	0.360
330.0	6.49E-21	0.200	340.0	1.44E-21	0.080	345.0	0.00E+00	0.020						

Photolysis File = ACET-93C

WL (nm)	Abs (cm^2)	QY	WL (nm)	Abs (cm^2)	QY	WL (nm)	Abs (cm^2)	QY	WL (nm)	Abs (cm^2)	QY	WL (nm)	Abs (cm^2)	QY
250.0	2.37E-20	0.760	260.0	3.66E-20	0.800	270.0	4.63E-20	0.640	280.0	5.05E-20	0.550	290.0	4.21E-20	0.300
300.0	2.78E-20	0.150	310.0	1.44E-20	0.050	320.0	4.80E-21	0.026	330.0	8.00E-22	0.017	340.0	1.00E-22	0.000
350.0	3.00E-23	0.000	360.0	0.00E+00	0.000									

Photolysis File = KETONE

WL (nm)	Abs (cm^2)	QY	WL (nm)	Abs (cm^2)	QY	WL (nm)	Abs (cm^2)	QY	WL (nm)	Abs (cm^2)	QY	WL (nm)	Abs (cm^2)	QY
210.0	1.10E-21	1.000	220.0	1.20E-21	1.000	230.0	4.60E-21	1.000	240.0	1.30E-20	1.000	250.0	2.68E-20	1.000
260.0	4.21E-20	1.000	270.0	5.54E-20	1.000	280.0	5.92E-20	1.000	290.0	5.16E-20	1.000	300.0	3.44E-20	1.000
310.0	1.53E-20	1.000	320.0	4.60E-21	1.000	330.0	1.10E-21	1.000	340.0	0.00E+00	1.000			

Photolysis File = GLYOXAL1

WL (nm)	Abs (cm^2)	QY	WL (nm)	Abs (cm^2)	QY	WL (nm)	Abs (cm^2)	QY	WL (nm)	Abs (cm^2)	QY	WL (nm)	Abs (cm^2)	QY
230.0	2.87E-21	1.000	235.0	2.87E-21	1.000	240.0	4.30E-21	1.000	245.0	5.73E-21	1.000	250.0	8.60E-21	1.000
255.0	1.15E-20	1.000	260.0	1.43E-20	1.000	265.0	1.86E-20	1.000	270.0	2.29E-20	1.000	275.0	2.58E-20	1.000
280.0	2.87E-20	1.000	285.0	3.30E-20	1.000	290.0	3.15E-20	1.000	295.0	3.30E-20	1.000	300.0	3.58E-20	1.000
305.0	2.72E-20	1.000	310.0	2.72E-20	1.000	312.5	2.87E-20	1.000	315.0	2.29E-20	1.000	320.0	1.43E-20	1.000
325.0	1.15E-20	1.000	327.5	1.43E-20	1.000	330.0	1.15E-20	1.000	335.0	2.87E-21	1.000	340.0	0.00E+00	1.000

Photolysis File = GLYOXAL2

WL (nm)	Abs (cm^2)	QY	WL (nm)	Abs (cm^2)	QY	WL (nm)	Abs (cm^2)	QY	WL (nm)	Abs (cm^2)	QY	WL (nm)	Abs (cm^2)	QY
355.0	0.00E+00	1.000	360.0	2.29E-21	1.000	365.0	2.87E-21	1.000	370.0	8.03E-21	1.000	375.0	1.00E-20	1.000
380.0	1.72E-20	1.000	382.0	1.58E-20	1.000	384.0	1.49E-20	1.000	386.0	1.49E-20	1.000	388.0	2.87E-20	1.000
390.0	3.15E-20	1.000	391.0	3.24E-20	1.000	392.0	3.04E-20	1.000	393.0	2.23E-20	1.000	394.0	2.63E-20	1.000
395.0	3.04E-20	1.000	396.0	2.63E-20	1.000	397.0	2.43E-20	1.000	398.0	3.24E-20	1.000	399.0	3.04E-20	1.000
400.0	2.84E-20	1.000	401.0	3.24E-20	1.000	402.0	4.46E-20	1.000	403.0	5.27E-20	1.000	404.0	4.26E-20	1.000
405.0	3.04E-20	1.000	406.0	3.04E-20	1.000	407.0	2.84E-20	1.000	408.0	2.43E-20	1.000	409.0	2.84E-20	1.000
410.0	6.08E-20	1.000	411.0	5.07E-20	1.000	411.5	6.08E-20	1.000	412.0	4.86E-20	1.000	413.0	8.31E-20	1.000
413.5	6.48E-20	1.000	414.0	7.50E-20	1.000	414.5	8.11E-20	1.000	415.0	8.11E-20	1.000	415.5	6.89E-20	1.000
416.0	4.26E-20	1.000	417.0	4.86E-20	1.000	418.0	5.88E-20	1.000	419.0	6.69E-20	1.000	420.0	3.85E-20	1.000
421.0	5.67E-20	1.000	421.5	4.46E-20	1.000	422.0	5.27E-20	1.000	422.5	1.05E-19	1.000	423.0	8.51E-20	1.000
424.0	6.08E-20	1.000	425.0	7.29E-20	1.000	426.0	1.18E-19	1.000	426.5	1.30E-19	1.000	427.0	1.07E-19	1.000
428.0	1.66E-19	1.000	429.0	4.05E-20	1.000	430.0	5.07E-20	1.000	431.0	4.86E-20	1.000	432.0	4.05E-20	1.000
433.0	3.65E-20	1.000	434.0	6.08E-20	1.000	434.5	6.08E-20	1.000	435.0	5.07E-20	1.000	436.0	8.11E-20	1.000
436.5	1.13E-19	1.000	437.0	5.27E-20	1.000	438.0	1.01E-19	1.000	438.5	1.38E-19	1.000	439.0	7.70E-20	1.000
440.0	2.47E-19	1.000	441.0	8.11E-20	1.000	442.0	6.08E-20	1.000	443.0	7.50E-20	1.000	444.0	9.32E-20	1.000
445.0	1.13E-19	1.000	446.0	5.27E-20	1.000	447.0	2.43E-20	1.000	448.0	2.84E-20	1.000	449.0	3.85E-20	1.000
450.0	6.08E-20	1.000	451.0	1.09E-19	1.000	451.5	9.32E-20	1.000	452.0	1.22E-19	1.000	453.0	2.39E-19	1.000
454.0	1.70E-19	1.000	455.0	3.40E-19	1.000	455.5	4.05E-19	1.000	456.0	1.01E-19	1.000	457.0	1.62E-20	1.000

Table A-3. (continued)

WL (nm)	Abs (cm^2)	QY	WL (nm)	Abs (cm^2)	QY	WL (nm)	Abs (cm^2)	QY	WL (nm)	Abs (cm^2)	QY	WL (nm)	Abs (cm^2)	QY
458.0	1.22E-20	1.000	458.5	1.42E-20	1.000	459.0	4.05E-21	1.000	460.0	4.05E-21	1.000	460.5	6.08E-21	1.000
461.0	2.03E-21	1.000	462.0	0.00E+00	1.000									

Photolysis File = MEGLYOX1

WL (nm)	Abs (cm^2)	QY	WL (nm)	Abs (cm^2)	QY	WL (nm)	Abs (cm^2)	QY	WL (nm)	Abs (cm^2)	QY	WL (nm)	Abs (cm^2)	QY
220.0	2.10E-21	1.000	225.0	2.10E-21	1.000	230.0	4.21E-21	1.000	235.0	7.57E-21	1.000	240.0	9.25E-21	1.000
245.0	8.41E-21	1.000	250.0	9.25E-21	1.000	255.0	9.25E-21	1.000	260.0	9.67E-21	1.000	265.0	1.05E-20	1.000
270.0	1.26E-20	1.000	275.0	1.43E-20	1.000	280.0	1.51E-20	1.000	285.0	1.43E-20	1.000	290.0	1.47E-20	1.000
295.0	1.18E-20	1.000	300.0	1.14E-20	1.000	305.0	9.25E-21	1.000	310.0	6.31E-21	1.000	315.0	5.47E-21	1.000
320.0	3.36E-21	1.000	325.0	1.68E-21	1.000	330.0	8.41E-22	1.000	335.0	0.00E+00	1.000			

Photolysis File = MEGLYOX2

WL (nm)	Abs (cm^2)	QY	WL (nm)	Abs (cm^2)	QY	WL (nm)	Abs (cm^2)	QY	WL (nm)	Abs (cm^2)	QY	WL (nm)	Abs (cm^2)	QY
350.0	0.00E+00	1.000	354.0	4.21E-22	1.000	358.0	1.26E-21	1.000	360.0	2.10E-21	1.000	362.0	2.10E-21	1.000
364.0	2.94E-21	1.000	366.0	3.36E-21	1.000	368.0	4.21E-21	1.000	370.0	5.47E-21	1.000	372.0	5.89E-21	1.000
374.0	7.57E-21	1.000	376.0	7.99E-21	1.000	378.0	8.83E-21	1.000	380.0	1.01E-20	1.000	382.0	1.09E-20	1.000
384.0	1.35E-20	1.000	386.0	1.51E-20	1.000	388.0	1.72E-20	1.000	390.0	2.06E-20	1.000	392.0	2.10E-20	1.000
394.0	2.31E-20	1.000	396.0	2.48E-20	1.000	398.0	2.61E-20	1.000	400.0	2.78E-20	1.000	402.0	2.99E-20	1.000
404.0	3.20E-20	1.000	406.0	3.79E-20	1.000	408.0	3.95E-20	1.000	410.0	4.33E-20	1.000	412.0	4.71E-20	1.000
414.0	4.79E-20	1.000	416.0	4.88E-20	1.000	418.0	5.05E-20	1.000	420.0	5.21E-20	1.000	422.0	5.30E-20	1.000
424.0	5.17E-20	1.000	426.0	5.30E-20	1.000	428.0	5.21E-20	1.000	430.0	5.55E-20	1.000	432.0	5.13E-20	1.000
434.0	5.68E-20	1.000	436.0	6.22E-20	1.000	438.0	6.06E-20	1.000	440.0	5.47E-20	1.000	441.0	6.14E-20	1.000
442.0	5.47E-20	1.000	443.5	5.55E-20	1.000	443.5	6.81E-20	1.000	444.0	5.97E-20	1.000	445.0	5.13E-20	1.000
446.0	4.88E-20	1.000	447.0	5.72E-20	1.000	448.0	5.47E-20	1.000	449.0	6.56E-20	1.000	450.0	5.05E-20	1.000
451.0	3.03E-20	1.000	452.0	4.29E-20	1.000	453.0	2.78E-20	1.000	454.0	2.27E-20	1.000	456.0	1.77E-20	1.000
458.0	8.41E-21	1.000	460.0	4.21E-21	1.000	464.0	1.68E-21	1.000	468.0	0.00E+00	1.000			

Photolysis File = BZCHO

WL (nm)	Abs (cm^2)	QY	WL (nm)	Abs (cm^2)	QY	WL (nm)	Abs (cm^2)	QY	WL (nm)	Abs (cm^2)	QY	WL (nm)	Abs (cm^2)	QY
299.0	1.78E-19	1.000	304.0	7.40E-20	1.000	306.0	6.91E-20	1.000	309.0	6.41E-20	1.000	313.0	6.91E-20	1.000
314.0	6.91E-20	1.000	318.0	6.41E-20	1.000	325.0	8.39E-20	1.000	332.0	7.65E-20	1.000	338.0	8.88E-20	1.000
342.0	8.88E-20	1.000	346.0	7.89E-20	1.000	349.0	7.89E-20	1.000	354.0	9.13E-20	1.000	355.0	8.14E-20	1.000
364.0	5.67E-20	1.000	368.0	6.66E-20	1.000	369.0	8.39E-20	1.000	370.0	8.39E-20	1.000	372.0	3.45E-20	1.000
374.0	3.21E-20	1.000	376.0	2.47E-20	1.000	377.0	2.47E-20	1.000	380.0	3.58E-20	1.000	382.0	9.90E-21	1.000
386.0	0.00E+00	1.000												

Photolysis File = ACROLEIN

WL (nm)	Abs (cm^2)	QY	WL (nm)	Abs (cm^2)	QY	WL (nm)	Abs (cm^2)	QY	WL (nm)	Abs (cm^2)	QY	WL (nm)	Abs (cm^2)	QY
250.0	1.80E-21	1.000	252.0	2.05E-21	1.000	253.0	2.20E-21	1.000	254.0	2.32E-21	1.000	255.0	2.45E-21	1.000
256.0	2.56E-21	1.000	257.0	2.65E-21	1.000	258.0	2.74E-21	1.000	259.0	2.83E-21	1.000	260.0	2.98E-21	1.000
261.0	3.24E-21	1.000	262.0	3.47E-21	1.000	263.0	3.58E-21	1.000	264.0	3.93E-21	1.000	265.0	4.67E-21	1.000
266.0	5.10E-21	1.000	267.0	5.38E-21	1.000	268.0	5.73E-21	1.000	269.0	6.13E-21	1.000	270.0	6.64E-21	1.000
271.0	7.20E-21	1.000	272.0	7.77E-21	1.000	273.0	8.37E-21	1.000	274.0	8.94E-21	1.000	275.0	9.55E-21	1.000
276.0	1.04E-20	1.000	277.0	1.12E-20	1.000	278.0	1.19E-20	1.000	279.0	1.27E-20	1.000	280.0	1.27E-20	1.000
281.0	1.26E-20	1.000	282.0	1.26E-20	1.000	283.0	1.28E-20	1.000	284.0	1.33E-20	1.000	285.0	1.38E-20	1.000
286.0	1.44E-20	1.000	287.0	1.50E-20	1.000	288.0	1.57E-20	1.000	289.0	1.63E-20	1.000	290.0	1.71E-20	1.000
291.0	1.78E-20	1.000	292.0	1.86E-20	1.000	293.0	1.95E-20	1.000	294.0	2.05E-20	1.000	295.0	2.15E-20	1.000
296.0	2.26E-20	1.000	297.0	2.37E-20	1.000	298.0	2.48E-20	1.000	299.0	2.60E-20	1.000	300.0	2.73E-20	1.000
301.0	2.85E-20	1.000	302.0	2.99E-20	1.000	303.0	3.13E-20	1.000	304.0	3.27E-20	1.000	305.0	3.39E-20	1.000
306.0	3.51E-20	1.000	307.0	3.63E-20	1.000	308.0	3.77E-20	1.000	309.0	3.91E-20	1.000	310.0	4.07E-20	1.000
311.0	4.25E-20	1.000	312.0	4.39E-20	1.000	313.0	4.44E-20	1.000	314.0	4.50E-20	1.000	315.0	4.59E-20	1.000
316.0	4.75E-20	1.000	317.0	4.90E-20	1.000	318.0	5.05E-20	1.000	319.0	5.19E-20	1.000	320.0	5.31E-20	1.000
321.0	5.43E-20	1.000	322.0	5.52E-20	1.000	323.0	5.60E-20	1.000	324.0	5.67E-20	1.000	325.0	5.67E-20	1.000
326.0	5.62E-20	1.000	327.0	5.63E-20	1.000	328.0	5.71E-20	1.000	329.0	5.76E-20	1.000	330.0	5.80E-20	1.000
331.0	5.95E-20	1.000	332.0	6.23E-20	1.000	333.0	6.39E-20	1.000	334.0	6.38E-20	1.000	335.0	6.24E-20	1.000
336.0	6.01E-20	1.000	337.0	5.79E-20	1.000	338.0	5.63E-20	1.000	339.0	5.56E-20	1.000	340.0	5.52E-20	1.000
341.0	5.54E-20	1.000	342.0	5.53E-20	1.000	343.0	5.47E-20	1.000	344.0	5.41E-20	1.000	345.0	5.40E-20	1.000
346.0	5.48E-20	1.000	347.0	5.90E-20	1.000	348.0	6.08E-20	1.000	349.0	6.00E-20	1.000	350.0	5.53E-20	1.000
351.0	5.03E-20	1.000	352.0	4.50E-20	1.000	353.0	4.03E-20	1.000	354.0	3.75E-20	1.000	355.0	3.55E-20	1.000
356.0	3.45E-20	1.000	357.0	3.46E-20	1.000	358.0	3.49E-20	1.000	359.0	3.41E-20	1.000	360.0	3.23E-20	1.000
361.0	2.95E-20	1.000	362.0	2.81E-20	1.000	363.0	2.91E-20	1.000	364.0	3.25E-20	1.000	365.0	3.54E-20	1.000
366.0	3.30E-20	1.000	367.0	2.78E-20	1.000	368.0	2.15E-20	1.000	369.0	1.59E-20	1.000	370.0	1.19E-20	1.000
371.0	8.99E-21	1.000	372.0	7.22E-21	1.000	373.0	5.86E-21	1.000	374.0	4.69E-21	1.000	375.0	3.72E-21	1.000
376.0	3.57E-21	1.000	377.0	3.55E-21	1.000	378.0	2.83E-21	1.000	379.0	1.69E-21	1.000	380.0	8.29E-24	1.000
381.0	0.00E+00	1.000												

Table A-4.   Values of chamber-dependent parameters used in the model simulations of the environmental chamber experiments for this study. [a]

Parm.	Value(s)	Discussion
Default Chamber Model		The following are the parameters for the default chamber effects model which was assumed to be the same in both sides of the chamber and to be unaffected by PDI exposure. They were used when simulating all experiments in this study.
k(1)	0.173 min^{-1} (run DTC587) - through - 0.156 min^{-1} (run DTC616)	Derived from linear fit to results of quartz tube NO_2 actinometry measurements carried out around the time of the experiments as a function of run number.
k(O3W)	1.5x10^{-4} min^{-1}	The results of the O_3 dark decay experiments in this chamber are reasonably consistent with the recommended default of Carter et al (1995c) for Teflon bag chambers in general.
k(N25I) k(N25S)	2.8 x10^{-3} min^{-1}, 1.5x10^{-6} - k$_g$ ppm^{-1} min^{-1}	Based on the N_2O_5 decay rate measurements in a similar chamber reported by Tuazon et al. (1983). Although we previously estimated there rate constants were lower in the larger Teflon bag chambers (Carter and Lurmann, 1990, 1991), we now consider it more reasonable to use the same rate constants for all such chambers (Carter et al., 1995c).
k(NO2W) yHONO	1.6x10^{-4} min^{-1} 0.2	Based on dark NO_2 decay and HONO formation measured in a similar chamber by Pitts et al. (1984). Assumed to be the same in all Teflon bag chambers (Carter et al, 1995c).
k(XSHC)	250 min^{-1}	Estimated by modeling pure air irradiations. Not important om affecting model predictions except for pure air or NO_x-air runs.
Side A Prior to PTI Exposure		Used for experiments carried out in Side A prior to PTI exposure. Applicable to runs DTC587A through DTC600A. This side of the chamber had been exposed to dilute auto exhaust prior to this program, and appeared to have somewhat higher than normal radical source.
RS/K1	0.091 ppb	Based on model simulations of n-butane - NO_x experiments as discussed by Carter et al (1995c,d). This value is the average of RS/K1 values which fit run DTC587A and other butane runs carried out in side A during this period.
E-NO2/K1	0.091 ppb	Results of pure air and acetaldehyde - air runs, which are sensitive to this parameter, indicate that RS/K1 and E-NO2/K1 tend to be within experimental variability of being the same. This would be expected if the radical source and NO_x offgasing are due to the same process, such as HONO offgasing. Therefore, it is assumed that E-NO2/K1 = RS/K1 unless there is evidence to the contrary.

_____

Parm.	Value(s)	Discussion

_____

<u>Side B Prior to PTI Exposure</u>		Used for experiments carried out in Side B prior to PTI exposure. Applicable to runs DTC587B through DTC603B. Characterization results indicate that until the time of PTI exposure Side B was not exposed to reactants significantly affecting chamber effects.
RS/K1	0.068 ppb	Average of radical source rate which fit data for n-butane - NO_x runs carried out during this period. The RS/K1 value which fit run DTC587B was 0.042 ppb, which is ~40% lower than this. However, this is within the variability observed for these experiments, especially when the apparent radical source is low.
E-NO2/K1	0.068 ppb	Assumed to be the same as RS/K1, as discussed above.
<u>Side A After PTI Exposure</u>		Used in runs in Side A after the reactor was exposed to PTI in run DTC600A. Applies to runs DTC600A through DTC618A.
RS/K1	0.207 ppb	Based on the results of run DTC607A.
E-NO2/K1	0.207 ppb	Assumed to be the same as RS/K1, as discussed above.
<u>Side B After PTI Exposure</u>		Used in runs in Side B after the reactor was exposed to PTI in run DTC604B. Applies to runs DTC604B through DTC618B.
RS/K1	0.073 ppb	Based on the results of run DTC607B.
E-NO2/K1	0.073 ppb	Assumed to be the same as RS/K1, as discussed above.

_____

[a] See Table A-2 for definitions of the parameters.